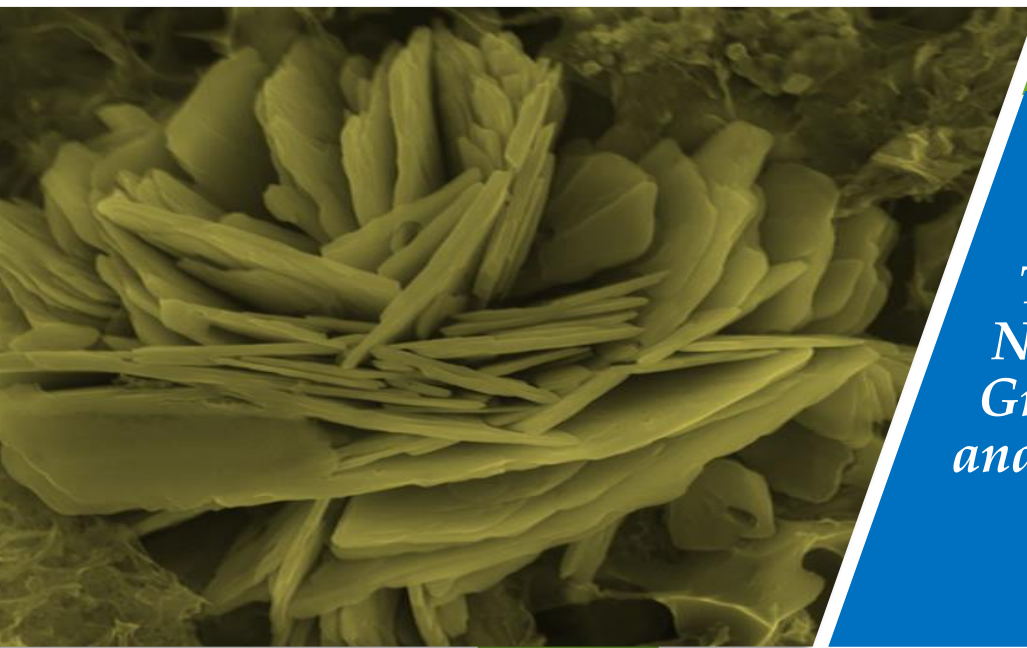




**UPM**  
UNIVERSITI PUTRA MALAYSIA  
BERILMU BERBAKTI



# iSAMN2021



*THEME:  
Nanoscale  
Green Synthesis  
and Applications*

PROCEEDING OF 5<sup>th</sup> INTERNATIONAL SYMPOSIUM ON  
ADVANCED MATERIALS AND NANOTECHNOLOGY  
9 – 10 December 2021

# Proceeding of 5<sup>th</sup> International Symposium on Advanced Materials and Nanotechnology

**Publisher:**

Institute of Nanoscience and Nanotechnology  
Universiti Putra Malaysia

2021



**International Symposium on Advanced Materials  
and Nanotechnology (iSAMN2021)**  
Nanoscale Green Synthesis and Applications  
December 9-10, 2021

Vol. 1, No.1, 2021  
eISSN 2811-4655

©Universiti Putra Malaysia 2021

All rights reserved. No part of this e-proceeding may be reproduced, stored in a retrieval system, or transmitted in any form, or by any means, electronic, mechanical, photocopying, recording or otherwise, without the prior permission of the copyright owner.

### **Editorial Board**

Dr. Umer Rashid  
Dr. Fatin Nabilah binti Mohd Faudzi  
Dr. Tan Tong Ling  
Dr. Nor Hapishah binti Abdullah  
Mohd Ali bin Mat Nong

### **Publisher's address:**

Institute of Nanoscience and Nanotechnology  
Universiti Putra Malaysia  
43400 UPM Serdang, Selangor,  
Malaysia

## TABLE OF CONTENT

No	Paper Title / Author (s)	Pages
<b>KEYNOTE PAPER</b>		
1.	Green Synthesized Nanomaterials as a Novel Support for the Immobilization of Some Industrial Enzymes and their Applications <i>Hayrunnisa Nadaroglu</i>	1
2.	Nanotechnology for Animal Health: Insights on Nanoparticles Applications in Poultry and Fish Farming <i>Mohamed Ibrahim Shaalan</i>	2
3.	Rapid and Low-cost Biosensing Platforms for the Detection of Infectious Agents & Toxins <i>Mohammed Zourob</i>	3
<b>INVITED PAPER</b>		
1.	Advanced Materials for Next Generation Power Source and Storage <i>Matsuda Atsunori</i>	4
2.	Functionalized Natural Rubber-Derived Carbon/Silica Nanocomposites for Catalytic Conversion of Glucose to 5-Hydroxymethylfurfural <i>Chawalit Ngamcharussrivichai</i>	6
3.	Lab-on-Flexible Printed Circuit board (LoFPCB) for Electrochemical Sensor and Sensing Platform <i>Asrulnizam Abdul Manaf</i>	8
4.	Electrical Response and Cell Viability Study of Breast Cancer Cell Treated in Aqueous Graphene Oxide Solution Deposited on IDE <i>Muhammad Mahyiddin Ramli</i>	10
5.	Development of a Microstrip Patch Antenna using Carbon based Charcoal for X-band Application <i>Zainab Yunusa</i>	12
6.	Kinetic Release Aspect of Naproxen Embedded on Boron-modified Carbon Nanodots as Multi-tasking Agent on Cancer Treatment <i>Zakki Fahmi</i>	14
7.	Doped and Un-doped Maghemite Nanoparticles for Magnetic Hyperthermia Application <i>Mohamed O. Lemine</i>	16
8.	Serine/Graphene Oxide modified Electrode for Electrochemical Determination of Uric Acid <i>Piyapong Asanithi</i>	18

No	Paper Title / Author (s)	Pages
9.	Niobium MXenes for Environmental Sensing Applications <i>Abdul Rasheed Pathath</i>	20
<b>FUNCTIONAL AND STRUCTURAL MATERIALS</b>		
1.	Versatile Graphene for a Myriad of Applications <i>Lim Hong Ngee and Izwaharyanie Ibrahim</i>	22
2.	Preparation and Sensing Characterization of Hybrid Iron Oxide-Reduced Graphene Oxide at Room Temperature <i>Nurul Athirah Abu Hussein and Huzein Fahmi Hawari</i>	24
3.	Biogenic Reduced Graphene Oxide and its Cytotoxicity Evaluation <i>Dharshini Perumal, Emmellie Laura Albert, Muhammad Amir Faiz and Che Azurahaman Che Abdullah</i>	26
4.	Optical, Structural, and Electrical Features of Polyaniline Synthesized by Camphor Sulphonic Acid <i>Mahnoush Beygisangchin, Suraya Abdul Rashid and Suhaidi Shafie</i>	28
5.	Resistless Nano-Etching of UV-Irradiated Vinyl-Functional Silsesquioxane Thin Film by Alcohol-Alkaline Solution <i>Siti Mariam Mohamad, Nurazilah Mohd Zainon, Syazana Abu Bakar, Nor Shahida Kader Basha, Farina Md Jamil and Mat Tamizi Zainuddin</i>	30
6.	A Review on Polymerization Method of Tuneable PNIPAAm-based Thermally Sensitive Nanogels <i>Nur Fathin Amirah binti Shafie, Mohd Yusof Hamzah and Roshafima Rasit Ali</i>	32
7.	Optimization of Gel Content and Swelling Properties of Hyaluronic Acid/Gracilaria Changgi Hydrogel <i>Maizatul Nurhafiqah Mohd Jupri, Norizah Abdul Rahman and Mansor Ahmad</i>	34
8.	Heat Treatment Affects the Formation of Copper Oxide Nanoparticles using the Precipitation-Thermal Oxidation Method <i>Nur Syuhada Mohd Haeizar, Che Anis Fawzi, Annie Maria Mahat and Nur Aimi Jani</i>	36
9.	Tailoring Localized Surface Plasmon Resonance of Added Ag Nanoparticles Er <sup>3+</sup> Ion Doped Glass System by Coupling Polarization Approach <i>Muhammad Siddiq Fadhil Sutrisno, S.K. Md Zain and R. Hisam</i>	38
10.	Impact Of Rare-Earth Lanthanum Ion Modifications on Magnetic Characteristics of Mechanically Alloyed Yttrium Iron Garnet Nanoparticles <i>Nurul Atiqah Mohd Pauzi and Rodziah Nazlan</i>	40
11.	Assessment of Various Organic Coatings on Magnetic Nanoparticles for Biomedical Applications	42

No	Paper Title / Author (s)	Pages
	<i>Nur Khalida Rahayu Zainon, Che Azurahaman Che Abdullah and Mohd Basyaruddin Abdul Rahman</i>	
<b>NANOELECTRONICS</b>		
12.	Modern Methods for Protecting Printed Circuit Boards Effects from Mechanical External Impact <i>Zainab Hussam Al-Araji, A.V. Turetsky and A.V. Bashkurov</i>	44
13.	Optimization of the Frequency Performance of Sige Heterojunction Bipolar Transistor (HBT) Integrated in a Bicmos 55 nm Technology <i>Lachkhab Chems El Ghizlane, Maya Lakhdara, Abdeaziz Boulghab and Saida Latreche</i>	46
<b>NANOMEDICINES</b>		
14.	Synthesis and Characterisation Chitosan-Carbon Dots with Loaded Mitomycin C for Bladder Cancer <i>Siti A'risyah Muhamad Ghadzali, Nor Azah Yusof and Jaafar Abdullah</i>	48
15.	The Toxicity Evaluation of Selected Nanoparticles on <i>Artemia salina</i> <i>Emmellie Albert, Nurul Anis Athirah Ab Aziz, Amir Faiz, Dharshini Perumal, Lau Gee Een, Ashreen Norman and Che Azurahaman Che Abdullah</i>	50
16.	Optimization, Characterization and Toxicity Studies of Gold Nanoparticles as Potential Biocompatible Carrier for Colon Cancer Treatment <i>Siti Nadiyah Zulkifli, Manali Haniti Zahid, Iskandar Zulkarnain Alias Mohamad Faizal Ibrahim and, Che Azurahaman Che Abdullah</i>	52
17.	Preparation, Cytotoxicity and Apoptotic properties of Gallic Acid Nanoparticles Against Human HepG2 Cell Lines <i>Abdelkader Hassani, Mohamed Lakhder Belfar, Zenkhri Louiza, Hakim Belkhalifa, Abdullah Hajar, Samiullah Saeed and Siti Aslina Hussain</i>	54
18.	Nano-Hydroxyapatite-based Scaffolds for the Delivery of Bone Morphogenetic Protein-2 (BMP-2) to Promote Bone Regeneration <i>Anis Syauqina Mohd Zaffarin, Shiow-Fern Ng, Min Hwei Ng, Haniza Hassan and Ekram Alias</i>	56
19.	Synthesis of Hydroxyapatite/Montmorillonite Nanocomposite as a Carrier for Methotrexate Drug <i>Rosnah Nawang, Mohd Zobir Hussein, Khamirul Amin Matori and Che Azurahaman Che Abdullah</i>	58
20.	Theranostic System Using Novel Chitosan-Based Nanoimmunosensing Antibody/Aptamer Assembly for Dual Application Sites of Bladder Cancer Cell Targeting and Drug Release	60

No	Paper Title / Author (s)	Pages
	<i>Fariza Aina Abd Manan and Nor Azah Yusof</i>	
21.	Structural and Antimicrobial Evaluation of Gamma Synthesized Ag/KIn Nanocomposites <i>Salmah Moosa, Anis Nadia Mohd Faisol Mahadeven and Kamyar Shameli</i>	62
<b>PHOTOCATALYSIS &amp; SEPARATION</b>		
22.	Hydrothermal Synthesized Stable and Reusable Tin Sulfide Filled Cellulose Photocatalysts and their Application in Dye Degradation <i>Jyoti Bala Kaundal and Y. C. Goswami</i>	64
23.	Photodegradation Performance by Zinc Oxide Filled in Cellulose Nanofibril Membranes and Aerogel for Decolouration of Organic Dye <i>Azima Azmi, Kam Sheng Lau, Siew Xian Chin, Sarani Zakaria and Chin Hua Chia</i>	66
24.	Synthesis and Characterization of TiO <sub>2</sub> Nanoparticles using Alkaline Fusion Method for Potential Photocatalyst Application <i>Muhammad Azri Muhd Yusop, Nurul Anis Athirah Ab Aziz, Amir Faiz, Dharshini Perumal, Lau Gee Een, Ashreen Norman and Che Azurahaman Che Abdullah</i>	68
<b>GREEN SYNTHESIS AND APPLICATIONS</b>		
25.	Physical Properties Characterization of Ancient Nanostructured Biomaterials (Nacre Layer) Retrieved using Ethylenediaminetetraacetic Acid (EDTA) <i>Nur Farahah Mohd Khairuddin, Nur Shuhada Zaharia, Mohd Luqman Mokhtar, Emmellie Laura Albert, Nicholas Khong and Che Azurahaman Che Abdullah</i>	70
26.	Synthesis of Thymol Encapsulated in Chitosan Nanoparticle for Active Food Packaging Application <i>Ruzanna Ahmad Shapi'I, Siti Hajar Othman, Mohd Nazli Naim and Intan Syafinaz Mohamed Amin Tawakkal</i>	72
27.	Influence of Grinding Techniques During Chromolaena Odorata Leaves Preparation Towards the Formation of Biosynthesized SnO <sub>2</sub> Nanoparticles <i>Irmaizatussyehdany Buniyamin, Rabiataladawiyah Md Akhir, Noor Asnida Asli, Zuraida Khusaimi and Mohamad Rusop Mahmood</i>	74
28.	The Effect of EM4 Addition to Stale Rice Substrate on the Production Potential of Methane in a Biogas Reactor <i>Kadek Saputra, M. Ramdhan Kirom and Asep Suhendi</i>	76
29.	Effect of Variation of Stale Rice and EM4 Rice Substrate Filling time on Methane Gas Production Potential using Mesophilic Biogas Reactor <i>Lely Gopar, M. Ramdhan Kirom and Asep Suhendi</i>	78



No	Paper Title / Author (s)	Pages
<b>NANOAGRICULTURE</b>		
30.	Preliminary Study on Methyl Jasmonate Nanoemulsion for Paddy Growth Modulation <i>Hazalina Zulkifli, Noor Azlina Masdor, Khalisanni Khalid, Nur Sabrina Wahid, Nor Fadilah Abd Halim, Shahida Hashim, Siti Nadzirah Padrillah, Nadia Izati Fadzil, Mohd Nor Mohd Rosmi, Nor Suzaida Mohd Nor, Ahmad Shazwan Ismail and Muhamad Shafiq Abd Karim</i>	80
31.	Effects of Carbon Quantum Dots on Growth of <i>Brassica juncea</i> under Grow Lights <i>Yamuna Chowmasundaram, Tong Ling Tan, Mohamad Fakri Zaky Bin Ja'afar, Rosimah Nulit, Mashitah Jusoh and Suraya Abdul Rashid</i>	82
32.	Cellulose-Based Hydrogel for Seed Germination <i>Swarna Devi Palanivelu, Kushairi Mohd Salleh, Keith Lindsey, Fareed Sairi, Muhamad Hafiz Che-Othman and Sarani Zakaria</i>	84
33.	Synthesis of Dazomet-Micelle Fungicide Nanodelivery System for Combating Ganoderma Disease in Oil Palm <i>Isshadiba Mustafa, Mohd Zobir Hussein, Abu Seman Idris, Nur Hailini Z. Hilmi and Sharida Fakurazi</i>	86
<b>NANOCELLULOSE</b>		
34.	Surface Modification of Nanocellulose: A Brief Overview <i>Nurul Ain Nadirah, Latifah Jasmani, Rafeadah Rusli and Sarani Zakaria</i>	88
35.	Preliminary Study of Cellulose Nanofibre Produced through Tri-Solvent Technique <i>Mohamad Zaki Abdullah, M Shuaib B M Saheed, Mohd Fazli Mohammat and Shahrul Nizam Md Salleh</i>	90
36.	Refinement Technique for Nanocellulose Extraction from Corn Cobs <i>Ismail Ibrahim (Al-Khateeb), Yusra M. Al-Obaidi and Sabri M. Hussain</i>	92
<b>ENVIRONMENTAL NANOTECHNOLOGY</b>		
37.	Investigation on Thermal Stability Behaviour and Mechanical Properties of Polyactic Acid-Based Polymer Composite Filled with Different Nanofillers <i>Natasha Ramli, Norkhairunnisa Mazlan, Yoshito Ando, Khalina Abdan and Zulkiflle Leman</i>	94
<b>MODELLING</b>		
38.	Excess Population of the Dipole Moment Controls the Total Moment in Bulk Tetrahydrofuran from Molecular Dynamics Simulation <i>Mohd Farid Ismail</i>	96





No	Paper Title / Author (s)	Pages
39.	Modelling Techniques of MTJ's in Spin-based Devices and its Results Comparison <i>Maryala Praveen and Atul Kumar Nishad</i>	98
40.	Simultaneous Extraction of Diffusion Length and Surface Recombination Velocity from an EBIC Line Scan Using Artificial Neural Networks <i>Souhaila Soualmia</i>	100
41.	Simulation of AI & ML Based Nano Mechanical Embedded Systems for Diagnostic Application Development in the Field of Bio-Medical Engineering <i>Madhu P. Asangi, Pavithra G. and T.C. Manjunath</i>	102
<b>NANOELECTRONICS</b>		
42.	Ambipolar effect in Field Effect Transistors Based on Transition-Metal Dichalcogenides <i>Mehmet Ertugrul</i>	104
<b>KEYNOTE PAPER</b>		
	Green Synthesized Nanomaterials as a Novel Support for the Immobilization of Some Industrial Enzymes and their Applications <i>Hayrunnisa Nadaroglu</i>	107

## **Green Synthesized Nanomaterials as a Novel Support for the Immobilization of Some Industrial Enzymes and Their Applications**

Hayrunnisa Nadaroglu\*

*Department of Food Technology, Erzurum Vocational Collage, Ataturk University, 25240 Erzurum, Turkey  
Department of Nano-Science and Nano-Engineering, Institute of Science and Technology, Ataturk University,  
25240 Erzurum, Turkey*

**Abstract:** Industrial enzymes immobilized on nano support materials are successfully used in the food industry, fuel, textile, paper and pulp, detergent, environment, medical and analytical fields. Nanoparticles obtained by green synthesis by using plant extracts in non-toxic, high yield, mild conditions were used for immobilization. Many different biodegradable nanoparticles or nanocomposite support materials have been used successfully in the immobilization of industrial enzymes. While pectin lyase, mannanase, lipase, protease, laccase, cellulase and chitinase enzymes were immobilized to the nanosupported materials, the activity and immobilization efficiency were preserved. As a result of the modification of the enzymes with Magnetic Fe<sub>3</sub>O<sub>4</sub> nanoparticles, the enzyme was easily recovered from the reaction medium. In addition, as a result of the immobilization of industrial enzymes, the steric bulk problem was minimized during the binding of the substrates to the active center.

From the findings obtained from our studies, it has been determined that the reusability of enzymes provides an average of over 80% activity preservation in 10 cycle reaction trials in almost all enzymes.

**Keywords:** Immobilization, Pectin lyase, Laccase, Mannanase, Phytase, Lipase, Chitinase

## **Nanotechnology for Animal Health: Insights on Nanoparticles Applications in Poultry and Fish Farming**

Mohamed Ibrahim Shaalan\*

*Department of Veterinary Pathology, Faculty of Veterinary Medicine, Cairo University, Egypt*

**Abstract:** Nanotechnology has become an extensive field of research due to the unique properties of nanoparticles (NPs), which enable novel applications. NPs show advantages of high absorption and bioavailability with higher effective delivering to the target tissue compared to the bulk particles. Nanomaterials show variable forms, sizes, shapes, surface modifications, charges and natures. Top-down and bottom-up methods are the common types of NPs preparation. There are different mechanisms through which NPs could exert their action. Nanoparticles have found their way into many applications in the field of medicine, including diagnostics, vaccination, drug and gene delivery. Veterinary medical research is no exception, in the poultry field, NPs have been considered in the diagnosis of infectious diseases, vaccines preparations, disinfection, production enhancement, detection of food adulteration and antimicrobial agents (antiviral, antibacterial, antiparasitic, antifungal) and antimycotoxins. In fish medicine, various nanoparticles have shown potent antimicrobial actions with particular emphasis on the antibiotic resistant bacteria. The development of nanoparticle-based vaccines against viral pathogens is a promising field in fish medicine research. Nanoparticles have gained much interest as a specific and sensitive tool for diagnosis of bacterial, fungal and viral diseases in aquaculture. Despite the wide benefits of using NPs in poultry and fish production, concerns about their safety should be regarded. Therefore, safety and hazards impact of NPs in animals must be carefully assessed.

**Keywords:** Nanoparticles, veterinary medicine, poultry, fish

## Rapid and Low-cost Biosensing Platforms for the Detection of Infectious Agents & Toxins

Mohammed Zourob

*Alfaisal University, Al Zahrawi Street, Al Maather, Al Takhassusi Rd, Riyadh 11533, Saudi Arabia.*

**Abstract:** According to the World Health Organization (WHO), infect 5-10% of the world population resulting in 3 to 5 million cases of severe illness and 290,000 to 650,000 annual deaths from viruses and respiratory pathogens. Early diagnosis and therapeutic intervention can ameliorate symptoms of infection and reduce mortality. The conventional diagnosis of viral infections has evolved over the years with diverse approaches, however, there are inherent short comings associated with these testing. There is an urgent need for the rapid and low-cost diagnostic assays, due to the enormous annual burden of the influenza diseases and associated mortality. In this presentation, we will cover our recent results in the development of use of soft and flexible diagnostic tools such as Q-tips, and flexible polymers as low-cost and easy to use colorimetric biosensing platforms. These swabs serve as sample collection, analytes pre-concentration as well as sensing tool. These platforms were tested for various bacteria e.g. E. Coli, Staphylococcus aureus, Campylobacter, Brucella, and viruses e.g. flu viruses, COVID19 and MERS CO V. The assay can be performed in field and at the patient bed's side by minimally skilled personnel without the need for instrumentation. Cross-reactivity assays did not show binding with other common respiratory viruses and pathogens. The detection limit for these viruses and pathogen equivalent to gold standard techniques but can be achieved within minutes.

## Advanced Materials for Next Generation Power Source and Storage

Atsunori. MATSUDA<sup>1</sup>

<sup>1</sup> Toyohashi University of Technology

(Department of Electrical and Electronic Information Engineering, Toyohashi, Aichi 441-8580, Japan)

\*E-mail: matsuda@ee.tut.ac.jp

**Abstract:** In 2020, Japan pledged to reduce greenhouse gas (GHG) emission in Japan to net zero by 2050, namely become carbon neutral and achieve a decarbonized society for the global warming control. Therefore, development of advanced materials and nanotechnologies for nextgeneration clean power source and efficient power storage devices are crucial for the achievement of the low-carbon society. In this invited lecture, I would like to describe the cutting-edge materials and technologies for fuel cells as clean power sources and for all solid-state lithium batteries as efficient power storages.

As for the clean power sources, fuel cells are one of the most important key devices. Polymer electrolyte fuel cells (PEFCs) using  $H_2$  have been practically applied as power sources of cogeneration systems such as ENE-FARM and electric vehicles such as Toyota MIRAI (Figure 1). The operation conditions of the PEFCs are generally restricted to be lower than

100°C and under high humidity due to the properties of commonly used perfluorosulfonate membranes like Nafion<sup>®</sup>. Protonconductive membranes with high conductivity in the medium temperature range (100–200°C) even under low humidity are highly required as the electrolytes for PEFCs. Since the operation of PEFCs in the medium temperature range improves the utilization of total electric power generated in the cells and depresses the poisoning of Pt catalysts with CO in the fuel gases. In addition, working of PEFCs under low humidity permits to reduce the weight and volume of humidifiers [1]. We have been studying composite electrolyte membranes composed of polybenzimidazole (PBI) and mechanochemically synthesized inorganic solid acid complex [2]. Cesium hydrogen sulfate-silicotungstic acid complex (CHS-WSiA) was mechanochemically synthesized, further pulverized in N,N-dimethylacetamide (DMAc) with wet milling, and then added to the PBI DMAc solution. A slurry thus prepared was cast in a petri dish, dried overnight in an electric oven, and peeled off to obtain CHS-WSiA PBI membrane. The addition of CHS-WSiA

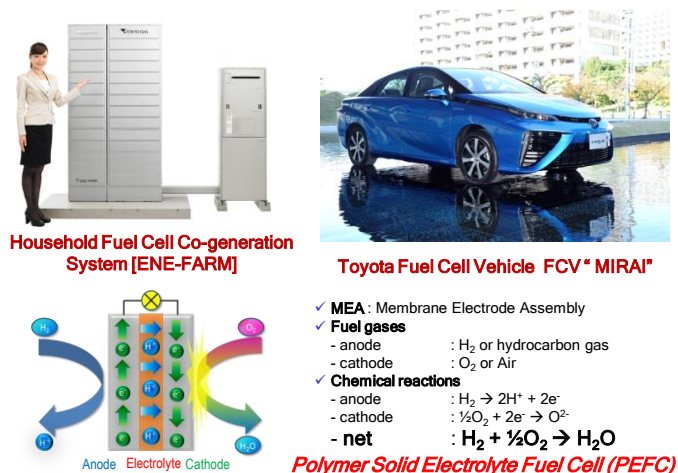


**Fig. 1.** Polymer electrolyte fuel cells (PEFC) and their practical applications.

improves the performance of the fuel cell, which can be ascribed to the enhancement of proton conductivity of the electrolyte membranes by the increase in proton conducting paths in the membranes. Pulverized submicron CHS-WSiA particles are highly dispersed in the PBI matrix and the homogeneous small amount  $\text{H}_3\text{PO}_4$ -doped PBI composite membranes achieve higher proton conductivity, lower overpotential, and better power density in the medium temperature range under anhydrous conditions.

As regards efficient power storages, the study of all-solid-state lithium ion battery (LIB) is becoming popular especially for electric vehicles (EVs) because the organic solvent used in the conventional LIB may be ignited at high temperature (Figure 2) [3]. The sulfide-based solid electrolytes are currently well known because of high lithium ion conductivity, nonflammability and unique elastoplastic property. Sulfide-based solid electrolytes for all-solid-state LIBs are usually synthesized by mechanical milling or melt-quenching. Recently, liquid phase synthesis has been introduced as a new route for sulfide-based lithium solid electrolytes. We

have developed new processing to synthesize  $\text{Li}_3\text{PS}_4\text{-LiI}$  (LPSI) from liquid phases [4]. In the preparation of LPSI, liquid-phase shaking (LS) method was applied.  $\text{Li}_2\text{S}$ ,  $\text{P}_2\text{S}_5$  and  $\text{LiI}$  were added to ethyl propionate and shaken to the mixture to obtain the LPSI precursor. After heat-treatment crystalline LPSI in nanosize was obtained. The prepared sample exhibited high ionic conductivity at room temperature of about  $6.0 \times 10^{-4} \text{ Scm}^{-1}$ . All-solid-state LIBs using LPSI as a solid electrolyte showed higher capacity and good charge-discharge performances as well as high thermal stability, which is promising for future LIB applications.

**Keywords:** Composite electrolyte, Solid acid, Fuel cell, Sulphide Electrolyte, All-Solid-State Li Battery

**ACKNOWLEDGMENT:** These works are partly supported by JSPS KAKEN, NEDO Advanced Fuel Cell (AFC) Project (JPNP20003), JST-ALCA-SPRING project (JPMJAL1301), and NEDO-SOLiD-EV Project (JPNP18003).

## REFERENCES

- [1] K.T. Adjemian *et al.*, *J. Electrochem. Soc.*, 149, 256 (2002).
- [2] S-Y. Oh, A. Matsuda *et al.*, *J. Mater. Chem.*, 20, 6359 (2010).
- [3] J. C. Bachman *et al.*, *Chem. Rev.*, 116 (1), 140 (2016).
- [4] Phuc, N.H.H., A. Matsuda *et al.*, *J. Power Sources*, 2017, 365, 7 (2017).

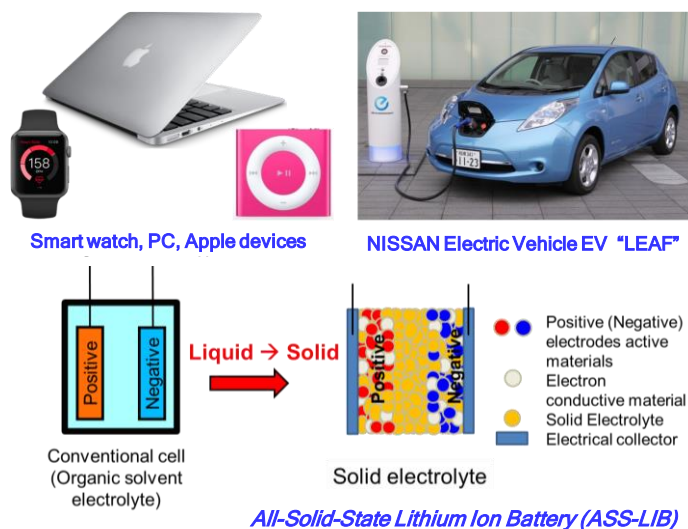


**Fig. 2.** Lithium ion battery (LIB) and all-solid-state LIB using solid electrolytes for future applications.



## Functionalized Natural Rubber-Derived Carbon/Silica Nanocomposites for Catalytic Conversion of Glucose to 5-Hydroxymethylfurfural

Satit Yousatit<sup>1,2</sup>, Ryota Osuga<sup>3</sup>, Junko N. Kondo<sup>4</sup>, Toshiyuki Yokoi<sup>4</sup> and Chawalit Ngamcharussrivichai<sup>1,2,5,\*</sup>

<sup>1</sup>Department of Chemical Technology, Faculty of Science, Chulalongkorn University, Bangkok 10330, Thailand

<sup>2</sup>Center of Excellence in Catalysis for Bioenergy and Renewable Chemicals (CBRC), Faculty of Science, Chulalongkorn University, Bangkok 10330, Thailand

<sup>3</sup>Institute of Multidisciplinary Research for Advanced Materials, Tohoku University, Miyagi, Japan

<sup>4</sup>Nanospace Catalysis Unit, Chemical Resources Laboratory, Tokyo Institute of Technology, Yokohama, Japan

<sup>5</sup>Center of Excellence on Petrochemical and Materials Technology (PETROMAT), Chulalongkorn University, Bangkok 10330, Thailand

\*Corresponding Author's Email: Chawalit.Ng@Chula.ac.th

**Abstract:** 5-Hydroxymethylfurfural (HMF) is an important platform molecule derived from biomass. This study aims at developing new bifunctional acid-base mesoporous carbon/silica (MCS) composites as solid catalysts for the selective conversion of glucose into HMF. The MCS material was prepared using a nanocomposite of natural rubber (NR) and hexagonal mesoporous silica (HMS) as a precursor. To obtain a series of bifunctional acid-base catalysts, the MCS surface was modified using post-synthesis methods in which the carbon moieties were decorated with sulfonic acid groups, whereas the silica matrix surface was grafted with 3-aminopropyl groups. The Brønsted basic sites facilitated not only the glucose–fructose isomerization but also promoted the generation of undesired humins. The acid/base ratio of bifunctional MCS catalysts determined the HMF yield and selectivity.

**Keywords:** carbon/silica composite, 5-hydroxymethylfurfural, hydrophobicity, acid catalyst, dehydration

### INTRODUCTION

5-Hydroxymethylfurfural (HMF) is an important platform compound for manufacturing various bio-based products. The glucose conversion into HMF is a two-step reaction process. Firstly, glucose is isomerized into fructose using Brønsted bases or Lewis acids. In the second step, fructose dehydration into HMF in the presence of Brønsted acid. However, various side reactions often accompany these processes, resulting in low HMF yield. Many researchers have attempted to develop novel solid materials with better catalytic performance and more environmentally friendly system for sustainable HMF production [1]. Mesoporous carbon/ silica (MCS) nanocomposites have attracted attention in catalysis application. The MCS can be functionalized with sulfonic acid group ( $-\text{SO}_3\text{H}$ ) by sulfonating with concentrated  $\text{H}_2\text{SO}_4$ , which are active for dehydrating fructose into HMF [2]. This study aims at developing new bifunctional acid base MCS composites as solid catalysts for the selective conversion of glucose into HMF.



## MATERIALS AND METHODS

The synthesis of MCS nanocomposites was conducted using NR/HMS material as a precursor, as previously reported [3]. The sulfonated MCS nanocomposites (MCS-SO<sub>3</sub>H) were prepared by sulfonation of MCS using aqueous H<sub>2</sub>SO<sub>4</sub> solution at different concentrations, while MCS was functionalized with 3-aminopropyltrimethoxysilane (APS) to prepare MCS-NH<sub>2</sub>. The bifunctional acid-base MCS nanocomposites (MCS-SO<sub>3</sub>H-NH<sub>2</sub>) was obtained by grafting MCS-SO<sub>3</sub>H with APS. Catalytic conversion of glucose was performed in a biphasic solvent (aqueous NaCl solution/THF) using a Teflon-lined stainless-steel autoclave. The reaction products were analyzed using a high-performance liquid chromatography.

## RESULTS AND DISCUSSION

The glucose conversion and HMF yield were enhanced over the MCS-SO<sub>3</sub>H-NH<sub>2</sub> catalysts. The basic sites promoted the isomerization of glucose to fructose and the formation of humins. The HMF yield increased with an increasing number of basic and acidic sites (Fig. 1). The highest HMF yield and glucose conversion of 39.4% and 86%, respectively, were obtained over MCS-18S-0.2N with an acid/base ratio of 0.10.

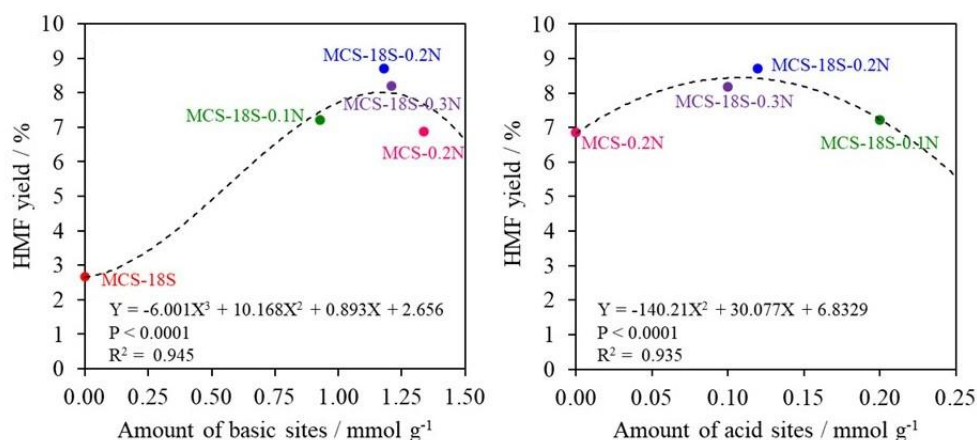


Fig. 1. Dependence of the HMF yield on number of basic and acid sites.

## CONCLUSIONS

The MCS-SO<sub>3</sub>H-NH<sub>2</sub> with acid-base bifunctionality has prospect for the glucose conversion into HMF. These catalysts not only have superior performance in the HMF synthesis but also exhibited good reusability.

## REFERENCES

- [1] Khumho R, Yousatit S, Ngamcharussrivichai C. *Catalysts* 2021, **11**, 887.
- [2] Tian X, Jiang Z, Jiang Y, Xu W, Li C, Luo L, Jiang Z. *RSC Adv.* 2016, **103**, 101526.
- [3] Yousatit S, Pitayachinchot H, Wijitrat A, Chaowamalee S, Nuntang S, Soontaranon S, Yokoi T, Ngamcharussrivichai, C. *Sci. Rep.* 2020, **10**, 12977.

## Lab-on-Flexible Printed Circuit board (LoFPCB) for Electrochemical Sensor and Sensing Platform

Mohd Syafiq Awang<sup>1</sup>, Nor Syafirah Zambry<sup>2</sup>, Beh Khi Khim<sup>1</sup>, Yazmin Bustami<sup>3</sup>, Hairul Hisham Hamzah<sup>4</sup>, Ismail Aziah<sup>2\*</sup> and Asrulnizam Abd Manaf<sup>1\*</sup>

<sup>1</sup>*Collaborative Microelectronic Design Excellence Centre (CEDEC), Sains@USM, Universiti Sains Malaysia, Level 1, Block C, No.10 Persiaran Bukit Jambul, 11900 Bayan Lepas, Pulau Pinang, Malaysia.*

<sup>2</sup>*Institute for Research in Molecular Medicine (INFORMM), Health Campus, Universiti Sains Malaysia (USM), 16150 Kubang Kerian, Malaysia.*

<sup>3</sup>*School of Biological Sciences, Universiti Sains Malaysia (USM), 11800 Gelugor, Malaysia.*

<sup>4</sup>*School of Chemical Sciences, Universiti Sains Malaysia (USM), 11800 Gelugor, Malaysia.*

*\*Corresponding Author's Email: [eeasrulnizam@usm.my](mailto:eeasrulnizam@usm.my), [aziahismail@usm.my](mailto:aziahismail@usm.my)*

**Abstract:** The present study aimed to develop a label-free miniaturised electrochemical biosensor based on aptamer and deoxyribonucleic acid (DNA) for typhoid and SARS-CoV2 detection, respectively. In these studies, the bioreceptors were immobilized on the working electrode and the electrochemical detection was performed using the differential-pulse voltammetry (DPV) technique. The results demonstrated that the applied strategies showed successful detection of both disease-causing pathogens. The presentation also will demonstrate the implementation the electrochemical sensor on flexible substrate.

**Keywords:** *Electrochemical biosensor, Salmonella typhi, Covid-19, lab on PCB.*

## INTRODUCTION

Lab-on-printed circuit board (LoPCB) is a device that integrates one or more laboratory functions into a single miniaturised chip [1]. This technology is getting attention in medical diagnostics as it provides less invasive, fast, specific and reliable detection of pathogens [2]. The traditional lab- centralised diagnostics of pathogens usually require expensive instruments, highly trained personnel, and long time-to-results [2]. In this study, the detection platform was developed based on the electrochemical sensing mechanism on screen-printed electrode (SPE) using a standard printed circuit board fabrication technique and flexible printed circuit board. A highly specific aptamer and DNA probe were used as the bioreceptor for target sensing and a successful detection was determined by the reduction in current in DPV measurement.

## MATERIALS AND METHODS

The SPE was fabricated based on a three-electrode system on a flame retardant 4 (FR-4) with gold working, counter and reference electrodes [3]. The fabrication of aptasensor for typhoid detection starts with the modification of the working electrode (WE) with graphene oxide (GO) to improve the current signal. Then, WE were functionalised with an aptamer specific for *Salmonella typhi* with the aid of EDC-NHS reagent, incubated, and rinse with PBS. Then, a

specific *Salmonella typhi* protein (100 ng/mL) was dropped onto the WE, incubated and rinsed with PBS. The fabrication of DNA sensor for SARS-COV2 starts with the functionalisation of WE with a thiolated ssDNA probe. Then, MCH solution was dropped onto the WE to reduce the non-specific binding of the DNA probe and rinsed. Then, the DNA target (1  $\mu$ M) was dropped onto the functionalised WE and incubated. Finally, the electrochemical detection for both developed biosensors was performed using DPV measurement in 50 mM potassium ferrocyanide (in 1 $\times$  PBS solution).

## RESULTS AND DISCUSSION

Figure 1 demonstrates the trends of current changes of developed aptasensor and DNA sensor.

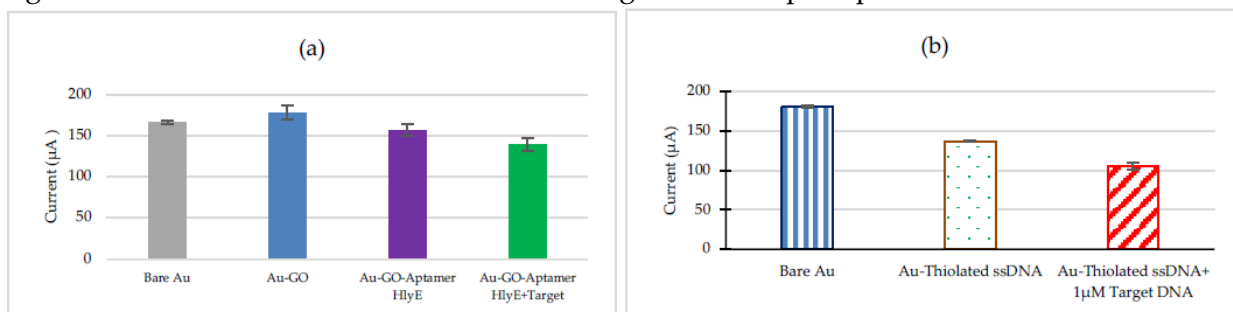


**Fig. 1:** (a) Current trends of *Salmonella* aptasensor after modified with GO, functionalised with aptamer and exposure to target protein. (b) Current trends of DNA sensor after functionalised with thiolated ssDNA and exposure to target DNA.

## CONCLUSIONS

In summary, we herein presented a low-cost, batch fabrication strategies for infectious disease detection (SARS-CoV2 and typhoid) on PCB, with highly selective aptamer and DNA probe as bioreceptor. The finding of these studies shows that our LoFPCB sensor is a promising diagnostic tool for disease detection.

**ACKNOWLEDGMENT:** The authors would like to express appreciation for the support of the sponsors Collaborative Research in Engineering, Science, and Technology (CREST) (304/CIPPM/6150181/C121).

## REFERENCES

- [1] Schönberger, M.; Hoffstetter, M. 6 - Emerging Trends. In; Schönberger, M., Hoffstetter, M.B.T.-E.T. in M.P.E. and M., Eds.; William Andrew Publishing, 2016; pp. 235–268 ISBN 978-0-323-37023-3.
- [2] Arshavsky-Graham, S.; Segal, E. Lab-on-a-Chip Devices for Point-of-Care Medical Diagnostics. In; Springer Berlin Heidelberg: Berlin, Heidelberg; pp. 1–19.
- [3] Beh, K.K.; Abd Manaf, A.; Oo, C.W.; Beh, K.P.; Yam, F.K.; Sawada, K. Comparative Studies of Graphitic Material Interaction with Flame Retardant 4 (FR-4) Substrate for Miniature Electrochemical-based pH Sensor. *Sensors Mater.* **2020**, 32, 2089–2103.

## Electrical Response and Cell Viability Study of Breast Cancer Cell Treated in Aqueous Graphene Oxide Solution Deposited on IDE

Muhammad M. Ramli<sup>1,2\*</sup>; A. S. Rosman<sup>1</sup>; N. S. Mazlan<sup>1</sup>; M. F. Ahmad<sup>1,2</sup>; D. S. C. Halin<sup>2</sup>, R. Mohamed<sup>3</sup>; Nurul H. Osman<sup>4</sup> and Ali H. Reshak<sup>2,5,6</sup>

<sup>1</sup>Faculty of Electronic Engineering Technology, Universiti Malaysia Perlis (UniMAP), Perlis, Malaysia.

<sup>2</sup>Geopolymer & Green Technology, Centre of Excellence (CEGeoGTech), Universiti Malaysia Perlis (UniMAP), Perlis, Malaysia.

<sup>3</sup>Advance Medical and Dental Institute, Universiti Sains Malaysia, Bertam, Jln Tun Hamdan Sheikh Tahir, 13200 Kepala Batas, Pulau Pinang, Malaysia.

<sup>4</sup>Applied Electromagnetic Lab 1, Department of Physics, Faculty of Science, Universiti Putra Malaysia, 43400 Serdang, Selangor, Malaysia.

<sup>5</sup>Physics Department, College of Science, University of Basrah, Basrah, Iraq

<sup>6</sup>Department of Instrumentation and Control Engineering, Faculty of Mechanical Engineering, CTU in Prague, Technicka 4, Prague 6 166 07, Czech Republic

\*Corresponding Autor's Email: mmahyiddin@unimap.edu.my

**Abstract:** Breast cancer is one of the most reported cancers that can lead to death. Despite the advances in diagnosis and treatment procedures, the possibility of cancer recurrences is still high in many cases. In this study, the cell viability and electrical response of GO, in terms of resistivity and impedance towards the breast cancer cells (MCF7) and normal breast cells (MCF10a), were investigated by varying the pH and concentration of GO. Based on the results obtained, as the pH of GO increased from pH 5 to pH 7, the number of viable MCF7 cells decreased while the number of viable MCF10a slightly increased after the incubation period of 48 hours. Similarly, the MCF7 also experienced higher cytotoxicity effects when treated with GO concentrations of more than 25 µg/mL. The findings from the electrical characterization of the cells observed that the number of viable cells has corresponded to the impedance of the cells. The electrical impedance of MCF7 decreased as the number of highly insulating viable cell membranes decreased. But in contrast, the electrical impedance of MCF10a increased as the number of highly insulating viable cell membranes increased. Hence, it can be deduced that the GO with higher pH and concentration influence the MCF7 cancer cell line and MCF10a normal breast cell.

**Keywords:** Graphene oxide (GO), Breast cancer cells (MCF7), Interdigitated electrode (IDE), Impedance

### INTRODUCTION

The objective of this paper is to study the effect of graphene oxide (GO) towards breast cancer cell line namely MCF7, when treated with different pH for 24 and 48 hours. The effect of the treatment are then measured based on electrical response and cell viability. It is believed that the treatment of GO will suppress the MCF7 formation hence inhibit the MCF7 cells.

### MATERIALS AND METHODS

The GO was synthesized and characterized in Faculty of Electronic engineering and Technology, Universiti Malaysia Perlis (UniMAP). The breast cancer cell (MCF7) was obtained from Advanced Medical and Dental Institute (AMDI, Universiti Sains Malaysia, USM). The electrical

characterization is done using LCR meter (Agilent E4980 20 Hz – 2 MHz Precision LCR (Inductance, Capacitance, Resistance) meter, USA).

## RESULTS AND DISCUSSION

The obtained GO was first characterized by using the Raman spectroscopy, XRD spectroscopy, FESEM, EDX spectroscopy and Thermogravimetric analysis (TGA) to confirm the graphitic nature, crystal structure, morphology, composition of elements and decarboxylation process respectively. For this research, a few layers of GO, with an average size of 0.56 to 0.96  $\mu\text{m}$  and an average thickness of 1.24 to 1.32 nm, were successfully produced by using the Hummer's method. The cell viability for both the MCF7 and MCF10a before and after treatment with GO was successfully determined by using the PrestoBlue cell viability assay. After treating both the MCF7 and MCF10a cells with three different pH (e.g., pH 5, 6 and 7) and time, it can be deduced that the GO of pH 7 was the most suitable pH to inhibit the MCF7 proliferation compared to pH 5 and pH 6, with the optimum incubation period at 24 hours. For the electrical characterization part, the electrical properties of MCF7 and MCF10a cells before and after exposures to GO were successfully demonstrated by using 10  $\mu\text{m}$ -gaps gold interdigitated electrodes connected to the LCR meter. It was proven that the capacitance reduction was due to the increase in highly insulating MCF7 and MCF10a cells membrane. When dropped on the electrode surface, the highly insulated cells membrane caused an increase in electrical Zcell and resistance.

## CONCLUSIONS

In conclusion, the electrical characterization and cell viability analyses of breast cancer cells using the GO deposited on IDE were successful.

**ACKNOWLEDGMENT:** The authors would like to acknowledge the support from the Fundamental Research Grant (FRGS) under a grant number of FRGS/1/2017/STG04/UNIMAP/02/1 given by the Ministry of Higher Education, Malaysia.

## REFERENCES

- [1] Barahuie, F. et al. Graphene oxide as a nanocarrier for controlled release and targeted delivery of an anticancer active agent, chlorogenic acid. *Mater. Sci. Eng. C* 74, 177–185 (2017).
- [2] Perini, G., Palmieri, V., Ciasca, G., Spirito, M. De & Papi, M. Unravelling the Potential of Graphene Quantum Dots in Biomedicine and Neuroscience. (2020).
- [3] Zhang, B., Wei, P., Zhou, Z. & Wei, T. Interactions of graphene with mammalian cells: Molecular mechanisms and biomedical insights. *Advanced Drug Delivery Reviews* vol. 105 145–162 (2016).
- [4] Mazlan, N. S. et al. Interdigitated electrodes as impedance and capacitance biosensors: A review. *AIP Conf. Proc.* 1885, (2017).
- [5] Wang, K., He, M. Q., Zhai, F. H., He, R. H. & Yu, Y. L. A novel electrochemical biosensor based on polyadenine modified aptamer for label-free and ultrasensitive detection of human breast cancer cells. *Talanta* 166, 87–92 (2017).



## Development of a Microstrip Patch Antenna using Carbon based Charcoal for X-band Application

Zainab Yunusa<sup>1\*</sup>, Intan Hasan<sup>2</sup> and Muhammad Asnawi<sup>2</sup>

<sup>1</sup>Department of Electrical Engineering, Bayero University Kano, P.M.B 3011 Kano, Nigeria

<sup>2</sup>Institute of Advanced Technology, Universiti Putra Malaysia, 43400 UPM Serdang, Selangor, Malaysia

\*Corresponding Autor's Email: zee2yunusa@gmail.com

**Abstract:** In this paper, we report the characterization of carbon based charcoal and its potential application as a conductive patch material for microstrip patch antenna. The charcoal was obtained locally from prosopisafricana tree and then crushed and milled to obtain nanometer sized powders. The milled powders were then mixed to form a thick paste and then screen printed onto FR4 substrate. Characterization was carried out using FESEM, EDX, Raman Spectroscopy and Electrical conductivity. The fabricated antenna was then measured using Vector Network Analyzer and the antenna was found to resonate 8.60 GHz with S11 value of -14.73 dB which shows that it has potential application for X-band applications.

**Keywords:** Microstrip patch antenna, Prosopisafricana, X-band applications

### INTRODUCTION

Microstrip antennas have the advantages of being compact in size, low cost and conformal which makes them very attractive. The conductive patch element of the microstrip patch antenna is usually made up of metal conductors such as copper, silver, tantalum etc [1]. However, the disadvantage of using metal conductor is corrosion overtime. This factor made researchers to explore other materials with less corrosive property in such as nanomaterials as a suitable replacement of these metals. Different types of materials have been used as radiating patch, or substrate material such as, Graphene [2] and carbon nano tube (CNT) [3], ferrites [4] etc. as radiating patch instead of pure metals [3]. Therefore, it becomes interesting to investigate the potential application of using carbon charcoal from (prosopisafricana tree) as a conducting patch element of microstrip patch antenna.

### MATERIALS AND METHODS

The charcoal was milled into nanosize and characterized using FESEM, EDX, Raman, electrical and thermal conductivity. The antenna was fabricated using the carbon-based charcoal as the patch material as shown in Fig.1.

### RESULTS AND DISCUSSION

Characterization results using EDX showed that the charcoal contains 97.45% Carbon and 2.55% weight of the elements and the Raman spectroscopy result showed the two peaks of D and G band with an  $I_D$  to  $I_G$  ratio of 0.8. The antenna was fabricated using thick film technology on FR4 substrate. A vector network analyzer was used to measure the S11 parameters which was found to be -14.73 dB resonating at 8.6 GHz. The bandwidth of the antenna is calculated to be 1.8 GHz.

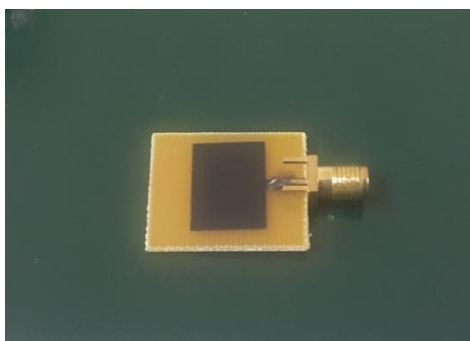


**Fig. 1.** Fabricated antenna using carbon based charcoal

## CONCLUSION

In this paper we report the development of carbon based microstrip patch antenna obtained from *prosopis Africana*. Results obtained showed that the antenna resonated at 8.6 GHz with a bandwidth of about 1.8 GHz and may have potential applications in X-band.

**ACKNOWLEDGMENT:** The authors would like to express appreciation for the support of the sponsors Bayero University Kano and Universiti Putra Malaysia.

## REFERENCES

- [1] Bansal, A., Gupta, R. A review on microstrip patch antenna and feeding techniques. *Int. j. inf. technol.* **12**, 149–154 (2020). <https://doi.org/10.1007/s41870-018-0121-4>
- [2] Shehu A.A. , Yunusa, Z., Hamidon, M. N Graphene Based Microstrip Patch Antenna for X Band Applications . of Innovative Journal Science and Engineering 2019 3(2): 57-65
- [3] V. Suryanarayana, M. Satya Anuradha and S. P. Douglas, "Bandwidth Enhancement of Multiwalled Carbon Nanotube Antenna Using Structural Modifications and DGS in X-Band Applications," *2021 International Conference on Computing, Communication, and Intelligent Systems (ICCCIS)*, 2021, pp. 792-797
- [4] I.H. Hasan, M.N. Hamidon, A. Ismail, I. Ismail, A.S. Mekki, M.A.M. Kusaimi, S. Azhari, R. Osman, YIG Thick Film as Substrate Overlay for Bandwidth Enhancement of Microstrip Patch Antenna, *IEEE Access*. (2018). doi:10.1109/ACCESS.2018.2842749.



## Kinetical Release Aspect of Naproxen Embedded on Boron-modified Carbon Nanodots as Multi-tasking Agent on Cancer Treatment

Dinar Fortuna Putri<sup>1</sup>, Aswandi Wibrianto<sup>1</sup> and Mochamad Zakki Fahmi<sup>1,2,\*</sup>

<sup>1</sup>Department of Chemistry, Universitas Airlangga, Surabaya 61115, Indonesia

<sup>2</sup>Supramodification Nano-Micro Engineering Research Group, Universitas Airlangga, Surabaya 60115, Indonesia

\*Corresponding Autor's Email: m.zakki.fahmi@fst.unair.ac.id

**Abstract:** The present study aim to synthesize boron doped carbon nanodots via hydrothermal method and further improved by varying the concentration of boron source. Naproxen drug is intentionally added on the nanomaterial to emerge a potency dual-purpose on both bioimaging agent and naproxen delivery. Several characterizations such XRD, FTIR and XPS analyses confirm well the nanomaterial design. Further UV-vis and photoluminescence observation showed excellent optical properties of the carbon dots with a quantum yield of 52.29%. A confocal micrograph and toxicity test of the carbon nanodots delivered naproxen efficiently with loading amount and loading efficiency of naproxen 28% and 65%, respectively.

**Keywords:** carbon nanodots, boron, naproxen, kinetical release

### INTRODUCTION

Carbon dots (CDs) can be a versatile material for future biomedical and bioimaging applications with unique fluorescence properties[1], excellent biocompatibility, and high water solubility [2]. Besides acting as a bioimaging agent, CDs can function as a drug delivery carrier, a substance used in the process of delivering chemical compounds or drugs to achieve targets or therapeutic effects in humans [3]. The fabrication procedure of doped-CDS is quite simple and low-cost due to the wide choice of cheap carbon sources. Moreover, boron doping on CDs progressively increasing the quantum yield of CDS owing to the p-type semiconductor effect, which comes from the boron elements. According to previous research, Boron-Carbon nanodots are not widely used in the field of bioimaging, but rather are applied in the detection of metal ions by the colorimetric method [4], detections of p-nitrophenol [5], dopamine examination [6], and sensors for acetone and dopamine [7]. Therefore, this research will report the results of synthesis and characterization of CDs nanoparticles doped with Boron atoms for bioimaging agents and naproxen delivery systems in HeLa cancer cells.

### MATERIALS AND METHODS

The synthesis of boron-carbon nanodots (BCD) begins with mixing citric acid and boric acid with variations in the concentration ratio of boric acid are citric acid. The mixture is inserted into Teflon autoclave and put into furnace for 4 h at 240 °C. The products were then dissolved with NaOH 0.1 N after the cooling process at room temperature. The solution then was further dialyzed on the membrane with a molecular weight cut-off (MWCO) of 1 kDa to specify the CDs size distribution and exclude by-products [8].

### RESULTS AND DISCUSSION

The hydrothermal method fundamentally is based on heating treatment, leads to the carbonization process at high temperatures (as showed on Figure 1). This process generates a rearrangement of the carbon structure of the citric acid and doping agent to form a graphene-like structure. Furthermore, a simple step for BCD synthesis was carried out by comparing the visual solution with visible light and under UV light. The fluorescence phenomenon's existence due to material emission originating from electron transitions in atomic orbitals indicates the formation of BCD themselves [9]. All of obtained BCDs perform good result on its structure and optical properties with naproxen release follow Korsmeyer-Peppas kinetical order.

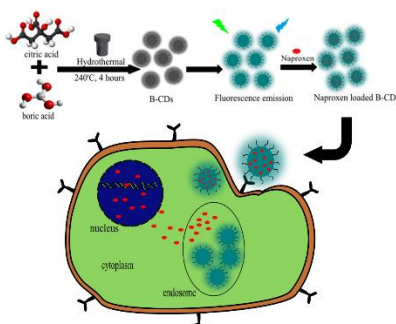


**Fig. 1** Synthesis route of BCD and N-BCD for inducing into HeLa cancer cell.

## CONCLUSIONS

Boron-carbon nanodots were successfully synthesized from citric acid using the hydrothermal method. From the results of confocal and toxicity tests, Boron-carbon nanodots have proven potential as candidates for bioimaging agents and naproxen delivery systems in HeLa cancer cells.

## REFERENCES

- [1] D. K. Dang, C. Sundaram, Y.-L. T. Ngo, J. S. Chung, E. J. Kim and S. H. Hur, *Sensors and Actuators B: Chemical*, 2018, **255**, 3284-3291.
- [2] Y. Z. Yang, N. Xiao, S. G. Liu, L. Han, N. B. Li and H. Q. Luo, *Materials Science and Engineering: C*, 2020, **108**, 110401.
- [3] G. Tiwari, R. Tiwari, B. Sriwastawa, L. Bhati, S. Pandey, P. Pandey and S. K. Bannerjee, *Int J Pharm Investig*, 2012, **2**, 2-11.
- [4] Y. Liu, W. Duan, W. Song, J. Liu, C. Ren, J. Wu, D. Liu and H. Chen, *ACS applied materials & interfaces*, 2017, **9**, 12663-12672.
- [5] N. Xiao, S. G. Liu, S. Mo, N. Li, Y. J. Ju, Y. Ling, N. B. Li and H. Q. Luo, *Talanta*, 2018, **184**, 184-192.
- [6] T. Tian, Y. He, Y. Ge and G. Song, *Sensors and Actuators B: Chemical*, 2017, **240**, 1265-1271.
- [7] Y. Liu, W. Li, P. Wu, C. Ma, X. Wu, M. Xu, S. Luo, Z. Xu and S. Liu, *Sensors and Actuators B: Chemical*, 2019, **281**, 34-43.
- [8] A. Wibrianto, S. Q. Khairunisa, S. C. Sakti, Y. L. Ni'mah, B. Purwanto and M. Z. Fahmi, *RSC Advances*, 2021, **11**, 1098-1108.
- [9] W. Li, W. Zhou, Z. Zhou, H. Zhang, X. Zhang, J. Zhuang, Y. Liu, B. Lei and C. Hu, *Angewandte Chemie*, 2019, **131**, 7356-7361.

## Doped and Un-doped Maghemite Nanoparticles for Magnetic Hyperthermia Application

O. M. Lemine<sup>1\*</sup>, Ibtessam Alotaibi<sup>1</sup>, Anfal Aldawood<sup>1</sup>, Saja Algessair<sup>1</sup>, N. Madkhali<sup>1</sup> and L. El Mir<sup>2</sup>

<sup>1</sup>Department of Physics, College of Sciences, Imam Mohammad Ibn Saud Islamic University (IMISU), Riyadh 11623, Saudi Arabia.

<sup>2</sup>Laboratory of Physics of Materials and Nanomaterials Applied at Environment (LaPhysMNE), Faculty of Sciences of Gabes, University of Gabes, Gabes 6072, Tunisia

\*Corresponding Author's Email: mamamin@imamu.edu.sa

**Abstract:** The heating efficiencies of  $\gamma$ -Fe<sub>2</sub>O<sub>3</sub>, (Gd, Co) doped  $\gamma$ -Fe<sub>2</sub>O<sub>3</sub> and hybrid  $\gamma$ -Fe<sub>2</sub>O<sub>3</sub>-TiO<sub>2</sub> NPs under an alternating magnetic field (AMF) have been investigated to evaluate their feasible use in magnetic hyperthermia. The NPs were synthesized by a modified sol-gel method and characterized by different techniques. Heating efficiency under an AC alternating magnetic field measurements showed that doped and un-doped samples display high heating ability and reached magnetic hyperthermia (42 °C) in relatively short times. The specific absorption rate (SAR) values calculated for  $\gamma$ -Fe<sub>2</sub>O<sub>3</sub> (up to 90 W/g) are higher than that obtained for  $\gamma$ -Fe<sub>2</sub>O<sub>3</sub>-TiO<sub>2</sub> (~ 40 W/g) and Gd (5%) (~50 W/g). The obtained high heating efficiencies suggest that the fabricated nanocomposites hold a great potential to be utilized in magnetic photothermal hyperthermia treatments.

**Keywords:** Magnetic hyperthermia, maghemite, iron oxides.

### INTRODUCTION

Magnetic fluid hyperthermia (MFH) is a cancer treatment method using the heat dissipated by magnetic NPs under an alternating magnetic field to kill the cancerous cells [1]. Magnetic iron oxides nanoparticles (NPs) are promising materials for MFH application. Among the iron oxides nanoparticles, maghemite ( $\gamma$ -Fe<sub>2</sub>O<sub>3</sub>) has advantage of relatively high saturation magnetization and it converts to hematite phase ( $\alpha$ -Fe<sub>2</sub>O<sub>3</sub>) at very high temperatures compared to magnetite (Fe<sub>3</sub>O<sub>4</sub>). Our previous works showed that heating and magnetism of  $\gamma$ -Fe<sub>2</sub>O<sub>3</sub> nanoparticles can be tuned by changing the size of nanoparticles [2]. Using alkaline earth and transition metal as dopants of NPs could be used also to tune the magnetic properties of NPs such as coercivity (H<sub>c</sub>), saturation (M<sub>s</sub>), Curie temperature and, subsequently the heating of the nanoparticles. We report a simple process using modified sol-gel strategy to synthesize maghemite and doped maghemite nanocomposites. We tested whether the presence of Gd, Co and TiO<sub>2</sub> affect magnetic properties and induce any effects on heating abilities.

### MATERIALS AND METHODS

The NPs were synthesized by a modified sol-gel method and characterized by different techniques. The structural properties are performed by X-ray diffraction (XRD), energy-dispersive X-ray spectrometer (EDAX) and X-ray Photoelectron Spectroscopy (XPS), while the

morphology is investigated by Transmission electron microscopy (TEM) and magnetic properties by SQUID.

## RESULTS AND DISCUSSION

X-ray diffraction points out that the doped and un-doped samples are mainly composed of maghemite phase ( $\gamma$ -Fe<sub>2</sub>O<sub>3</sub>). Magnetic characterization showed that doping induces increasing of saturation, while coercivity and field remain negligible, indicating superparamagnetic behavior [3,4]. The heating efficiency of the obtained nanoparticles was studied under an alternating magnetic field and as a function of concentration, frequency and amplitude of the applied magnetic field. The dependence of specific absorption rate (SAR) with concentration of Gd, Co and TiO<sub>2</sub>, field amplitude and frequency is analyzed in terms of structure and magnetic properties. Our results show that the ILP and SAR values differ slightly between the doped and un-doped samples but both have high heating efficiency and reach magnetic hyperthermia temperature (42°C) in relatively short times. As an example, figure 1 shows the the increase in temperature and SAR values for  $\gamma$ -Fe<sub>2</sub>O<sub>3</sub> and  $\gamma$ -Fe<sub>2</sub>O<sub>3</sub>-TiO<sub>2</sub> nanoparticles for H<sub>0</sub> =170 Oe and f = 332.5 kHz .



**Fig. 1.** . Temperature increases at H<sub>0</sub>=170 Oe and f =332.8 kHz and SAR values as function of concentration.

## CONCLUSIONS

Modified sol-gel method was employed to synthesize doped and un-doped  $\gamma$ -Fe<sub>2</sub>O<sub>3</sub> nanoparticles with small sizes and good uniformity for magnetic hyperthermia applications. The high crystallinity, superparamagnetic behaviors and good SAR values make these NPs promising candidates for hyperthermia application.

## REFERENCES

- [1] A. Jordan, P. Wust, H. Föhling, W. John, A. Hinz, R. Felix Int. J. Hyperth. Off. J. Eur. Soc. Hyperthermic Oncol. North Am. Hyperth. Gr. 9 (1993) 51–68.
- [2] O.M. Lemine, K. Omri , L. El Mir , M Iglesias, V Velasco, P Crespo, P de la Presa, Houcine Bouzid, Ali A. Yousif and A. Hajry, Journal of Alloys and Compounds 607 (2014) 125–131
- [3] Ibtesam Alotaibi, M. Alshammari, Saja Algessair, N. Madkhali, N. AbdelAll, M. Hjiri, Sharif AbuAlrub, L. El Mir and O.M. Lemine, Physica B (2021), 14,5691.
- [4] O. M. Lemine, Nawal Madkhali , Marzook Alshammari , Saja Algessair, Abbasher Gismelseed , Lassad El Mir , Moktar Hjiri, Ali A. Yousif and Kheireddine El-Boubbou , Materials (2021), 14,5691.

## Serine/Graphene Oxide modified Electrode for Electrochemical Determination of Uric acid

Pattanan Oungkanitanon<sup>1</sup>, Sarawut Cheunkar<sup>2</sup>, Watchara Liewwrian<sup>1,3</sup> and Piyapong Asanithi<sup>1,3\*</sup>

<sup>1</sup>Department of Physics, Faculty of Science, King Mongkut's University of Technology Thonburi, Bangkok 10140

<sup>2</sup>School of Bioresources and Technology, King Mongkut's University of Technology Thonburi, Bangkok 10140

<sup>3</sup>ThEP Center, Commission of Higher Education, 328 Si Ayuthaya Rd.

\*E-mail: piyapong.asa@mail.kmutt.ac.th

**Abstract:** In this study, serine/graphene-oxide (SER/GO) modified electrode was used for determination of uric acid (UA) in the interference of ascorbic acid (AA) and dopamine (DA) using differential pulse voltammetry (DPV). In general, the DPV potential peaks of UA, AA and DA are overlapped to form single peak and difficult to separate them into three peaks [1]. Here, we showed that serine/graphene-oxide (SER/GO) modified electrode was able to overcome this limitation. SER/GO-modified screen-printed electrode (SER/GO SPE) was prepared by coating GO on the working electrode of SPE and then SER was electrochemically deposited on GO-modified SPE via cyclic voltammetry (- 1V to 1V, for 10 cycles). The modified electrode was characterized by FTIR, SEM and contact angle measurement. The selectivity and sensitivity of the SER/GO SPE for determining UA in the interference of AA and DA was studied. The DPV results showed that SER/GO SPE was able to separate the oxidation peak potentials of AA, DA and UA into three well-defined peaks at -15 mV, 210 mV and 370 mV, respectively. The calibration curve of UA detection in the interference of AA (5 mM) and DA (50  $\mu$ M) was in the range of 5  $\mu$ M – 90  $\mu$ M and the limit of detection (LOD) was 3.87  $\mu$ M.

**Keywords:** Electrochemistry, Graphene oxide, Serine, Sensor, Uric acid

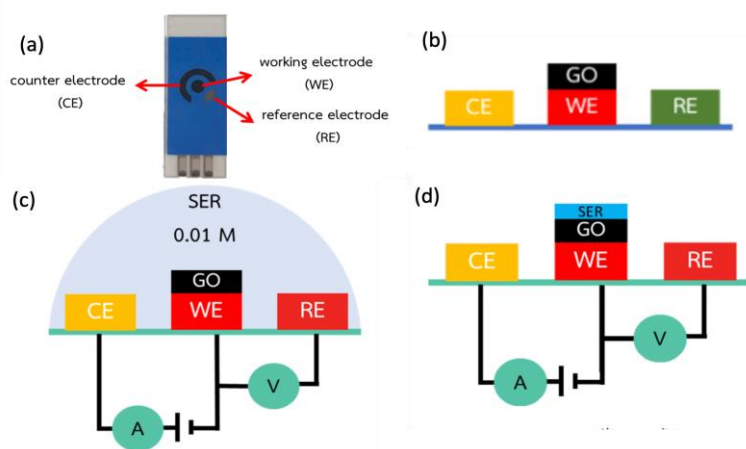


**Fig. 1** (a) Screen-printed electrode, (b) GO deposition on working electrode, (c) Electrochemical deposition of SER on GO-modified SPE, (d) SER/GO SPE for determination of UA.



**ACKNOWLEDGMENT:** We would like to thank the Scholarship from Faculty of Science, KMUTT for supporting P. Oungkanitanon for M.Sc. study and the National Research Council of Thailand (NRCT) for supporting with research fund.

## **REFERENCE**

[1] Ensafi A A, Taei M, Khayamian T and Arabzadeh A 2010 Highly selective determination of ascorbic acid, dopamine, and uric acid by differential pulse voltammetry using poly (sulfonazo III) modified glassy carbon electrode Sens. Actuator B-Chem. 147(1) 213–21



## Niobium MXenes for Electrochemical Sensing Applications

P Abdul Rasheed\*

*Department of Biological Sciences and Engineering, Indian Institute of Technology Palakkad, Palakkad 678 557,  
Kerala, India*

*\*Corresponding Author's Email: [abdulrasheed@iitpkd.ac.in](mailto:abdulrasheed@iitpkd.ac.in)*

**Abstract :** Recently, 2D MXenes have been used as an ideal material for electrochemical sensing applications owing to their distinctive properties such as excellent electrical conductivity and hydrophilicity [1]. Recently, niobium-based MXenes such as Nb<sub>2</sub>CT<sub>x</sub> and Nb<sub>4</sub>C<sub>3</sub>T<sub>x</sub> have emerged as attractive materials for various applications due to their unique properties and potential applications. The Nb<sub>2</sub>CT<sub>x</sub> and Nb<sub>4</sub>C<sub>3</sub>T<sub>x</sub> are prepared by acid etching of their MAX phases Nb<sub>2</sub>AlC and Nb<sub>4</sub>AlC<sub>3</sub>, respectively [2]. We have found that Nb<sub>4</sub>C<sub>3</sub>T<sub>x</sub> is having higher electrochemical activity than Nb<sub>2</sub>CT<sub>x</sub> and the higher electrochemical activity of Nb<sub>4</sub>C<sub>3</sub>T<sub>x</sub> can be attributed to the higher n' value of Nb<sub>4</sub>C<sub>3</sub>T<sub>x</sub> (n=3) compared to Nb<sub>2</sub>CT<sub>x</sub> where n=1 [3].

**Keywords:** MXene, Niobium, Electrochemical sensors, sensitivity.

### INTRODUCTION

By utilizing this high electrochemical activity of Nb<sub>4</sub>C<sub>3</sub>T<sub>x</sub>, we have introduced Nb<sub>4</sub>C<sub>3</sub>T<sub>x</sub> for sensitive electrochemical detection of Pb<sup>2+</sup> in the cathodic potential on glassy carbon electrode based on anodic stripping voltammetry analysis [4]. This developed sensor exhibited a detection limit of 12 nM with promising stability. To enhance the selectivity of electrochemical detection of Pb<sup>2+</sup>, lead-binding DNA oligonucleotide as a molecular recognition element has been introduced which binds to Au nanoparticles/Nb<sub>4</sub>C<sub>3</sub>T<sub>x</sub> MXene (Au@Nb<sub>4</sub>C<sub>3</sub>T<sub>x</sub>) modified glassy carbon electrode. The Au@Nb<sub>4</sub>C<sub>3</sub>T<sub>x</sub> nanocomposite was synthesized by *in situ* reduction method which results in pseudo-spherical gold nanoparticles (AuNPs) with 10–40 nm size distributions on the surface of Nb<sub>4</sub>C<sub>3</sub>T<sub>x</sub> nanosheets. Here, the direct quantification of Pb<sup>2+</sup> with ultrahigh selectivity is possible by utilizing the selective binding property of Pb<sup>2+</sup> with G-rich sequences which results in the formation of G-quadruplex structures [5]. The lead-binding DNA is modified with thiol groups to allow the self-assembly of s-DNA on Au@Nb<sub>4</sub>C<sub>3</sub>T<sub>x</sub> surface through Au-S bond. The detection method does not consist of any electrochemical deposition step compared to the anodic stripping analysis usually used for the detection of heavy metal ions. The direct detection of Pb<sup>2+</sup> can be done by using differential pulse voltammetry analysis after incubating the electrode in the analyte solution. The developed DNA-Au@Nb<sub>4</sub>C<sub>3</sub>T<sub>x</sub> sensor has reached a detection limit of 4 nM with a linear range of 10 nM to 5 μM along with high selectivity and stability. To investigate the electrochemical behavior of the Nb MXenes in the anodic potential window, cyclic voltammetry analysis was conducted in the potential range of 0 to 1.0 V in phosphate buffer. The anodic oxidation was observed for both Nb<sub>2</sub>CT<sub>x</sub> and Nb<sub>4</sub>C<sub>3</sub>T<sub>x</sub> with onset potential around +0.5 V. However, the peak current is higher for Nb<sub>4</sub>C<sub>3</sub>T<sub>x</sub> and it can be attributed to its higher electron transfer kinetics than Nb<sub>2</sub>CT<sub>x</sub> [6]. This shows that the partial oxidation of Nb<sub>2</sub>CT<sub>x</sub> and Nb<sub>4</sub>C<sub>3</sub>T<sub>x</sub> occurs during the anodic scan above +0.5V. This oxidation behavior of both Nb MXenes is



entirely different from  $Ti_3C_2T_x$ , where irreversible oxidation of  $Ti_3C_2T_x$  occurred upon exposure to an anodic potential around 0.43V [7]. Since the oxidation onset potential for both Nb MXenes starts at +0.5 V, another cyclic voltammogram was run below the onset potential +0.5V to evaluate the stability below the onset potential. The results showed that there is a negligible current difference after multiple scans which shows that  $Nb_2CT_x$  and  $Nb_4C_3T_x$  are electrochemically stable up to a potential of 0.5V [3]. By utilizing this electrochemical stability, we have used  $Nb_4C_3T_x$  for sensing of small biomolecules such as dopamine which is having the oxidation peak in the anodic potential window. The detailed electrochemical analysis showed that  $Nb_4C_3T_x$  can be used as an immobilization platform for sensitive detection of DA with wide linear range and detection limit of 23 nM [3]. These works demonstrate the high potential of  $Nb_4C_3T_x$  towards the development of different electrochemical sensors and potential of  $Nb_4C_3T_x$  as an efficient immobilization platform for DNA oligonucleotides for various biomedical and sensing applications.

## REFERENCE

- [1] Rasheed, P. A.; Pandey, R. P.; Rasool, K.; Mahmoud, K. A. *Sensors and Actuators B: Chemical* **2018**, 265, 652.
- [2] Zhao, S.; Meng, X.; Zhu, K.; Du, F.; Chen, G.; Wei, Y.; Gogotsi, Y.; Gao, Y. *Energy Storage Materials* **2017**, 8, 42.
- [3] Abdul Rasheed, P.; Pandey, R. P.; Gomez, T.; Jabbar, K. A.; Prenger, K.; Naguib, M.; Aïssa, B.; Mahmoud, K. A. *Electrochemistry Communications* **2020**, 119, 106811.
- [4] Rasheed, P. A.; Pandey, R. P.; Gomez, T.; Naguib, M.; Mahmoud, K. A. *RSC Advances* **2020**, 10, 24697.
- [5] Yu, S. H.; Lee, C.-S.; Kim, T. H. *Nanomaterials* **2019**, 9, 817.
- [6] Nayak, P.; Jiang, Q.; Mohanraman, R.; Anjum, D.; Hedhili, M. N.; Alshareef, H. N. *Nanoscale* **2018**, 10, 17030.
- [7] Lorencova, L.; Bertok, T.; Dosekova, E.; Holazova, A.; Paprckova, D.; Vikartovska, A.; Sasinkova, V.; Filip, J.; Kasak, P.; Jerigova, M.; Velic, D.; Mahmoud, K. A.; Tkac, J. *Electrochimica Acta* **2017**, 235, 471.

## Versatile Graphene for a Myriad of Applications

Lim Hong Ngee<sup>1\*</sup>, Izwaharyanie Ibrahim<sup>2</sup>

<sup>1</sup>Department of Chemistry, Faculty of Science, Universiti Putra Malaysia, 43400 UPM Serdang, Selangor Darul Ehsan, Malaysia.

<sup>2</sup>Functional Nanotechnology Devices Laboratory (FNDL), Institute of Nanoscience and Nanotechnology, Universiti Putra Malaysia, 43400 UPM Serdang, Selangor, Malaysia

\*Corresponding Autor's Email: hongngee@upm.edu.my

**Abstract:** Graphene is a true wonder material and has the potential to generate disruptive technologies. To harness the exceptional physical properties of graphite often require its dispersion into aqueous or organic media. Herein, we reported the first work on graphene where a nickel-metal-organic framework/graphene oxide/graphene nanoplatelets electrode was prepared and assembled in a symmetrical coin cell and pouch cell. The construction offered superior capacitive properties that may overcome the drawbacks of poor electrical conductivity and stability of pristine metal-organic framework, as attested by the capacity retention of more than 80% after more than 20,000 cycles. In the second work, graphene, when combined with cadmium sulphide nanorods and gold nanoparticles, was able to increase the photocurrent of a sensor, making it more sensitive and selective to heavy metal copper detection. In the third work, graphene was employed as a scaffold for targeted drug delivery application. Graphene was decorated with magnetite nanoparticles to guide the drugs, quercetin, to a specific site of interest using a guided external magnetic field.

**Keywords:** Graphene, Supercapacitor, Photoelectrochemical Sensor, Drug Delivery.

### INTRODUCTION

The difficulties in processing graphene, in particular, graphene's poor colloidal stability in most common solvents has become a great challenge for commercial development of the graphene-based product [1]. Herein, we highlight a simple, nondestructive method for preparing a water-dispersible graphene powder, coined as Versatile Graphene which is quickly dispersed in any solvent by bath sonication. In this work, the as-produced Versatile Graphene was employed in three different applications. The first work, Ni-MOF/GO/GNP electrode material synthesized via a combination of in-situ method and microwave-assisted synthesis was utilized as a supercapacitor electrode material. Next, the second work, CdS NRs/Au QDs with modified graphene has successfully been designed for superior environmental monitoring devices based on the photoelectrochemical (PEC) detection of  $\text{Cu}^{2+}$ . Lastly, rGO-Fe<sub>3</sub>O<sub>4</sub> nanocomposite was synthesized to be used as a drug carrier targeted for lung cancer treatment that can be controlled by external magnetic field in order to enhance the specificity of the delivery system.

### MATERIALS AND METHODS

Ni-MOF/GO/GNP, CdS NRs/Au QDs/graphene QDs and rGO-Fe<sub>3</sub>O<sub>4</sub> were synthesized via microwave-assisted synthesis, reflux and *in-situ* approach, respectively.

## RESULTS AND DISCUSSION

The long cycling performance of the Ni-MOF/GO/GNP supercapacitor electrode was evaluated as a coin cell at a current density of 1 A/g, as shown in Figure 1A. The supercapacitor of Ni-MOF/GO/GNP electrode retained up to 85.6% of its original capacitance after 20,000 cycles at 1 A/g with an average specific capacitance of 80.55 F/g. As depicted in Figure 1B, the photocurrent intensity decreased upon an increase in the concentration of  $\text{Cu}^{2+}$  ions for CdS/Au/graphene QD photoelectrode. The standard calibration curve for  $\text{Cu}^{2+}$  detection showed a good correlation coefficient of 0.9998 with detection limit (LoD) of 2.27 nM. The as-synthesized rGO- $\text{Fe}_3\text{O}_4$ -GL-PF shows slightly lower LE and LC of quercetin compared to previous report, the current nanocomposite possesses an excellent superparamagnetic property, which can be controlled via external magnetic field for targeting purpose (Figure 1C).

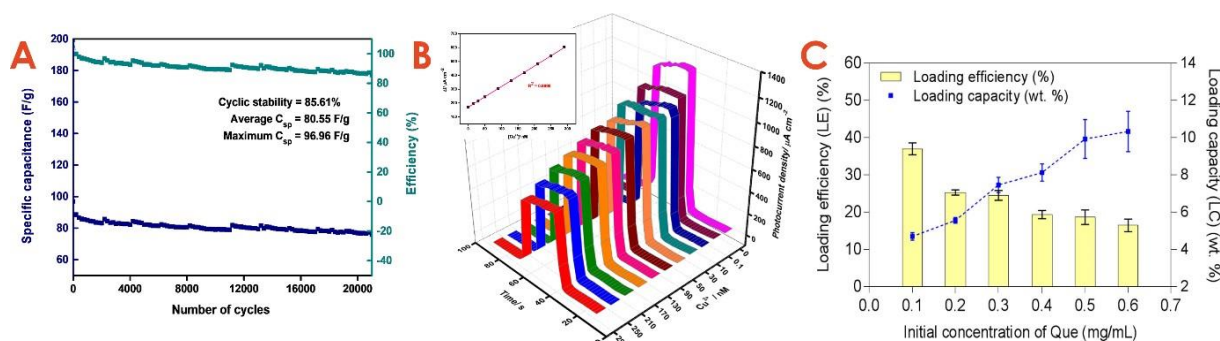


**Fig. 1-** (A) Cyclic stability of coin-cell Ni-MOF/GO/GNP supercapacitor. (B) Photocurrent vs. time of CdS/Au/graphene QDs photoelectrode for consecutive additions of  $\text{Cu}^{2+}$  in concentrations of 0.1–290 nM at 0 V vs. Ag/AgCl. Inset of calibration curve between  $\Delta I$  and  $[\text{Cu}^{2+}]$ . (C) The LE and LC of Que on rGO- $\text{Fe}_3\text{O}_4$ -GL-PF. Reproduce from ref.[2-4].

## CONCLUSIONS

In conclusion, we have highlighted the use of the Versatile Graphene for a myriad of applications such as supercapacitor, photoelectrochemical sensor and drug delivery. The remarkable higher specific capacitance, lower limit of detection and cytotoxicity was depicted for the nanocomposite materials in the presence of the novel and eco-friendly Versatile Graphene products.

## REFERENCES

- [1] Mohan, V. B.; Lau, K. T.; Hui, D.; Bhattacharyya, D. *Composites Part B: Engineering* **2018**, 142, 200-220.
- [2] Ibrahim, I.; Zheng, S.; Foo, C.; Huang, N.; Lim, H. *Journal of Energy Storage* **2021**, 43, 103304.
- [3] Ibrahim, I.; Lim, H. N.; Huang, N. M.; Jiang, Z.-T.; Altarawneh, M. *Journal of hazardous materials* **2020**, 391, 122248.
- [4] Lee, X. J.; Lim, H. N.; Gowthaman, N.; Rahman, M. B. A.; Abdullah, C. A. C.; Muthoosamy, K. *Appl. Surf. Sci.* **2020**, 512, 145738.

## Preparation and Sensing Characterization of Hybrid Iron Oxide-Reduced Graphene Oxide at Room Temperature

Nurul Athirah Abu Hussein<sup>1</sup>, Huzein Fahmi Hawari<sup>1\*</sup>

<sup>1</sup>Department of Electrical and Electronics Engineering, Universiti Teknologi PETRONAS, 32610 Seri Iskandar, Perak, Malaysia

\*Corresponding Autor's Email: huzeinfahmi.hawari@utp.edu.my

**Abstract:** This research looked into a 10MHz quartz crystal microbalance (QCM) sensor based on reduced graphene oxide (RGO) and Iron Oxide which was deposited on it and the sensing mechanism towards 100ppm acetone and ethanol was investigated. The hybrid materials were created through the process of synthesis using in-situ method and deposited on the QCM using a drop cast method. The response and recovery time for the hybrid materials towards 100ppm acetone and 100ppm ethanol were 13s/39s and 25s/22s, respectively. The hybrid material-based QCM sensor is extremely sensitive and reversible, making it suitable for human health and environmental safety applications.

**Keywords:** Quartz crystal microbalance (QCM), Hybrid materials, Volatile Organic Compound (VOC), Sensing Application

### INTRODUCTION

In recent years, there have been further advancement in the comprehension of metal oxide that can be exploited for gas sensing application and new material hybridization have been recognized that may improve the sensor performance such as lowering the operating temperature of Metal Oxide Semiconductor (MOX) sensor [1, 2]. Carbon Nanotubes and graphene stand out among the carbon-based materials due to their high carrier mobility, high quality crystal lattices, and low electrical noise. Carbon nanomaterials can therefore be synthesised by functionalizing or combining them with other materials to create hybrid platforms with improved sensing capability, for the detection of volatile organic compound (VOC) [3]. As a result, in this study, we will functionalize graphene with metal oxide nanomaterial to open a large energy gap in graphene via the quantum confinement effect in order to increase sensor performance.

### MATERIALS AND METHODS

#### A. Materials and Experimental Procedure

Iron (II) Chloride Tetrahydrate ( $\text{FeCl}_2 \cdot 4\text{H}_2\text{O}$ ), Iron (III) Chloride Hexahydrate ( $\text{FeCl}_3 \cdot 6\text{H}_2\text{O}$ ), Iron (III) Nitrate ( $\text{Fe}(\text{NO}_3)_3 \cdot 9\text{H}_2\text{O}$ ), Nitric acid (65%), Hydrochloric acid (37%), Ascorbic Acid and Graphene oxide (GO) paste (95 wt% purity) was purchased from Merck. Iron Oxide is synthesized using Massart's procedure as stated in previous study [4]. The RGO was also prepared according to the previous study [5]. The hybrid nanomaterials was prepared by in-situ method where the Iron Oxide was added into the GO paste solution for a better homogeneity.

## RESULTS AND DISCUSSION

The results of the sensor's response are given in frequency shift  $\Delta f$ , which may be calculated using  $\Delta f = (f_{air} - f_{gas})$ , where  $f_{air}$  and  $f_{gas}$  are the frequencies of QCM at air flow and gas flow (acetone and ethanol vapor) conditions, respectively [6]. The response of the as-prepared QCM sensor was 3749 Hz and 4397 Hz for 100 ppm acetone and ethanol respectively. The interaction between the vapor molecules and the hybrid materials resulted in changes on the absorbate mass on the QCM electrode's surface. Thus, changes in the frequency shift are obtained. Four similar cycles were obtained for both acetone and ethanol vapor sensing. This shows that the as-prepared sensor has strong reversibility and reproducibility. The response and recovery time obtained for 100ppm acetone was 13s and 39s respectively while for 100ppm ethanol, the response and recovery time was 25s and 22s respectively. For 100ppm acetone, the response time was faster compared to the response time for 100ppm ethanol. Because the van der Waals bonds are intrinsically weak, the absorbate desorbs readily when exposed to air. Such molecular desorption shows that the sensing device has recovered well.

## CONCLUSIONS

The as-synthesized hybrid Iron Oxide-RGO materials have successfully lowered down the working temperature of the conventional MOX sensor. The response and recovery time for both 100ppm acetone and 100ppm ethanol are 13s/39s and 25s/22s respectively. This shows that the hybrid materials have great synergistic effect. However, further studies need to be done in order to further investigate the physical and chemical analysis of the hybrid materials.

**ACKNOWLEDGMENT:** The authors would like to express appreciation for the support of the sponsors [Project Code = FRGS/1/2019/TK04/ UTP/02/7].

## REFERENCES

- [1] Zhang C, Luo Y, Xu J, Debliquy M. *Sensors and Actuators A: Physical*, 2019, **289**.
- [2] Li Z, Li H, Wu Z, Wang M, Luo J, Torun H, Hu PA, Yang C, Grundmann M, Liu X, Fu YQ. *Materials Horizons*, 2019, **6**, 3.
- [3] Andre RS, Sanfelice RC, Pavinatto A, Mattoso LHC, Correa DS. *Materials & Design*, 2018, **156**.
- [4] Athirah NAH, Ang BC, Wong YH, Ong BH, Aqilah AB. *Materials Research Express*, 2018, **5**, 6.
- [5] Gupta M, Athirah N, Fahmi Hawari H. *Indonesian Journal of Electrical Engineering and Computer Science*, 2020, **18**, 3.
- [6] Huang X, Bai Q, Hu J, Hou D. *Sensors*, 2017, **17**, 8.



## Biogenic Reduced Graphene Oxide and its Cytotoxicity Evaluation

Dharshini Perumal<sup>1</sup>, Emmellie Laura Albert<sup>2</sup>, Muhammad Amir Faiz<sup>3</sup>, and Che Azurahaman  
Che Abdullah<sup>1, 2, 3\*</sup>

<sup>1</sup>Biophysics Laboratory, Department of Physics, Faculty of Science, Universiti Putra Malaysia, 43400 UPM  
Serdang, Selangor, Malaysia

<sup>2</sup>Nano Synthesis and Characterization Laboratory, Institute of Nanoscience and Nanotechnology, Universiti  
Putra Malaysia, 43400 UPM Serdang, Selangor, Malaysia

<sup>3</sup>UPM MAKNA Cancer Research Laboratory, Institute of Bioscience, Universiti Putra Malaysia, 43400 UPM  
Serdang, Selangor, Malaysia

\*Corresponding Author's Email: azurahaman@upm.edu.my

**Abstract:** Green nanotechnology is blooming in various sectors. We employed fabrication of green reduced graphene oxide (rGO) using the leaf extract of *Elaeis guineensis* and investigated the toxicity of the graphene oxide (GO) and rGO using brine shrimp assay. The rGO synthesis was conducted by adding leaf extract to the GO suspension and refluxed. The synthesized rGO were characterized using various analytical techniques and its toxicity effect was performed on marine model. The characterizations result revealed that we successfully synthesized green rGO. Brine shrimp assay-based toxicity shows that rGO is less toxic and biocompatible compared to GO.

**Keywords:** Green, Graphene oxide, Reduced graphene oxide, Toxicity, Brine shrimp

### INTRODUCTION

Graphene is the thinnest and lightest material with prominent properties. This offers an enormous potential for application in various sectors. The synthesis of high-quality graphene in an eco-friendly manner remains a major challenge. Green technology opens new windows in the synthesis of green graphene oxide (GO) reduction using plant extracts [1]. Plant extracts are readily available, renewable, economical and environmentally friendly in nature. The present study focuses on the synthesis of rGO using extracts from leaves of *Elaeis guineensis* and evaluate the toxicity effect using brine shrimp assay on marine model organism, *Artemia salina*. Brine shrimp assay was used as it is a rapid process, requires relatively small amount of sample and inexpensive. Herein we present the data on structural and optical properties as well as toxicity evaluation. Based on the characterization data by XRD, and TEM revealed that we successfully synthesized green rGO and the toxicity effect on *A. salina* shows that synthesized rGO is dose- dependent. The potential application of the prepared rGO will be on biomedical applications.

### MATERIALS AND METHODS

The graphene oxide (GO) was prepared by slight modification of Improved Hummers method [2]. For the synthesis of rGO, plant extracts were mixed with the GO solution and refluxed under oil bath. After the completion of the reaction process, the deoxygenation of GO was observed by a visual color changing from brown to black. Prepared samples were characterized by means

of XRD and TEM. To study the effect of the samples on the hatchability of the cysts, seven different concentrations of the sample solution were prepared. Generally, the cysts were hatched in 96-well plates, and each well were added with 200 $\mu$ L of sample solution. Ten cysts were added into each well, and three wells were used for each concentration. All plates were incubated at room temperature under a continuous illumination. The hatchability of the cysts in each concentration was detected using a microscope [3].

## RESULTS AND DISCUSSION

The peaks from XRD data confirms that GO and rGO was successfully formed with the presence of  $2\theta$  for GO=  $10.5^\circ$  and rGO=  $24.5^\circ$ . The rGO has almost similar  $2\theta$  peak as graphite at  $26.6^\circ$ . The oxidation of graphite is proportional to the increasing distance between each plane which is 0.33 nm (Graphite) to 0.84 nm (GO). The reduction also gives the outcome of broadening peak and decrease in d-spacing distance to 0.36 nm (rGO) [4]. TEM images of GO show wrinkly surface and synthesized rGO surface was found to be corrugated on the edges [5]. This data shows a successful synthesis of GO and rGO. For the toxicity study, hatching percentage of the *A. Salina* exposed to the GO and rGO (various concentration) were counted at different timepoint such as 18 h, 24 h and 48 h. The study reveals that rGO is less toxic and dose dependent.

## CONCLUSIONS

A simple, yet cost-effective and stable plant- derived rGO was successfully prepared. The synthesized rGO showed excellent biocompatible on *A. salina*. Our future work will be on the incorporation of metal nanoparticles and rGO for potential synergistic effect, which may open a new avenue for cancer treatments.

**ACKNOWLEDGMENT:** The authors are grateful for the financial support from the Ministry of Higher Education of Malaysia under Fundamental Research Grant Scheme (FRGS) (Vot. no. 5524949) and Dana Tautan Grant (DT0021) from UPM.

## REFERENCES

- [1] M. Fahiminia, N. S. Shamabadi, M. Nasrollahzadeh, and S. Mohammad Sajadi, "Phytosynthesis of Cu/rGO using Euphorbia cheiradenia Boiss extract and study of its ability in the reduction of organic dyes and 4-nitrophenol in aqueous medium," *IET Nanobiotechnology*, vol. 13, pp. 202–213, 2019.
- [2] D. C. Marcano *et al.*, "Improved synthesis of graphene oxide," *ACS Nano*, vol. 4, no. 8, pp. 4806– 4814, 2010.
- [3] S. Zhu, F. Luo, W. Chen, B. Zhu, and G. Wang, "Toxicity evaluation of graphene oxide on cysts and three larval stages of *Artemia salina*," *Sci. Total Environ.*, vol. 595, pp. 101–109, 2017.
- [4] G. Medha, C. Sharmila, and G. Anil, "Green Synthesis and Characterization of Nanocrystalline Graphene Oxide," *Int. Res. J. Sci. Eng.*, pp. 29–34, 2017.
- [5] D. Hou, Q. Liu, H. Cheng, H. Zhang, and S. Wang, "Green reduction of graphene oxide via *Lycium barbarum* extract," *J. Solid State Chem.*, vol. 246, pp. 351–356, 2017.



## Optical, Structural, and Electrical Features of Polyaniline Synthesized by Camphor Sulfonic Acid

Mahnoush Beygisangchin<sup>1,2</sup>, Suraya Abdul Rashid<sup>1,\*</sup> and Suhaidi Shafie<sup>2</sup>

<sup>1</sup>Material Processing and Technology Laboratory, Institute of Advanced Technology, Universiti Putra Malaysia, 43400 UPM Serdang, Selangor, Malaysia

<sup>2</sup>Functional Device Laboratory, Institute of Advanced Technology, Universiti Putra Malaysia, 43400 UPM Serdang, Selangor, Malaysia

\*Corresponding Author's Email: suraya\_ar@upm.edu.my

**Abstract:** PANI in its pure pattern has low conductivity. The electrical conductivity can be improved using charge defects in its doped structures. In this study, the influence of Camphor sulfonic acid (CSA) on preparation, and characterization of PANI was investigated through the chemical polymerization method by Fourier transform infrared (FT-IR), UV-visible (UV-vis), field emission scanning electron microscopy (FE-SEM), and four-point probe. The morphology of typical nanoflakes in PANI was changed to nanorods in PANI doped CSA. The conductivity was also improved from  $2.50 \times 10^{-2}$  to 2.7 S/cm in PANI doped CSA due to decreasing band gap from 2.9 to 2.5 eV.

**Keywords:** Polyaniline; PANI; Camphor sulfonic acid; Electronics; Conductivity.

### INTRODUCTION

PANI is a kind of polymer compound that is used in electrochromic glasses, solar cells, and sensor owing to special electrical and optical properties [1,2]. PANI in its pure pattern has low conductivity, and the electrical conductivity can be improved by adding some dopants. Camphor sulfonic acid (CSA) has an exceptional impact on electrical conductivity due to having soluble solvents such as cresol which can be performers into conductive PANI layers [3]. Furthermore, CSA components can interact with amine/imine hydrogens that improve the polymer's electrical features. The current work is related to the use of CSA doped PANI in emeraldine salt as a dopant for obtaining high conductivity through the chemical synthesis of PANI. Prepared samples were characterized using UV-visible (UV-vis), Fourier transform infrared (FT-IR), field emission scanning electron microscopy (FE-SEM), X-ray diffraction (XRD), and four-point probe.

### MATERIALS AND METHODS

The PANI in emeraldine salt was synthesized according to the recent literature [4]. In a standard process, Aniline (2.24 g) was dissolved in 120 ml of PTSA in 0.4 M and trailed with cooling and stirring for one h. APS (0.68 g) dissolved in PTSA (0.4 M) and added dropwise. An ice bath was used to keep the temperature between 0 and 5 °C. For a further 3 hours, the mixture was stirred. This PANI is doped with CSA in 0.4M CSA to the PANI chain repeat at ambient temperature for an additional 3 h [5].

## RESULTS AND DISCUSSION

FT-IR results of PANI and PANI doped CSA structures were mostly the same as shown in Fig. 1(a), and it evaluated the intensity proportion of quinoid/benzenoid rings. The major vibration band at  $1653\text{ cm}^{-1}$  might be because of the C=N extension of benzene and quinoid rings. The valance band and conduction band were produced by orbital  $\pi$  and  $\pi^*$ , respectively. The energy transformation between valance band and conduction band is termed band gap, which defines the optical features of PANI. The UV-vis findings showed when the PANI is doped, a polaronic band is formed between the band gaps of the polymer. The conductivity was originated to be just the inverse of its band gap.

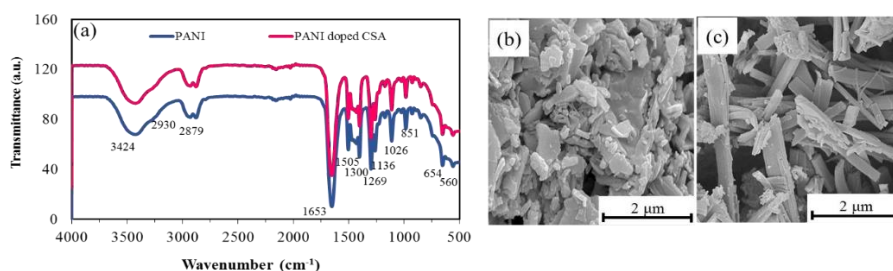


**Fig. 1.** PANI, and PANI doped CSA; (a) FT-IR analysis, FE-SEM image (b) of PANI, and (c) PANI doped CSA.

By adding CSA, the morphology transformed from typical nanoflakes in PANI to nanorods in PANI doped CSA as shown in Fig. 1(b) & (c). Also, the conductivity of PANI doped CSA (2.7 S/cm) was higher than PANI ( $2.50 \times 10^{-2}$  S/cm) due to the physical structural features of PANI doped CSA.

## CONCLUSIONS

PANI and PANI doped CSA were synthesized with the chemical oxidation method. The UV-vis findings demonstrated that conductivity will be increased by decreasing band gap. Using additional CSA content, the structure displays a transformation in morphology from typical nanoflakes PANI to nanorods. The conductivity was improved from 0.025 in PANI to 2.7 (S/cm) in PANI doped CSA.

## REFERENCES

- [1] Beygisangchin, M.; Abdul Rashid, S.; Shafie, S.; Sadrolhosseini, A.R.; Lim, H.N. *Polymers (Basel)*. **2021**, *13*, 2003.
- [2] Ramanavicius, S.; Ramanavicius, A. *Polymers (Basel)*. **2021**, *13*, 1–19.
- [3] Geethalakshmi, D.; Muthukumarasamy, N.; Balasundaraprabhu, R. *J. Mater. Sci. Mater. Electron.* **2015**, *26*, 7797–7803.
- [4] Usman, F.; Dennis, J.O.; Seong, K.C.; Yousif Ahmed, A.; Meriaudeau, F.; Ayodele, O.B.; Tobi, A.R.; Rabih, A.A.S.; Yar, A. *Results Phys.* **2019**, *15*, 102690.
- [5] Saravanan, S.; Joseph Mathai, C.; Anantharaman, M.R.; Venkatachalam, S.; Prabhakaran, P.V. *J. Phys. Chem. Solids* **2006**, *67*, 1496–1501.

## Resistless Nanoetching of UV-Irradiated Vinyl-functional Silsesquioxane Thin Film by Alcohol-Alkaline Solution

Siti Mariam Mohamad<sup>1</sup>, Nurazilah Mohd Zainon<sup>1</sup>, Syazana Abu Bakar<sup>1</sup>, Nor Shahida Kader Basha<sup>1</sup>, Farina Md Jamil<sup>2</sup> and Mat Tamizi Zainuddin<sup>1\*</sup>

<sup>1</sup>Industrial Centre of Innovation in Biomedical, SIRIM Berhad, Kulim HiTech Park 09000 Kulim Kedah, Malaysia

<sup>2</sup>Industrial Centre of Innovation in Nanotechnology, SIRIM Berhad, Kulim HiTech Park 09000 Kulim Kedah, Malaysia

\*Corresponding Autor's Email: tamizi@sirim.my

**Abstract:** Defining optical thin film-based components such as waveguides, microlens, etc. typically encounter dimensional-based challenges especially when it comes to nano-dimensional features processing. This work focused on the optimisation of wet etching process on the photosensitive organic-inorganic thin film in which desired pattern from UV-exposed photolithographic technique was successfully defined. Dissolution of the non-exposed areas was performed using a mixture of alcohol-alkaline solution and parameters such as concentration of etchant and etching time have been studied for the impact on morphology, topography, and optical properties. The optical properties of film thickness indicated that the non-exposed areas experienced thickness loss with low etchant contributed to the steady-state thickness reduction than the higher concentration of etchant used, whereas the refractive index is maintained throughout the process. Changes in topography properties indicated that surface features of arithmetical surface mean height, Sa and the average roughness, Ra exhibited that film smoothness and textural gross shapes are greatly enhanced by the combination of composition of etchant ions and etching duration. Elongation of etching impact on surface morphology was analyzed and a schematic etching phases based on sequential morphological observation on organic-inorganic thin film is outlined.

**Keywords:** Thin film, organic-inorganic, etching, UV micropatterning

### INTRODUCTION

Recently, optical waveguides have been widely produced by various 'hard' deposition techniques such as flame hydrolysis deposition (FHD), plasma chemical vapor deposition (P-CVD) and etc. On the other hand, sol gel technique which employed chemical synthesis route offers more rapid and less expensive production cost that has been the most important issues for the waveguides fabrication industries. However, both 'hard' deposition techniques and conventional inorganic based sol gel method still require photoresist deposition as masker during photolithographic process to define pertinent microscopic architectures of the pattern. Photoresist consists of high molecular weight polymer e.g. resin, usually give rise to contamination on the pattern and the solvents they used to it place severe compatibility restrictions on the substrate. Therefore, many researchers have been developing novel materials and processes for the photoresist and mask reduction in photolithography. Apart from that, etching techniques such as wet etching and reactive ion etching (RIE) also play important role in defining the pattern by contributing multiple steps. This work focuses on the optimization of the

wet etching process using NaOH alkaline solution on the silica based organic-inorganic hybrid sol gel thin film in order to define optical components.

## RESULTS AND DISCUSSION

Micropatterning involving UV light irradiation has been applied on the thin film with presence of negative type photomask. It promoted organic cross-linked network by undergo addition photopolymerization C=C double bonds of vinylic groups. Such polymerization also densified the irradiated area and increased refractive index. Shrinkage in the irradiated areas was observed to be close to that of the unirradiated area of the film. Thus, the influence of the neighboring unirradiated areas on the shrinkage of the film during UV irradiation should be relatively small. Wet etching was performed using controlled solution of NaOH:H<sub>2</sub>O:EtOH. Unirradiated area was completely dissolved and removed by etching, whereas no significant decreased was observed for irradiated area after etching. This suggests that the UV-irradiated area has high chemical durability against the alcohol-alkaline etching solution due to the densification facilitated by addition photopolymerization. The optical properties of film thickness indicated that the non-exposed areas experienced thickness loss with low etchant contributed to the steady-state thickness reduction than the higher concentration of etchant used, whereas the refractive index is remains at 1.42 which is comparable to silica material throughout the process. FTIR showed that for longer etching duration, irregular shapes of peak correspond to hydroxyl groups appear for unirradiated areas, whereas the peaks remain unchanged for irradiated areas. Optical micrograph also correlated with this phenomenon by showing losses channel structure for longer etching time. This indicated that etching time is significant factor in order to form optimum unirradiated areas dissolution. Smooth surface with areal roughness, Sa and profile roughness, Ra values around 70 to 110 nm has been observed during each etching points for the 1 and 2% NaOH indicating the realization of compacted structure and precised patterned for film etched at low concentration of NaOH. Elongation of surface morphology indicated the events of etching process started from micropores formation to bulk lift-off has been observed and the schematic etching phases has been defined and outlined.

## CONCLUSIONS

Controlling etching solution at below 2% at specific etching time of 15 s by using shorter alkyl group alcohol governed more definitive pattern transfer through UV-micropatterning technique.

**ACKNOWLEDGMENT:** The authors would like to express appreciation for the support of the SIRIM Industrial Research Fund [SR-21-0008 'Nanostructured Organosilsesquioxane Thin Film for Hazardous Antibacterial and Antiviral Applications].

## REFERENCES

- [1] Minami T. *J Sol-Gel Sci Technol.*, 2013, **65**, 4-11
- [2] Bidaud C, Berling D, Jamon D. *Sci Rep.*, 2021, **11**, 5075

## A Review on Polymerization Method of Tuneable PNIPAAm-based Thermally Sensitive Nanogels

Nur Fathin Amirah Shafie<sup>1,2</sup>, Mohd Yusof Hamzah<sup>2</sup>, Roshafima Rasit Ali<sup>1</sup>

<sup>1</sup>Malaysia-Japan International Institute of Technology, University Teknologi Malaysia, 54100 Kuala Lumpur, Malaysia.

<sup>2</sup> Nanotechnology Laboratory, Radiation Processing Technology, Malaysian Nuclear Agency, 43000 Kajang, Selangor, Malaysia.

\*Corresponding Author's Email: [m\\_yusof@nuclearmalaysia.gov.my](mailto:m_yusof@nuclearmalaysia.gov.my)

**Abstract:** Drug delivery research has gained popularity recently. One of the most explored areas was the synthesis of nanogels for drug delivery. Nanogels with stimuli-responsive properties have improved the category of smart polymers. These materials are ideal for drug carriers because they react appropriately to their environments and their release profile can be changed to allow for high-efficiency drug transportation. Thermally sensitive nanogels are designed to react to changes in temperature, prompting therapeutic drug release. To date, the most researched thermally sensitive nanogels based on their Lower Critical Solution Temperature (LCST) is Poly(N-isopropyl acrylamide) or PNIPAAm. This paper reviews alternative polymerization processes for thermally sensitive PNIPAAm-based nanogels and recent advancements in drug delivery applications.

**Keywords:** Smart polymers, Stimuli-responsive polymers, Thermo-responsive nanogels, Lower critical solution temperature

### INTRODUCTION

Cancer is a severe medical issue that continues to plague the globe. Targeted drug delivery may reduce the cost and risk of conventional chemotherapy methods. The ability of stimulus-responsive nanocarriers for targeted drug delivery to release targeted material in different stimuli, such as temperature and pH, has been recognized and attributed [1]. With its LCST, next to the tumour site temperature, the thermo-responsive delivery system is a promising cancer-targeting method. This study discusses the fundamentals of LCST and several polymerization processes used to create thermo-responsive nanogels for drug administration, with current and future research challenges associated.

### THERMO-RESPONSIVE SYSTEMS

Thermo-sensitive polymers have been extensively studied for their LCST tailoring for targeted drug administration. LCST nanogels were the most studied among binary thermo-responsive nanogels. The thermal-responsive drug carriers can preferably hold their cargo at physiological temperatures (37 °C) and release the cargo at an LCST (Fig. 1) slightly above physiological temperature (40 to 45°C) at the target site of heated cancer cells.



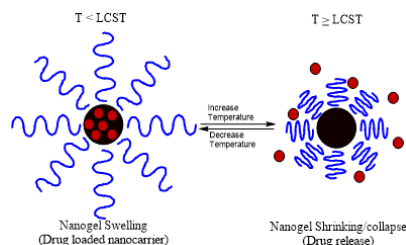


**Fig. 1.** Mechanism of Thermo-Responsive Nanogels

## POLYMERIZATION METHOD

Free radical polymerization is a common polymerization method in thermo-responsive drug delivery systems [2]. Although toxicities associated with multistep synthesis are avoided [3], the main radicals are generated using an initiator and have an unregulated molecular weight distribution due to the necessary radical-radical termination events. Some promising techniques for overcoming these drawbacks are Atom Transfer Radical Polymerization (ATRP) and Reversible Addition-Fragmentation Chain Transfer (RAFT) polymerization. However, the lack of an appropriate catalyst system [13] to control polymerization behaviour is linked to ATRP rarity in drug delivery applications. RAFT polymerization seeks to manage the exact structure of nanogels, strengthen mechanical properties, respond quickly to external heat stimuli, and control drug release [4]. Nevertheless, this process frequently uses AIBN, a thermal initiator creating radicals.

## CONCLUDING REMARKS AND FUTURE PERSPECTIVES

Even though the preceding polymerization methods are well equipped with tuneable LCSTs, these multistep techniques produced thermo-sensitive polymers and required chemical cross-linkers, initiators or accelerators. These materials are known carcinogens and irritants, and their disposal at the end of the process is cost-prohibitive. This is an essential aspect since drug delivery nanogels should be free of hazardous components. So, if certain nanogels can cure cancer in a patient, they must not include any carcinogens. Otherwise, the treatment will fail. The single-step, non-carcinogenic, green irradiation polymerization at room temperature is intended to solve the carcinogen issue. The review sought to show that research on PNIPAAm synthesis and polymerization methods using this thermo-responsive nanogel is progressing. Many substantial obstacles remain to improve the clinical appropriateness of these materials polymerization approaches.

## REFERENCES

- [1] M. Chountoules, N. Naziris, N. Pippa, P. Pispas, and C. Demetzos, Stimuli-responsive nanocarriers for drug delivery, In: Holt, S.s. (ed.), Elsevier, Greece, 2020, pp. 99-121.
- [2] M. A. Macchione, C. Biglione, and M. Strumia. *Polymers (Basel)*. 2018, **10**, 5.
- [3] S. Pentlavalli, P. Chambers, B. N. Sathy, M. O'Doherty, M. Chalanqui, D. J. Kelly, T. Haut-Donahue, H. O. McCarthy, and N. J. Dunne. *Macromol Biosci*. 2017, **17**, 11.
- [4] T. Ugurlu. *Turk J Pharm Sci*. 2012, **9**, 3.



## Optimization of Gel Content and Swelling Properties of Hyaluronic Acid/*Gracilaria changgi* Hydrogel

Maizatul Nurhafiqah Mohd Jupri<sup>1</sup>, Norizah Abdul Rahman<sup>1,2\*</sup> and Mansor Ahmad<sup>1</sup>

<sup>1</sup>Department of Chemistry, Faculty of Science, Universiti Putra Malaysia, 43400 UPM, Serdang, Selangor Darul Ehsan, Malaysia

<sup>2</sup>Materials Synthesis and Characterization Laboratory, Institute of Advanced Technology, Universiti Putra Malaysia, 43400 Serdang, Selangor, Malaysia

\*Corresponding author: a\_norizah@upm.edu.my

**Abstract:** In this study, HA/*Gracilaria changgi* seaweed (Gc) hydrogel with various ratio of HA to Gc were synthesized using chemical crosslinking method. The preparation of HA/Gc hydrogel was optimised using three parameters; concentration of 1-ethyl-3-[3-(dimethylamino)-propyl]carbodiimide (EDC), ratio of HA to Gc, and pH values. Therefore, only effect of HA/Gc against concentration of EDC on gel content will be discussed. The optimum ratio of gel content was found at 70:30 ratio of HA/Gc with 30 mM of EDC in pH 6.0. As HA was composited with Gc, the gel content and swelling studies of the HA/Gc hydrogel film improved when compared to HA alone.

**Keywords:** Hyaluronic acid, *Gracilaria changgi*, hydrogel, crosslinker, 1-Ethyl-3-[3-(dimethylamino)-propyl]carbodiimide (EDC).

### INTRODUCTION

Hyaluronic acid (HA) is a natural linear anionic polysaccharide. However, the mechanical properties of HA based hydrogel are commonly very poor *in vitro* environment and rapidly degrade *in vivo* system which limit its use in biomedical application [1, 2]. The physicochemical properties and stability of HA can be improved by pre-modified with crosslinkable functional groups or by adding a crosslinker directly and three-dimensional (3D) network is formed [1, 3]. *Gracilaria Changgi* (Gc) is an edible seaweed that can be found in various places in Malaysia. Due its chemical composites and structure, it can also be utilized into the hydrogel matrix. There are many studies have been carried out on the modification of HA based hydrogel, however, to the best of our knowledge, no study has been reported on HA blend *Gracilaria changgi* seaweed hydrogel. In this study, HA and Gc were chosen as the main materials and were synthesized using chemical crosslinking method for hydrogel formulation due to their excellent properties in drug delivery applications, such as biocompatibility and non-toxic.

### MATERIALS AND METHODS

The raw *Gracilaria Changgi* (Gc) seaweed was obtained from coastal area of Sabah. The hyaluronic acid (HA) and the 1-Ethyl-3-[3-(dimethylamino)-propyl]carbodiimide (EDC) were purchased from the Sigma-Aldrich. A dried Gc seaweed was washed and soaked for few days. The seaweed was rinsed and dried for few days. Seaweed was cut and ground into powder form. After sieved, it was kept in desiccators. The parameter was varied to prepare HA/Gc 0.5% (w/v) which were concentration of EDC and ratio of HA to Gc. The samples were left for 3 days at 37°C. Later the gel content were measured and calculated based on the formula stated in Kanafi et al [4].

## RESULTS AND DISCUSSION

Figure 1 shows the gel content of several ratio of HA/Gc hydrogel composition at different concentration of crosslinker. A maximum percentage of gel content was obtained at 30 mM of EDC for all ratio of HA to Gc which may be explained by the formation of denser and tighter hydrogels network structure in polymer chain. Moreover, the gel content increased as the ratio of HA to Gc decreased from 100:0 (HA hydrogel) to 70:30. The hydrogel of HA/Gc with ratio of HA to Gc of 60:40 and 50:50, had a lower percentage of gel content because they have lower percent of HA which give less side chain for crosslinking reaction. Thus, 70:30 ratio of HA/Gc hydrogels were chosen to proceed to the next optimization parameter of HA/Gc hydrogels because of their high gel content which is suitable for drug-loading.

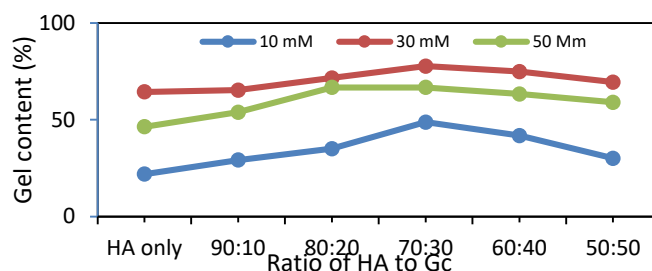


**Fig.1.** Effect of different concentration of EDC on gel content of HA/Gc hydrogels at different HA to Gc ratio.

## CONCLUSION

In summary, the chemical crosslinking method was used and a non-toxic and biocompatible of HA/Gc hydrogel film was prepared. The optimum formation of hydrogel was obtained at ratio 70:30 HA/Gc with 30 mM concentration of EDC in pH 6.0. This preliminary work has illustrated the potential of crosslinked HA/Gc as a drug carrier. Due to the nature of hydrogel, HA/Gc hydrogel may also be suitable for application, like wound dressing.

## REFERENCES

- [1] Perez, L.A., et al., *Hyaluronic Acid Hydrogels Crosslinked in Physiological Conditions: Synthesis and Biomedical Applications*. Biomedicines, 2021. **9**(9).
- [2] Collins, M.N. and C. Birkinshaw, *Investigation of the swelling behavior of crosslinked hyaluronic acid films and hydrogels produced using homogeneous reactions*. Journal of Applied Polymer Science, 2008. **109**(2): p. 923-931.
- [3] Wang, M.-D., et al., *Novel crosslinked alginate/hyaluronic acid hydrogels for nerve tissue engineering*. Frontiers of Materials Science, 2013. **7**(3): p. 269-284.
- [4] Kanafi, N.M., N.A. Rahman, and N.H. Rosdi, *Citric acid cross-linking of highly porous carboxymethyl cellulose/poly(ethylene oxide) composite hydrogel films for controlled release applications*. Materials Today: Proceedings, 2019. **7**: p. 721-731.

## Heat Treatment Affects the Formation of CopperOxide Nanoparticles using the Precipitation-Thermal Oxidation Method

Nur Syuhada Mohd Haeizar<sup>1,2</sup>, Che Anis Fawzi<sup>1</sup>, Annie Maria Mahat<sup>3</sup> and Nur Aimi Jani<sup>1,2,3,\*</sup>

<sup>1</sup>Faculty of Applied Sciences, Universiti Teknologi MARA, 40450 UiTM Shah Alam, Selangor, Malaysia

<sup>2</sup>Electrochemistry and Corrosion Lab, Faculty of Applied Sciences, Universiti Teknologi MARA, 40450 UiTM Shah Alam, Selangor, Malaysia

<sup>3</sup>Centre for Functional Materials and Nanotechnology, Institute of Science, Universiti Teknologi MARA, 40450 UiTM Shah Alam, Selangor, Malaysia

\*Corresponding Autor's Email: nuraimi\_jani@uitm.edu.my

**Abstract:** In this study, Copper Oxide (CuO) nanoparticles were produced using the precipitation thermal oxidation method. In order to identify the influence of sintering temperature to the growth structure of CuO, the surface structure and crystallinity of the materials was investigated by field emission scanning electron microscope (FESEM) and X-ray diffraction (XRD). FESEM result shows that, the nanoparticles production at different sintering temperatures of 300 °C and 400 °C, changed with temperature. At 300 °C of sintering temperature, the formation of CuO nanoparticles was formed with more uniform structure. As the temperature increased to 400 °C, the nanoparticles size growth and started to agglomerate. Furthermore, the XRD results indicate prominent peaks at 35.86° and 39.21°, indicating the presence of CuO phase.

**Keywords:** Copper oxide, Precipitation process, Nanoparticles, Growth formation

### INTRODUCTION

Copper oxide (CuO) in a form of nanoparticles have been extensively studied due to the high surface area characteristic compared to its bulk structure. CuO with a direct bandgap of 1.3–1.7 eV, has attracted significant attention due to their physicochemical properties which potentially used for various applications including catalysis, antimicrobial agents, and optoelectronic devices [1]. The best method in producing CuO nanoparticles is precipitation thermal oxidation method as compared to sol-gel, hydrothermal, and microwave assisted method which commonly encounters problems such as high temperature condition and complicated experimental setups [2,3].

### MATERIALS AND METHODS

The CuO nanoparticles were synthesized using simple precipitation thermal oxidation method inspired by Jiang et al. (2018). The precursor solution was prepared with mixing 2.0 g of cupric acetate, 5 mL of water, and 45 mL of ethylene glycol in conical flask. The mixture was heated and stirred for 5 hours at 110 °C. The precipitate was filtered and heated for 2 hours at 80 °C. Subsequently, the precipitate was thermally treated for 1 hours at temperature 300 °C and 400 °C.

## RESULT AND DISCUSSION

The structural properties and crystallinity of CuO nanoparticles at different sintering temperatures from 300 °C - 400 °C were observed through XRD patterns as in Fig. 1. Diffraction sharp peaks at  $2\theta$  values of 32.78, 35.86°, 39.21°, 49.26°, and 54.01° were assigned to (1 1 0), (002), (1 1 1), (2 0 2), (0 2 0), and (− 1 1 3) which correspond to the monoclinic structure of CuO [4]. The higher peak intensity observed, hence the degree of crystallinity increases as a result of oxide growth and removal of grain boundaries during sintering [5]. From FESEM analysis, inset (a) and (b) shows that the particles size increases from 300 °C to 400 °C. Nanoparticle structure well distributed at 300 °C compared to 400 °C.

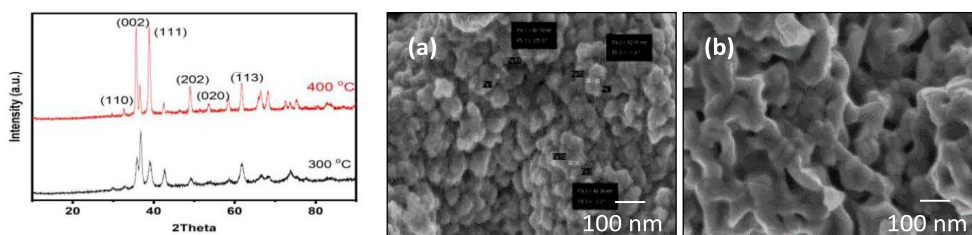


**Fig. 1.** XRD pattern of CuO sintered 1 hour at different temperature for 300 °C and 400 °C, respectively. Inset (a) and (b) are the FESEM images of CuO at 300 °C and 400 °C.

## CONCLUSIONS

In this study, CuO nanoparticles were formed using a precipitation thermal oxidation method, with varying sintering temperature. The structure and size of the nanoparticles have been affected as well as their structural properties with the shift in sintering temperature. CuO sintered at 300 °C shows the best nanoparticles structure compared to 400 °C.

**ACKNOWLEDGEMENT:** The authors would like to express their gratitude to Faculty of Applied Sciences and Research Management Centre of Universiti Teknologi MARA Shah Alam. [Lestari Grant: 600-IRMI 5/3/LESTARI (030/2019) and GPK Grant: 600-RMC/GPK 5/3 (140/2020)]

## REFERENCES

- [1] Gupta, D., et al., *Facile synthesis of Cu<sub>2</sub>O and CuO nanoparticles and study of their structural, optical and electronic properties*. Journal of Alloys and Compounds, 2018. **743**: p. 737-745.
- [2] Nikam, A.V. and A.H. Dadwal, *Scalable microwave-assisted continuous flow synthesis of CuO nanoparticles and their thermal conductivity applications as nanofluids*. Advanced Powder Technology, 2019. **30**(1): p. 13-17.
- [3] Jiang, T., et al., *Cu<sub>2</sub>O@ CuO core-shell nanoparticles as photocathode for p-type dye sensitized solar cell*. Journal of Alloys and Compounds, 2018. **769**: p. 605-610.
- [4] Veisi, H., et al., *Biosynthesis of CuO nanoparticles using aqueous extract of herbal tea (Stachys Lavandulifolia) flowers and evaluation of its catalytic activity*. Scientific Reports, 2021. **11**(1): p. 1983.
- [5] Shaheen, M., et al., *Efficient surfactant modified copper oxide nanoparticles for solar light driven water purification*. Optical Materials, 2021. **122**: p. 111688.

## Tailoring Localized Surface Plasmon Resonance of Added Ag Nanoparticles Er<sup>3+</sup> Ion Doped Glass System by Coupling Polarization Approach

M.S. Sutrisno<sup>1,2</sup>, S.K. Md Zain<sup>3</sup> and R. Hisam<sup>1\*</sup>

<sup>1</sup>Faculty of Applied Sciences, Universiti Teknologi MARA, 40450 Shah Alam, Selangor, Malaysia

<sup>2</sup>University of Cyberjaya, Persiaran Bestari, Cyber 11, 63000 Cyberjaya, Selangor Darul Ehsan, Malaysia

<sup>3</sup>Optical Materials Research Group, Faculty of Science, Universiti Teknologi Malaysia, 81310 Skudai, Johor, Malaysia

\*Corresponding Author's Email: rosdiana@uitm.edu.my

**Abstract:** The coupling polarization  $\xrightarrow{PEr^{3+}:NP}$  of LSPR was investigated using the 20Li<sub>2</sub>O-xBi<sub>2</sub>O<sub>3</sub>-(78-x)TeO<sub>2</sub>-1Er<sub>2</sub>O<sub>3</sub>-1Ag glass system with electrical polarizability of spherical particle  $\chi$  and Clausius-Mosotti relation polarizability  $\alpha_L$  approximations.

**Keywords:** localized surface plasmon resonance, polarizability, Er<sup>3+</sup> ion doped glass

### INTRODUCTION

Since the beginning of the twenty-first century, there has been a lot of research on the interaction of light with metal nano-objects associated with a dielectric medium, one of which is the surface plasmon effect [1]. Surface plasmon effects such as localized surface plasmon resonance (LSPR) and their interaction with dielectric medium which is glass in our work are sensitive to slight changes such as changes in glass composition [2]. Hence, our work intends to determine the effect of dielectric host glass to LSPR by describing the coupling  $\xrightarrow{PEr^{3+}:NP}$  mechanism between Ag NP and Er<sup>3+</sup> ion doped dielectric glass.

### MATERIALS AND METHODS

The Er<sup>3+</sup> ion doped glasses were made using a melt-quenching process with the chemical formula 20Li<sub>2</sub>O-xBi<sub>2</sub>O<sub>3</sub>-(78-x)TeO<sub>2</sub>-1Er<sub>2</sub>O<sub>3</sub>-1Ag glass samples. The optical absorption on the glass samples was measured using a double-beam Shimadzu UV-VIS spectrophotometer with a wavelength range of 200-2500 nm.

### RESULTS AND DISCUSSION

The interaction of spherical core shell nanostructures with the host glass medium at  $4I_{15/2} \rightarrow 4I_{13/2}$  excitation transition using the electrostatic approximation where the electrical polarizability  $\chi$  can be determined by the dielectric permittivity of Ag's  $\epsilon_m$  particle and also host glass  $\epsilon_d$  respectively. Furthermore, another approach of the conventional local-response Drude model for the response of the Ag nanoparticle may be investigated with consideration of Ag NP volume where the quasistatic optical polarizability  $\alpha_L$  is supplied by Clausius-Mossotti relation [3]. It is observed that both  $\chi$  and  $\alpha_L$  is initially increase at  $x < 7$  mol% before a large drop at  $x = 7$  mol% (Fig. 2) with increasing Bi<sub>2</sub>O<sub>3</sub> concentration. However, opposite trend between  $\chi$  and  $\alpha_L$  are observed for  $x > 7$  mol% where an increase of  $\chi$  is observed of at  $x = 11$  mol% but  $\alpha_L$  is approximately constant.



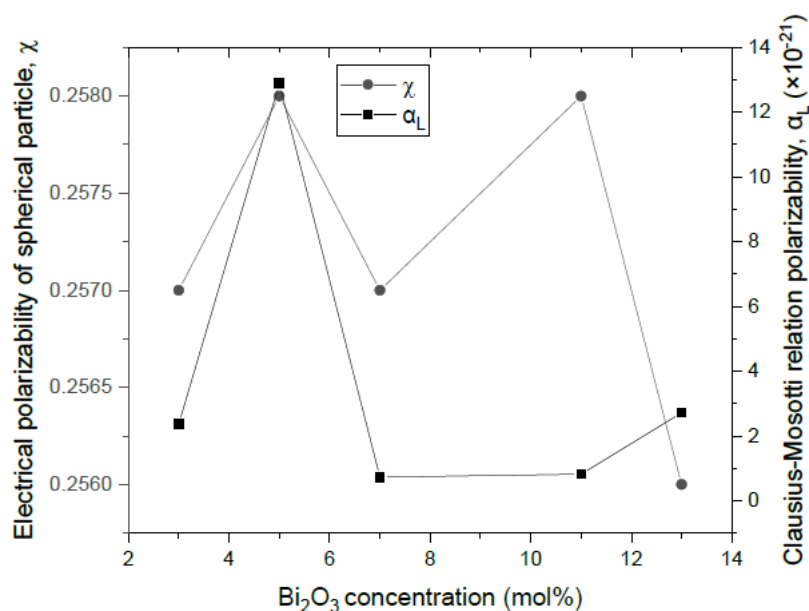


**Fig. 1.** The electrical polarizability of spherical particle,  $\chi$  and Clausius-Mosotti relation polarizability,  $\alpha_L$  of  $4I_{15/2} \rightarrow 4I_{13/2}$  excitation transition for  $20\text{Li}_2\text{O}-x\text{Bi}_2\text{O}_3-(78-x)\text{TeO}_2-1\text{Er}_2\text{O}_3-1\text{Ag}$  glass system.

## CONCLUSIONS

The  $20\text{Li}_2\text{O}-x\text{Bi}_2\text{O}_3-(78-x)\text{TeO}_2-1\text{Er}_2\text{O}_3-1\text{Ag}$  glass system had been fabricated and the coupling polarization  $\overline{\text{P}_{Er3+}:NP}$  of LSPR had been determined by means of electrical polarizability of spherical particle,  $\chi$  and Clausius-Mosotti relation polarizability,  $\alpha_L$  approximation. The highest coupling polarization  $\overline{\text{P}_{Er3+}:NP}$  is suggested at  $x = 5$  mol% indicated from high  $\chi$  and  $\alpha_L$  at that region hence can contribute to maximum LSPR before a contrast trend between both  $\chi$  and  $\alpha_L$  is observed at  $x=11$  mol%.

**ACKNOWLEDGMENT:** The authors express gratitude to the Research Management Centre (RMC) and Universiti Teknologi MARA, Malaysia for funding this research under the Strategic Research Partnership Grant 100-RMC/5/3/SRPGOV (005/2021).

## REFERENCES

- [1] Kreibig, U., & Vollmer, M. (2013). Optical properties of metal clusters (Vol. 25). Springer Science & Business Media.
- [2] Rivera, V. A. G., Silva, O. B., Ledemi, Y., Messaddeq, Y., & Marega Jr, E. (2014). *Collective plasmon-modes in gain media: Quantum emitters and plasmonic nanostructures*. Springer.
- [3] Raza, S., Stenger, N., Kadkhodazadeh, S., Fischer, S. V., Kotesha, N., Jauho, A. P., ... & Mortensen, N. A. (2013). Blueshift of the surface plasmon resonance in silver nanoparticles studied with EELS. *Nanophotonics*, 2(2), 131-138.



## Impact of Rare-Earth Lanthanum Ion Modifications on Magnetic Characteristics of Mechanically Alloyed Yttrium Iron Garnet Nanoparticles

Nurul Atiqah Mohd Pauzi<sup>1</sup> and Rodziah Nazlan<sup>1\*</sup>

<sup>1</sup>Faculty of Industrial Sciences and Technology, Universiti Malaysia Pahang, Lebuhraya Tun Razak,  
26300 Gambang, Pahang, Malaysia

\*Corresponding Author's Email: rodziah@ump.edu.my

**Abstract:** The influence of different lanthanum (La) content on structural, microstructural and magnetic properties of YIG was reported. The nanosized powders of  $Y_{3-x}La_xFe_5O_{12}$  with  $x=0.1$  to 0.5 were synthesized using mechanical alloying technique. The particle size of as-milled samples showed an increment from 38 to 53 nm with increasing La content. However, all magnetic parameters showed reduction with La content which is attributed to the paramagnetic nature of La rare earth ions at room temperature.

**Keywords:** Yttrium iron garnet, nanoparticles, lanthanum dopant, microstructure, magnetic properties

### INTRODUCTION

Yttrium Iron Garnet (YIG;  $Y_3Fe_5O_{12}$ ) is one of soft ferromagnetic materials with complex cubic crystal structure. Due to its strong negative superexchange interactions between magnetic moments of  $Fe^{3+}$  ions in octahedral and tetrahedral sublattices, YIG is largely utilized in high frequency microwave and magneto-optical applications [1]. As well as microstructure, the magnetic properties of YIG is largely dependent on stoichiometric composition of the materials. As  $Y^{3+}$  ions that accommodated the dodecahedral sublattice in YIG play a dominant contribution to the stoichiometric stability of YIG [2], therefore it is of interest if the stability of YIG can be maintained whilst changing the magnetic properties of YIG by rare-earth substitution in YIG crystal structure. As the magnetic properties of YIG is highly dependent on its crystal structure which can be tailored by composition variation of YIG, a study on substituting YIG with different  $La^{3+}$  ion contents is being studied.

### MATERIALS AND METHODS

High purity (>99.9%) starting powders of  $Fe_2O_3$ ,  $Y_2O_3$  and  $La_2O_3$  were used in synthesizing  $Y_{3-x}La_xFe_5O_{12}$  ( $x = 0.0$  to 0.5 with 0.1 increment) based on stoichiometric proportions. The powder mixtures were mechanically alloyed for 6 hours and shaped into toroidal specimens before being sintered at 1400 °C with a heating rate of 4 °C/min. The samples were then characterized using High Resolution Transmission Electron Microscopy (HRTEM) for nanoparticle size confirmation, X-ray Diffractometer (XRD) for structural analysis, Fourier Transform Infrared Spectroscopy (FTIR) for chemical bonding determination, Field Emission Scanning Electron Microscope (FESEM) for morphological analysis and both Vibrating Sample Magnetometer (VSM) and LCR- meter was used for magnetic and thermo-magnetic characteristics analyses respectively.

## RESULTS AND DISCUSSION

The as milled samples of YIG with different La concentrations showed increased in particle size with increases of La content from 38 to 53 nm. XRD spectra showed all the samples possess a single garnet phase structure with a space group of  $la-3d$  after sintering at 1400 °C regardless of La content. The XRD peak intensity increased with increasing La, proving that  $La^{3+}$  ions lead to increased crystallization by improving the atomic structure arrangement in comparison to that of pure YIG sample. The lattice constant also increases as the  $La^{3+}$  ion content increases due to larger ionic radius of  $La^{3+}$  ion (1.88 Å) as compared to  $Y^{3+}$  ion (1.02 Å) [3]. However, saturation magnetization showed a reduction with increasing  $La^{3+}$  ion content from 26.7 to 21.3 emu/g. Coercivity, remanence and Curie temperature were also observed to decrease as tabulated in Table 1 which is attributed to the paramagnetic nature of La ions at room temperature, that weakens the superexchange interactions between magnetic moments sublattices of YIG crystal system. This results in a reduction of net magnetic moment thus deteriorated the overall magnetic properties of the samples.

**Table 1.** Magnetic parameters for pure and La-substituted YIG

Samples	Coercivity, H (G)	Magnetization, $M_s$ (emu/g)	Retentivity, $M_r$ (emu/g)
YIG	3.99	26.66	0.36
La-YIG 0.1	3.80	26.24	0.32
La-YIG 0.2	4.96	25.58	0.99
La-YIG 0.3	4.63	24.03	0.39
La-YIG 0.4	3.92	20.87	0.29
La-YIG 0.5	4.12	21.33	0.30

## CONCLUSIONS

The effect of La substitutions on physical and magnetic properties of YIG was successfully reported. With increases of  $La^{3+}$  content, the crystallization and particles morphology have been improved. In contrast, magnetic characteristics showed reduction with increasing La content.

## ACKNOWLEDGEMENT

Financial support from Ministry of Higher Education under Fundamental Research Grant Scheme (FRGS) No. FRGS/1/2021/TK0/UMP/02/54 is greatly appreciated.

## REFERENCES

- [1] Yu H, Zeng L, Lu C, Zhang W, Xu G. *Mater. Charact.* 2011, **62**(4), 378-381.
- [2] Guillot M. Magnetic Properties of Ferrites, *Materials Science and Technology*, 2006.
- [3] Singh G. Chemistry of Lanthanides and Actinides, *Discovery Publishing House*, 2007.

## Assessment of Various Organic Coatings on Magnetic Nanoparticles for Biomedical Applications

Nur Khalida Rahayu Zainon<sup>1,2</sup>, Che Azurahaman Che Abdullah<sup>1,2,3</sup> and Mohd Basyaruddin Abdul Rahman<sup>2,4</sup>

<sup>1</sup>Department of Physics, Faculty of Science, Universiti Putra Malaysia, 43400 UPM Serdang, Selangor, Malaysia

<sup>2</sup>UPM-MAKNA Cancer Research Laboratory, Institute of Bioscience, Universiti Putra Malaysia, 43400 UPM Serdang, Selangor, Malaysia.

<sup>3</sup>Material Synthesis and Characterization Laboratory (MSCL), Institute of Advanced Technology (ITMA), Universiti Putra Malaysia, 43400 UPM Serdang, Selangor, Malaysia

<sup>4</sup>Department of Chemistry, Faculty of Science, Universiti Putra Malaysia, 43400 UPM Serdang, Selangor, Malaysia

\* Corresponding Author's email: azurahaman@upm.edu.my

**Abstract:** Magnetic nanoparticles (MNPs) have unique magnetic properties, good biocompatibility and targeting ability that make it an invaluable gem for application in nanomedicines. However, naked MNPs are easily oxidized, hydrophobic in nature and intrinsically unstable. Therefore, stabilizer like surfactant and polymer are necessary to prevent particles aggregation and to assist further functionalization with other nanoparticles, ligands or therapeutic agents depending on the chosen applications. In this research, lipid based oleic acid surfactant (OA) and polymer based polyethylene glycol (PEG) were used to coat the surface of the nanoparticles. MNP, MNP-OA, and MNP-PEG with average particle size of  $9.7 \pm 1.7\text{nm}$ ,  $7.1 \pm 1.3\text{nm}$ , and  $7.2 \pm 1.1\text{nm}$  were successfully synthesised.

Keywords: magnetic nanoparticles, iron oxide, PEG, oleic acid, superparamagnetic

### INTRODUCTION

Surface coatings can be categorized into two main groups, namely organic (surfactants, biomolecules, polymers) and inorganic (metals/ non-metals, silica, metal oxides). This study focused on the usage of organic coatings that employ functional reactive groups, such as hydroxyl, amino, carboxyl and aldehyde groups for further interactions [1]. Our subjects of interest are lipid-based oleic acid (OA) and polymer-based polyethylene glycol (PEG) to be tested as coating materials for MNPs. Although multiple research have been conducted using both types of coating agents, there is lack of information on the effect of the coatings to the physical and chemical properties of MNP itself [2]. The nature of surface coatings and their structural arrangement on the nanoparticles will influence the size, magnetization values, biocompatibility and biodistribution of the nanoparticles in the body.

### MATERIALS AND METHODS

Ferrous chloride tetrahydrate ( $\text{FeCl}_2 \cdot 4\text{H}_2\text{O}$ ), ferric chloride hexahydrate ( $\text{FeCl}_3 \cdot 6\text{H}_2\text{O}$ ) and oleic acid were purchased from Sigma-Aldrich (US). Ammonia solution (25%), ethanol ( $\text{C}_2\text{H}_5\text{O}$ ) and PEG 2000 were purchased from R&M Chemical. Magnetic nanoparticles (MNP) were synthesized using co-precipitation method as previously reported. 5.4g of  $\text{FeCl}_3 \cdot 6\text{H}_2\text{O}$  and 1.98g  $\text{FeCl}_2 \cdot 4\text{H}_2\text{O}$  was mixed with 150ml of deionized water before mixed with 20ml ammonium hydroxide

solution. The solution was stirred at 45°C under vigorous stirring (800rpm) for 1 hour. The resulting precipitates were then washed several times with deionized water to remove the impurities. The samples then dried in oven overnight at 70°C. For MNP-OA, 6ml, 8ml and 10ml of oleic acid were added to the precipitates of MNP respectively, followed by stirring at 80°C for 1 hour. MNP-PEG nanoparticles were prepared by dissolving 1g, 2g and 3g of PEG 2000 respectively in 100ml water. 1g of iron oxide nanoparticles were added and mixed with each PEG solutions for the duration of 18 hour. Both samples were then centrifuged and washed several times with acetone to remove the impurities. The sediments were dried in oven overnight at 70°C.

## RESULTS AND DISCUSSION

Transmission electron microscopy (TEM) revealed a uniform distribution and spherical shape for the nanoparticles, with an average particle size of  $9.7 \pm 1.7\text{nm}$ ,  $7.1 \pm 1.3\text{nm}$ , and  $7.2 \pm 1.1\text{nm}$  for MNP, MNP-OA, and MNP-PEG, respectively. The reduction in particle size following coating demonstrated that OA and PEG are capable of controlling particle size and preventing aggregation of naked MNPs. Ms values of 63.95 emu/g, 62.55 emu/g, and 63.91 emu/g were obtained for all three types of MNPs. This value is considered appropriate for biomedical field applications.

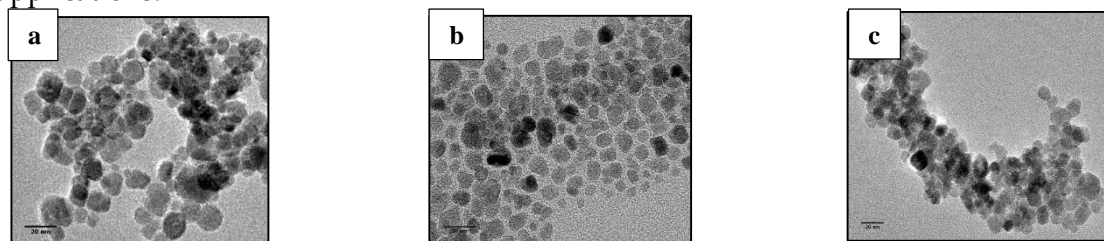


**Fig. 1** TEM images of a) MNP, b) MNP-OA6 and c) MNP-PEG2

## CONCLUSION

Based on the physical and optical analysis (XRD, FTIR, TGA), we deduced that the best concentration ratio for both coated MNPs were MNP-OA6 and MNP-PEG2. Excess amount of coating will hamper MNPs targeting ability, while inadequate amount of coating will not serve its purpose in preventing agglomeration of MNPs.

**ACKNOWLEDGEMENT:** The project was supported in part by Malaysian Institute for Innovative Nanotechnology (NanoMITe) (Vote No. 5526306) and IPS Grant (Vot No. 9618800) financed by Universiti Putra Malaysia.

## REFERENCES

- [1] Hedayatnasab, Z., Abnisa, F., and Daud, W. M. A. W. (2017). Review on magnetic nanoparticles for magnetic nanofluid hyperthermia application. *Materials & Design*, 123, 174-196.
- [2] Keskin, T., Yalcin, S., and Gunduz, U. (2018). Folic acid functionalized PEG coated magnetic nanoparticles for targeting anti-cancer drug delivery: Preparation, characterization and cytotoxicity on Doxorubicin, Zoledronic acid and Paclitaxel resistant MCF-7 breast cancer cell lines. *Inorganic and Nano-Metal Chemistry*, 48(2), 150-159.

## Modern Methods for Protecting Printed Circuit Boards Effects from Mechanical External Impact

Z.H.M. Al-Araji <sup>1</sup>, A.V. Turetsky <sup>2</sup> and A.V. Bashkirov <sup>2</sup>

<sup>1</sup>University of Baghdad, Baghdad, Iraq

<sup>2</sup> Voronezh State Technical University, Voronezh, Russia

\*Corresponding Autor's Email: zainab.alaraje.1975@gmail.com

**Abstract:** To ensure the protection of electronic devices (RES) in general and printed circuit boards as the central part, any malfunction in their work leads to the failure of the electronic device. This article reviews the nature and conditions of external influences and chooses a method to reduce their impact on RES performance. This paper describes the most common methods for minimizing external mechanical influences on electronic means, and numerical data demonstrates the effectiveness and validates a simulation environment designed to predict the optimal design of radio-electronic devices using Creo simulations.

**Keywords:** Deformation, radio-electronic blocks, printed circuit board, vibration analysis.

### INTRODUCTION

The printed circuit board is the basic building block of all electronic devices. Shock and vibration applied to a printed circuit board can if severe, enough, damage the connected electronic components. External mechanical influences cause 30 to 50 per cent of the failures in the operation of radio-electronic equipment (RES) and lead to a decrease in the accuracy, stability and reliability of the actuating device. As a result of mechanical influences (vibrations, shocks, etc.), the following types of damage occur [3] like violation of sealing due to the appearance of cracks in metal-to-glass joints, welded and glue seams; failure of detachable and one-piece electrical contacts; complete destruction of the body or its individual parts from mechanical resonance and fatigue; displacement of the position of the controls and settings; breakage of assembly connections; peeling of printed conductors; layering of multilayer printed circuit boards.

### MATERIALS AND METHODS

In this paper, there has tested a four-layer PCB. The PCB is modelled as an isotropic plate with similar material properties.

### RESULTS AND DISCUSSION

Finite element (FE) simulation model for PCB with a concentrated mass instead of the components .

- a. *Frequency offset* - An increase in the mounting points of the boards from four to seven increases the natural vibration frequency by more than 3 times.



- b. *Vibration damping* - Another way to protect against mechanical influences is vibration damping due to the inclusion of special layers of vibration-absorbing materials in the design of the printed circuit board.

## CONCLUSIONS

This paper has described and validated a simulation environment designed to predict the optimum design of radio-electronic devices using Creo simulation. External influences have a significant impact on the operation of electronic equipment. Therefore, an essential task of the designer is to carefully consider the parameters of external influences and the choice of an adequate method of protecting electronic equipment. An increase in the rigidity of structures leads to a shift in the spectrum of frequencies of free vibrations beyond the upper limit of the frequency range of external influences and allows you to exclude resonance phenomena. To eliminate resonance oscillations, the frequency of free changes of the fundamental tone must be at least an octave higher than the upper frequency of external influences, i.e.,  $f_{o1} / f_B > 2$ . You can control the stiffness of the structures of functional units like the choice of the method of fixing the boards; geometric dimensions of the PP; the use of stiffeners, shells, frames in the construction; the use of vibration-absorbing mastics, adhesives.

**ACKNOWLEDGMENT:** The authors gratefully acknowledge the Strength of Material Laboratory at the Voronezh State Technical University for providing the experimental assistances.

## REFERENCES

- [1] T. L. A. Sysuev V. A., Yankov R. V., Lysenko A. V., Almametov V. B., "Modern Means of Protecting Onboard Radio Electronic Devices From External Mechanical Effects Completed," vol. 1, no. 177, pp. 70–74, 2020.
- [2] NK Yurkov, "Risks of failure of complex technical systems," vol. 1, no. 5, 2014.
- [3] Yu. N. K. Frolov SI, Goryachev NV, Tankov GV, Kochegarov II, "On Some Problems of Reliable-Oriented Design of On-Board Researches In," pp. 155-156, 2017.



## Optimization of the Frequency Performance of SiGe Heterojunction Bipolar Transistor (HBT) Integrated in a BiCMOS 55nm Technology

Chems El Ghizlane Lachkhab<sup>1,\*</sup>, Maya Lakhdara<sup>1,\*</sup>, Abdeaziz Boulghab<sup>1</sup> and Saida Latreche<sup>1</sup>

<sup>1</sup>Laboratoire Hyperfréquences et Semi-conducteurs, Département d'Electronique, Université des frères Mentouri  
Constantine 1, PO Box 25017, Constantine, Algeria

\*Corresponding Author's Email: chamsghizlene21.06@gmail.com, l\_maya1@yahoo.fr

**Abstract:** This work presents an optimization of the frequency performance of a new technology of a SiGe Heterojunction Bipolar Transistor, realized in an industrial BiCMOS55 process technology with a DPSA-SEG (Double Poly-silicon, Self -Aligned, Selective Epitaxial Growth) architecture, with characteristic frequencies ( $f_T / f_{max} = 320 / 370$  GHz). The aim of this work is to optimize the doping of the intrinsic and extrinsic base on the dynamic characteristics of HBT, The doping of the extrinsic base significantly affects compared to the doping of the intrinsic base on the frequencies  $f_T$  and  $f_{max}$ .

**Keywords:** Transistor, Heterojunction, BiCMOS055, HBT, SiGe.

### INTRODUCTION

In the context where the smallest is the fastest make law, STMicroelectronics realizes a new technology of HBT (BiCMOS55), with characteristic frequencies ( $f_T / f_{max} = 320 / 370$  GHz) [1]. The purpose of this work is to optimize the frequency performance with the doping of the intrinsic and extrinsic base of the BiCMOS055, in order to increase the cut-off frequencies.

### The structure studied under COMSOL Multiphysics

The studied structure is a NPN HBT. This structure is a DPSA-SEG with cut-off frequencies of ( $f_T / f_{max} = 320 / 370$  GHz). The latter consists of a collector module formed by a localized location SIC, a heavily doped layer and a collector well. The Emitter-base module is composed of two parts , a mono crystalline intrinsic part based on Si/SiGe and another polysilicon extrinsic less doped than that of intrinsic . In this architecture, deep trench insulation is used to isolate the transistor from the rest of its plate environment, and Shallow trench isolation is used to isolate the device core from the collector contact [2]. The final structure of this technology is shown in Fig. 1(a) and Fig. 1(b) represents the simulated structure under COMSOL software.

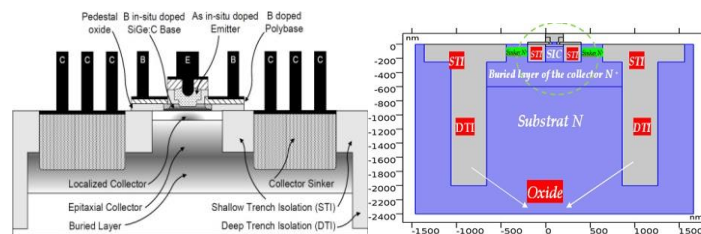


**Fig.1.** (a) Schematic structure of the HBT SiGe integrated in the BiCMOS 55 [3] (b)Representation of the simulated BiCMOS 55 structure by COMSOL.

## RESULTS AND DISCUSSION

In this section, we will first simulate the frequency performance of the HBT. The results obtained under COMSOL software of the BiCMOS55nm are represented on Fig.2, the maximum values are in the order of  $f_T / f_{max} = 334 / 397 \text{ GHz}$ . These frequencies correspond perfectly to the order of the performance of BiCMOS55 manufactured by STMicroelectronics ( $f_T / f_{max} = 330 / 390 \text{ GHz}$ ) [3].

### Optimizing the $f_T$ and $f_{max}$ frequencies for doping the extrinsic base

The base resistance is a key parameter in the dynamic performance of HBT and it is inversely proportional to  $f_{max}$ . Based on the simulation results obtained (Fig. 3) which illustrates the optimization of the  $f_{max}$  as a function of the doping of extrinsic base. It is noted that when the concentration increases, the resistance of the poly base considerably decreases. This decrease in frequency in turn results in an increase of  $f_{max}$ . However, the  $f_T$  increases but slightly with this doping (Fig. 4). This latter is greater than the increase in the intrinsic base.

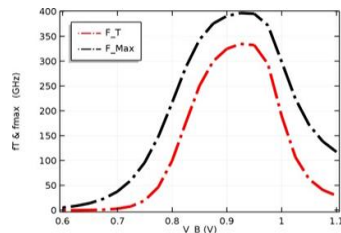


**Fig.2.** Frequencies  $f_T$  and  $f_{max}$  obtained by the simulation

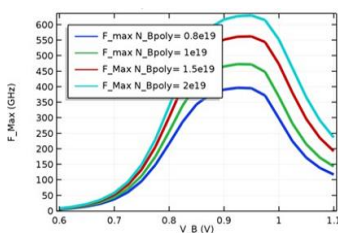


**Fig.3.** Variation of  $f_{max}$  as a function of poly-base doping.

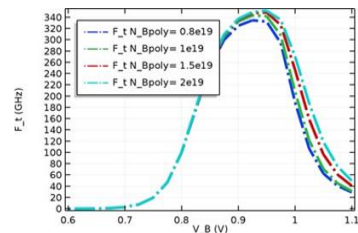


**Fig.4.** Variation of  $f_T$  as a function of poly-base doping.

## CONCLUSIONS

The presented work is about the optimization of the HBT dynamic characteristics (BiCMOS055 technology) using the COMSOL Multiphysics software. Doping of both bases (intrinsic and extrinsic), we have noticed that the doping of the extrinsic base has a significant influence in relation to the doping of the intrinsic base on the  $f_T$  and  $f_{max}$  frequencies. The frequency  $f_{max}$  reaches  $630 \text{ GHz}$  for a  $2 \times 10^{19} \text{ cm}^{-3}$  poly silicon base doping. The THz path seems traced but no doubt, that reaching this frequency will require on the one hand to further improve our knowledge of HBT, and to pursue technological innovations.

## REFERENCES

- [1] Rücker H, Heinemann B, "High-performance SiGe HBTs for next generation BiCMOS technology", *semicond. Sci. Technol.* 33, 2018, pp.6.
- [2] Chevalier P et al, "Nanoscale SiGe BiCMOS Technologies: From 55 nm Reality to 14 nm Opportunities and Challenges", in *Proc. BCTM*, 2015, pp. 80-87.
- [3] V. VU, "Recherche et Evaluation d'une Nouvelle Architecture de Transistor Bipolaire à Hétérojonction Si/SiGe pour la Prochaine Génération de Technologie BiCMOS", Ph.D.thesis, 2016

## Synthesis and Characterisation Chitosan-Carbon Dots with Loaded Mitomycin C for Bladder Cancer

Siti A'risyah Muhamad Ghadzali<sup>1</sup>, Nor Azah Yusof<sup>2\*</sup> and Jaafar Abdullah<sup>1,2</sup>

<sup>1</sup>Institute of Advanced Technology, 43400 Universiti Putra Malaysia, Selangor, Malaysia

<sup>2</sup>Department of Chemistry, Faculty of Science, Universiti Putra Malaysia, 43400 UPM Serdang, Selangor, Malaysia

\*Corresponding Autor's Email: azahy@upm.edu.my

**Abstract:** This research focused on synthesis and characterization of chitosan-carbon dots with mitomycin C loaded for bladder cancer treatment. Hydrothermal treatment method used for synthesis nanocarrier which is Carbon dots (CDs). Fluorescence spectroscopic shows an emission wavelength at 466 nm which correspond to excitation wavelength 375 nm. The size of carbon dots measured by using High Resolution-Transmission electron spectroscopy with particle size distribution Of 5.71 nm. Carbon dots has spherical shape.

**Keywords:** carbon dots, chitosan, drug delivery, nanocarriers

### INTRODUCTION

Bladder cancer is under top ten common cancer worldwide [1]. Men are highly diagnosed with bladder cancer rather than women. From previous study bladder cancer can be treated by conventional technique based on Intravesical instillation of Bacillus Calmette-Geurin (BCG) which there are still recurrence after the treatment [2]. Therefore, development of Chitosan-Carbon (CS-CDs) dots with loaded mitomycin C (MMC) is introduce to control rate, time and place of release. It is also less toxic and biocompatible. This study to improve the therapeutic effect and to improve the efficacy of drug by the use of chitosan-based CDs. The achievement of this research is Carbon dots (CDs) were synthesized from citric acid and ethylenediamine as the pre-cursors under hydrothermal carbonization process. Then further conjugation with Chitosan (CS) for encapsulation MMC drug.

### MATERIALS AND METHODS

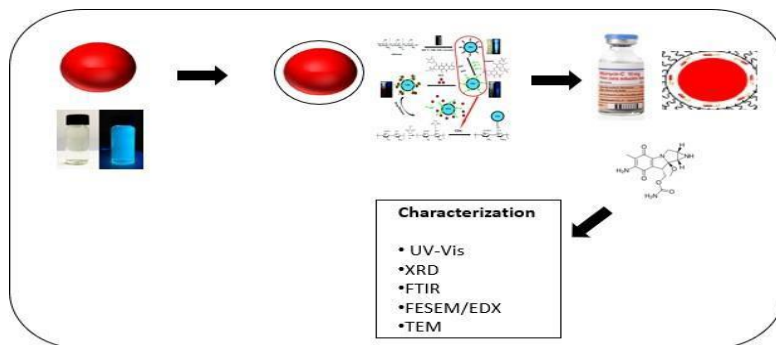


**Fig.1:** The schematic diagram illustrates the procedure of this research which is preparation of chitosan-carbon dots with loaded mitomycin C.

## RESULTS AND DISCUSSION

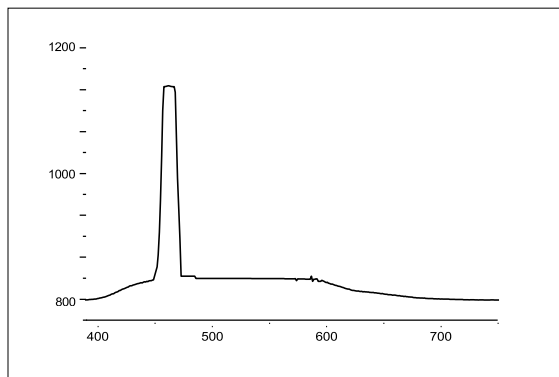


**Fig. 2:** Emission peak of CDs at 466 nm

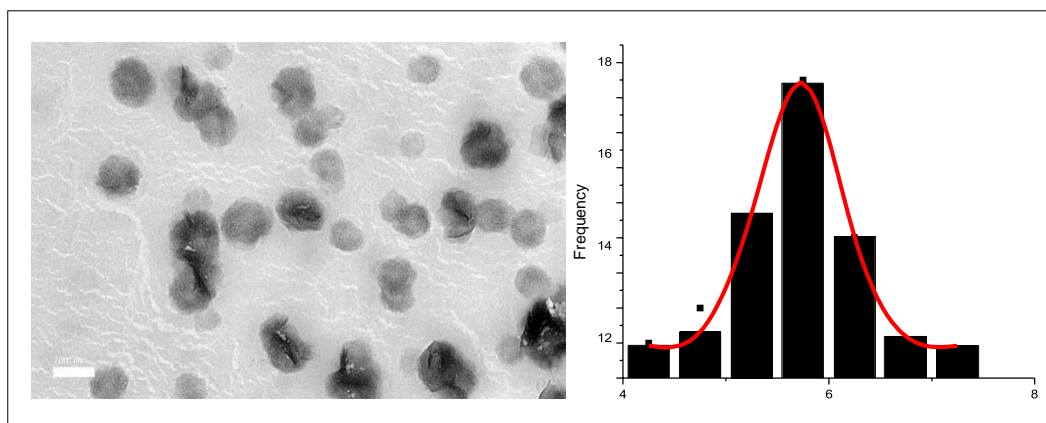


**Fig. 3:** a) HR-TEM images of CDs - EDA and b) histogram show a particle size distribution CD -EDA

## CONCLUSIONS

In conclusion, chitosan-carbon dots have been successfully developed with loaded mitomycin C. This research is contributed to non-muscle invasive bladder cancer treatment. To improve the therapeutic effect of the drug.

## REFERENCES

- [1] Saginala, K.; Barsouk. A.; Aluru, J. K.; Rawla. P.; Padala, S. A.; Barsouk. A.; Epidemiology of Bladder Cancer. Med. Sci. 2020, 8, 15.
- [2] Shelley, M. D.; Wilt. T. J.; Court. J.; Coles. B.; Kynaston. H.; Mason. M. D. Intravesical bacillus Calmette- Guérin is superior to mitomycin C in reducing tumour recurrence in high-risk superficial bladder cancer: A meta-analysis of randomized trials. BJU International 2004;93(4):485.

## The Toxicity Evaluation of Selected Nanoparticles on *Artemia Salina*

Emmellie Laura Albert<sup>1</sup>, Nurul Anis Athirah Ab Aziz<sup>2</sup>, Amir Faiz<sup>3</sup>, Dharshini Perumal<sup>3</sup>, Lau Gee Een<sup>3</sup>, Ashreen Norman<sup>1</sup>, and Che Azurahaman Che Abdullah<sup>1,3,4\*</sup>

<sup>1</sup>Nano Synthesis and Characterisation Laboratory, Institute of Nanoscience and Nanotechnology, Universiti Putra Malaysia, 43400 Serdang, Selangor, Malaysia.

<sup>2</sup>Department of Physics, Faculty of Science, Universiti Teknologi Malaysia, Jalan Hikmah, 81310 Skudai, Johor, Malaysia

<sup>3</sup>Biophysics Laboratory, Department Physics, Faculty of Science, Universiti Putra Malaysia, 43400 Serdang, Selangor, Malaysia.

<sup>4</sup>UPM-MAKNA Cancer Research Laboratory Institute of Bioscience, Universiti Putra Malaysia, 43400 Serdang, Selangor, Malaysia

\*Corresponding Author's Email: azurahaman@upm.edu.my

**Abstract:** This study investigated the toxicity of different kind of nanoparticles such as iron (III) oxide, graphene oxide, zinc oxide, and titanium oxide to *Artemia Salina* (*A. Salina*). The nanoparticles are of special interest due to their exceptional physicochemical properties. They are used in a wide range of application thus it is inevitably release to marine ecosystem. *A. Salina* is selected as the model organism to test the marine toxicity because it is the primary food for most marine animal. Hatching rate of *A. Salina* expose to the nanoparticles was observed and analyse to understand the toxicity of nanoparticles toward *A. Salina*.

**Keywords:** *Artermia Salina*, Toxicity, Nanoparticles, Iron (III) Oxide, Graphene Oxide, Titanium Dioxide, and Zinc Oxide

## INTRODUCTION

Nanoparticles (NPs) such as Iron (III) Oxide (IO), Graphene Oxide (GO), Zinc Oxide (ZnO) and Titanium Dioxide (TiO<sub>2</sub>) are of special interest due to their exceptional physicochemical properties, which make them highly suitable and desirable for many consumer products and industrial technologies. All the NPs will eventually infiltrate aquatic habitats, particularly marine ecosystems [1,2], hence it is imperative to understand their biological impact to the ecosystem. The purpose of this study is to look at the ecological imbalance possibilities of NPs (IO, GO, RGO, ZnO, and TiO<sub>2</sub>) in crustaceans like *A. Salina*, which are at the top of the food chain. We examined the hatchability of capsulated cysts following NPs exposure in order to determine the adverse reactions that occur after prolonged acute exposure.

## MATERIALS AND METHODS

All NPs are successfully fabricated in the Biophysics Laboratory at UPM. NPs suspension with different concentration were prepared by simply mixing it with artificial saltwater. Twenty (20) capsulated cysts were put inside the 96-well plates, and each well contained 200uL test solution. All plates were incubated at 28 °C under a continuous illumination. A microscope was used to determine the hatchability of capsulated cysts in each treatment at various time

points.

## RESULTS AND DISCUSSION

The uptake of NPs by *A. Salina* was observed using a microscope. After exposure, larvae started to ingest the nanoparticles. Gradually, the gut became almost completely filled with the nanoparticle, as indicated by the presence of a dark line inside the gut. Finally, *A. Salina* excreted the accumulated nanoparticle. All NPs responded dose dependently to the hatching rate of the cyst [3–5]. The dosage, on the other hand, is dependent on the type of NP. Acute exposure of nanoparticles to *A. Salina* cysts and larvae alters hatchability and physiological parameters significantly. The toxic effects of nanoparticles were taken into account.

## CONCLUSIONS

The toxicity of the NPs to *A. Salina* depends on the type of NPs. When exposed to nanoparticles, *A. Salina* is able to survive at low concentrations of IO, GO, and TiO<sub>2</sub>. But when *A. Salina* are exposed to ZnO synthesised from palm oil leaves and roselle, they cannot hatch.

**ACKNOWLEDGMENT:** The authors are grateful for the financial support from the Ministry of Higher Education of Malaysia under Fundamental Research Grants Scheme (FRGS) (Vot. No. 5524949) and Dana Tautan Grant (DT0021) from UPM.

## REFERENCES

- [1] Scown TM, Van Aerle, R, Tyler CR, *Crit. Rev. Toxicol.*, 2010, **40**, 653–670.
- [2] Xiaoxiao C, Xing Z, Rui L, Hanchao Y, Zhisong L, Xu Y, *Open J. Ecol.*, 2012, 2012.
- [3] Zhu S, Xue MY., Luo F, Chen WC., Zhu B, Wang GX., *Environ. Pollut.*, 2017, **230**, 683–691.
- [4] Danabas D, Ates M, Ertit Tastan B, Cicek Cimen IC, Unal I, Aksu O, Kutlu B, *Sci. Total Environ.* 2020, **711**, 134869.
- [5] Ates M, Daniels J, Arslan Z, Farah IO, Rivera HF, *Environ. Sci. Process. Impacts* 2013, **15**, 225–233.



## Optimization, Characterization and Toxicity Studies of Gold Nanoparticles as Potential Biocompatible Carrier for Colon Cancer Treatment

Siti Nadiah Zulkifli<sup>1,3</sup>, Manali Haniti Zahid<sup>2</sup>, Iskandar Zulkarnain Alias<sup>2</sup>, Mohamad Faizal Ibrahim<sup>4</sup> and Che Azurahanim Che Abdullah<sup>1,3</sup>

<sup>1</sup>*Institute of Nanoscience and Nanotechnology (ION2), Universiti Putra Malaysia, 43400 Serdang, Selangor*

<sup>2</sup>*Department of Chemical Pathology, School of Medical Sciences, Health Campus, Universiti Sains Malaysia, 16150 Kubang Kerian, Kelantan*

<sup>3</sup>*Department of Physics, Faculty of Science, Universiti Putra Malaysia, 43400 Serdang, Selangor*

<sup>4</sup>*Department of Bioprocess Technology, Faculty of Biotechnology and Biomolecular Science, Universiti Putra Malaysia, 43400 Serdang, Selangor*

\*Corresponding Author: [azurahanim@upm.edu.my](mailto:azurahanim@upm.edu.my)

**Abstract:** The gold nanoparticles (AuNPs) used in this research were chosen due to their widespread use in a variety of applications. Recent studies have discovered numerous advantages of AuNPs over other nanomaterials, owing primarily to highly optimised protocols for the development of AuNPs in a variety of sizes and shapes with unique properties. Both chemical and green synthesis approaches were successfully synthesized by modifying the Turkevich method. This is significant because it relates to the environmental safety of their manufacturing processes. X-ray diffraction (XRD), ultraviolet visible spectrophotometry (UV-Vis), and Fourier transform infrared (FTIR) spectroscopy were used for characterization. After that, the toxicity of AuNPs was tested using brine shrimp for determining the safety of a nanocarrier for colon cancer treatment.

**Keywords:** Gold Nanoparticles (AuNPs), Chemical Synthesis, Green Synthesis, Turkevich Method

### INTRODUCTION

For over a decade, nanoparticles have been evaluated and used in a variety of industrial applications. AuNPs have generated considerable interest due to their diverse properties that make them suitable for future biomedical applications. AuNPs are widely used in a variety of biomedical applications due to their small size to volume ratio and high thermal stability (Tiwari et al. 2011). Citrate's reduction and capturing capacity have been demonstrated to be related to its structure, specifically the hydroxyl group attached to the carboxyl group (Bartosewicz et al., 2018). This research employs a modified Turkevich method to synthesis AuNPs and investigates the effect of parameter on the synthesized AuNPs to achieve optimized products. This research compared the characterization of two methods.

### MATERIALS AND METHODS

At room temperature, a few mL of gold precursor was stirred, and then diluted sodium citrate was added to the solutions for the modified Turkevich's Method. Gold solution changes colour

from light yellow to dark red wine, indicating the presence of AuNPs. The same procedure was repeated for green synthesis, but with tea polyphenols in place of the citrate solution.

## RESULTS AND DISCUSSION

Due to its simplicity, the modified Turkevich's Method is regarded as the most representative and frequently used technique for the synthesis of AuNPs. FTIR analysis revealed the presence of various functional groups in the synthesized AuNPs, as depicted in figure 1, while figure 2 shows the hatching rate of brine shrimp. FTIR spectroscopy detected the presence of different functional groups in the synthesized AuNPs and the findings were shown in figure 1.

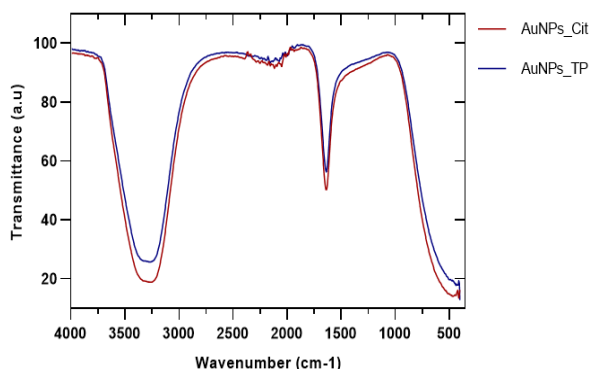


**Fig. 1** FTIR spectra of synthesized AuNPs by citrate and tea polyphenols

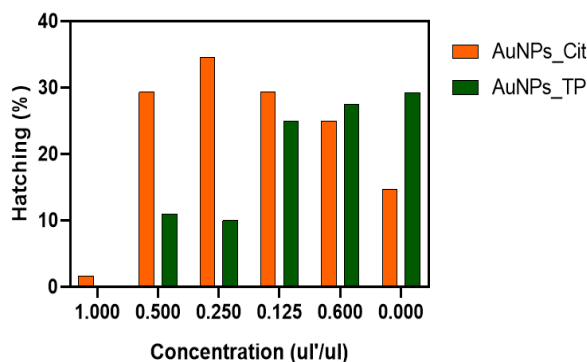


**Fig. 2.** Hatching rate of brine shrimp *Artemia nauplii* treated with AuNPs synthesized by chemical and biological methods.

## CONCLUSIONS

A comparative analysis of the characterization of two methods was conducted. Both chemical and green synthesis approaches were successfully synthesized by modifying the Turkevich method. These AuNPs were synthesized via the reduction of citrate and tea polyphenols, which act as a reducing and capping agent, respectively. AuNPs have been tested for toxicity in biomedical applications using brine shrimp.

## REFERENCES

- [1] Tiwari, P. M., Vig, K., Dennis, V. A., & Singh, S. R. (2011). Functionalized gold nanoparticles and their biomedical applications. *Nanomaterials*, 1(1), 31-63.
- [2] Irvani, S. (2011). Green synthesis of metal nanoparticles using plants. *Green Chemistry*, 13(10), 2638-2650.
- [3] Bartosewicz, B., Bujno, K., Liszewska, M., Budner, B., Bazarnik, P., Płociński, T., & Jankiewicz, B. J. (2018). Effect of citrate substitution by various  $\alpha$ -hydroxycarboxylate anions on properties of gold nanoparticles synthesized by Turkevich method. *Colloids and Surfaces A: Physicochemical and Engineering Aspects*, 549, 25-33.
- [4] Jafarizad, A., Safaei, K., Gharibian, S., Omid, Y., & Ekinci, D. (2015). Biosynthesis and in-vitro study of gold nanoparticles using *Mentha* and *Pelargonium* extracts. *Procedia Materials Science*, 11, 224-230.

## Preparation, Cytotoxicity and Apoptotic Properties of Gallic Acid Nanoparticles Against Human HepG2 Cell lines

Abdelkader Hassani<sup>1,2</sup>, Mohamed Lakhder Belfar<sup>1</sup>, Zenkhri Louiza<sup>1</sup>, Hakim Belkhalifa<sup>3</sup>,  
Abdullah Hajar<sup>4</sup>, Samiullah Saeed<sup>5</sup> and Siti Aslina Hussain<sup>2,\*</sup>

<sup>1</sup>Department of Chemistry, Faculty of Mathematics and Material Sciences, University of kasdi Murbah, Ouargla, Algeria.

<sup>2</sup>Department of Chemical and Environmental Engineering, University Putra Malaysia, Serdang 43400, Malaysia.

<sup>3</sup>Scientific and Technical Research Center in Physicochemical Analysis, Bou-Ismaïl, Tipaza, Algeria

<sup>4</sup>Department of Nutrition Sciences, Faculty of Allied Health Sciences, International Islamic University Malaysia, 25200, Kuantan, Malaysia

<sup>5</sup>Department of Anaesthesiology and Critical Care, Faculty of Medecine, International Islamic University Malaysia, 25200, Kuantan, Malaysia

\*Corresponding Author's Email: [aslina@upm.edu.my](mailto:aslina@upm.edu.my)

**Abstract:** Gallic acid (GA) is considered as a phenolic compound whose therapeutic effects are often limited by its rapid metabolism and removal. To increase GA bioavailability, gum arabic was used to encapsulate it in nanoparticles. The size and physicochemical properties of prepared gallic acid nanoparticles (GANPs) were studied. The main objective of this study was to investigate how gallic acid nanoparticles (GANPs) affected the in vitro cytotoxicity of human liver cancer HepG2 and normal liver Chang cells. The cytotoxicity activity of GA nanoparticles toward Chang and liver cancer HepG2 cells was assessed based on MTT (3-(4,5-dimethylthiazol-2-yl)-2,5-diphenyltetrazolium bromide). colorimetric test, cell cycle flow cytometry analysis, and Trypan blue assay. GANPs inhibited HepG2 cells growth in the MTT assay ( $IC_{50} = 10.13 \mu\text{g/mL}$ ), with less toxicity in Chang cells ( $IC_{50} = 41.27 \mu\text{g/mL}$ ) after 72h. In the trypan blue assay, the number of viable HepG2 cells exhibited a sharp decline until  $(3.5 \pm 0.64 \times 10^5 \text{ cells/mL})$  after 72 h of incubation. GANPs exhibited strong cytotoxicity toward HepG2 cells through induction of apoptosis and suppression of proliferation.

**Keywords:** Gallic acid, HepG2 cells, liver Chang cells, nanoparticles.

### INTRODUCTION

To date, researchers have focused on the extraction of compounds from plants in order to improve the efficiency of anticancer treatments such as flavonoids [1,2]. Gallic acid is a natural triphenol extracted from plants and used for various biological and pharmaceutical applications [3,5]. Gum arabic is a polymer extracted naturally from Acacia species that is used in a range of therapeutic applications as an emulsifier or stabilizer [6]. The current research aims to assess the cytotoxicity of GANPs against Human liver cancer (HepG2) and normal liver Chang cell line based on various tests.

### RESULTS AND DISCUSSION

GANPs have been successfully synthesized using the freeze-drying process. Gum arabic was

given as an amorphous substance in this diffraction. The GANPs displayed a significant toxicity against HepG2 cells at high concentration (100  $\mu\text{g/mL}$ ) and a considerable decrease of cell viability at low concentration (1.56  $\mu\text{g/mL}$ ) as depicted in Figure 1. The results mentioned that GANPs induced cell cycle in the HepG2 cells treated with IC<sub>50</sub> levels of GANPs recorded by MTT assay for 24, 48, and 72 hours. Moreover, GANPs exhibited a time-dependent effect on the cell cycle of normal Chang cells at IC<sub>50</sub> concentrations.

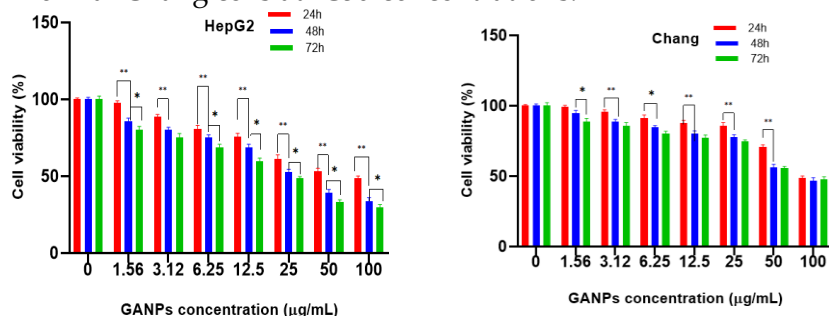


**Fig.1.** Cytotoxicity effects of GANPs treatment in HepG2 (A) and Chang cells (B) and doxorubicin treatment in HepG2 (C) and Chang cells (D) after 24, 48, and 72 hours of treatment.

The cytotoxicity effect of GANPs might be due to its ability to induced marked apoptotic cell death after 24h of exposure. Therefore, after 72 hours of incubation in this study, a decrease in the accumulation of G2/M phase was related to an apoptotic cell death representing the main inducer of toxicity.

## CONCLUSION

GANPs exhibited potent cytotoxicity effect against human liver cancer HepG2 cells as it decreased the cell viability after 72 h of treatments. The HepG2 cells were more sensitive to GANPs as it has a lower IC<sub>50</sub> value (IC<sub>50</sub> = 10.13 after 72 h) in compared to the normal Chang cells. The in vitro selective inhibitory activity of GANPs revealed the antitumor activity of this phenolic compounds as a novel antitumor agent candidate for the treatment of liver cancer.

## REFERENCES

- [1] Benavente-Garcia O, Castillo J, Marin F.R, Ortun A. *J. Agric. Food Chem*, 2015,**45**,1–96.
- [2] Galati G, Brien P.J.O. *Free Radic. Biol. Med*, 2004,**37**,287–303.
- [3] Aborehab1 N.M, Osama N. *Cancer Cell Int*, 2019,**19**,154 .
- [4] OwyY, Stupans I. *Curr. Drug Metab*, 2003, **4**, 241–248.
- [5] Luciane A, Savi Paulo C, Leal T.O, Rober R, Ricardo J, Nunes R.A. *Drug Res*, 2005,**75**, 66–75.
- [6] Ali B. *Phytomedicine*,2011, **18**, 1176–1180.

## Nano-Hydroxyapatite-based Scaffolds for the Delivery of Bone Morphogenetic Protein-2 (BMP-2) to Promote Bone Regeneration

Anis Syauqina Mohd Zaffarin<sup>1</sup>, Shiow-Fern Ng<sup>2</sup>, Min Hwei Ng<sup>3</sup>, Haniza Hassan<sup>4\*</sup> and Ekram Alias<sup>1\*</sup>

<sup>1</sup>Department of Biochemistry, Faculty of Medicine, Universiti Kebangsaan Malaysia, 56000 Bandar Tun Razak, W.P. Kuala Lumpur, Malaysia

<sup>2</sup>Faculty of Pharmacy, Universiti Kebangsaan Malaysia, 50300 Kuala Lumpur, W.P. Kuala Lumpur, Malaysia

<sup>3</sup>Centre for Tissue Engineering and Regenerative Medicine, Universiti Kebangsaan Malaysia, 56000 Bandar Tun Razak, W.P. Kuala Lumpur, Malaysia

<sup>4</sup>Department of Human Anatomy, Faculty of Medicine and Health Sciences, Universiti Putra Malaysia, 43400 UPM Serdang, Selangor, Malaysia

\*Corresponding Authors' Email: ekram.alias@ppukm.ukm.edu.my (E.A.); nizahassan@upm.edu.my (H.H.)

**Abstract:** Bone morphogenetic protein-2 (BMP-2) is an osteoinductive protein that used to induce bone regeneration. However, the limitation of using BMP-2 for therapy include its burst release upon administration and short half-life. Nano-hydroxyapatite (nHA) is widely used as an orthopedic biomaterial and vehicle for the delivery of various drugs. This systematic review aims to critically evaluate the effectiveness of nHA-based scaffolds in promoting bone regeneration and whether the conjugation of BMP-2 further improves osteogenesis. After a thorough literature screening process, only 8 articles were considered eligible for this review. nHA-based scaffolds were able to induce bone regeneration, and the incorporation of BMP-2 and other proteins further improved the bone formation process.

**Keywords:** nano-hydroxyapatite, bone morphogenetic protein, scaffolds, bone regeneration.

### INTRODUCTION

Bone morphogenetic protein-2 (BMP-2) belongs to the large family of transforming growth factor-beta (TGF- $\beta$ ) which has a good osteoinductive property [1]. Despite this benefit, its application in therapy is limited due to short half-life and burst release upon administration [2]. Hence, a delivery vehicle is required to prolong the bone-forming activity and reduce the required amount of BMP-2. Nano-hydroxyapatite (nHA) has an excellent biodegradability and osteoconductivity [3]. It has a small particle size of less than 100 nm and mimics the bone minerals which will provide a suitable surface for drugs and cells adhesion [4,5]. The aim of this review is to critically analyze the literatures obtained from different databases, specifically on the application of BMP-2-loaded-nHA scaffold in promoting bone regeneration in vivo. Generally, all studies showed that nHA-based scaffolds successfully induced bone regeneration in animal models with artificial bone defects. The conjugation of BMP-2 and other bioactive molecules were found to further enhance and accelerate the bone regeneration process.

### MATERIALS AND METHODS

The literature search was conducted on two databases (Scopus and Ebscohost) with a combination of specific keywords. Articles will be excluded if the nHA was used in dental



application, not nano-sized, biomaterials other than nHA was used, study only reported the characterization of nHA as a delivery vehicle, outcomes were not measured in bone tissues, studies did not apply nHA for bone regeneration, nHA was not used as a delivery vehicle, and study only reported the toxicity. Non-primary studies, case reports, proceedings abstracts, editorials, letters, comments to the editor, reviews, meta-analyses and book chapters were also excluded. Full-text articles were retrieved, screened, and the relevant details were extracted.

## RESULTS AND DISCUSSION

### 1.1 *Studies Selection and Characteristics*

At the end of the screening process, a total of 14 articles reported the application of nHA as a delivery system for various drugs and bioactive molecules. However, with regards to the scope of the current review, only 8 articles that applied nHA-based scaffold for the delivery of BMP-2 were included in this review. All eligible articles involved different animal models with large or critical-sized defects created on the bone or induced with an open fracture.

### 1.2 *Effect of BMP-2-loaded nHA-based Scaffold on Bone Regeneration*

All studies reported that animals implanted with nHA-based scaffolds showed an effective bone regeneration compared to animals with untreated defects. Furthermore, the conjugation of nHA-based scaffolds with BMP-2 alone or in combination with vascular endothelial growth factor (VEGF), basic fibroblast growth factor (bFGF) or zoledronic acid (ZA) further improve the bone regeneration process. The conjugation of BMP-2 with nHA resulted in a controlled and sustained release of BMP-2, hence, the BMP-2-induced bone formation is prolonged.

## CONCLUSIONS

In summary, nHA-based scaffolds were able to promote bone regeneration in animal models with artificial bone defects. The conjugation of BMP-2 with nHA-based scaffolds also enhanced and accelerated the bone regeneration process. Although it can be proposed that nHA may be a suitable delivery vehicle for BMP-2, the effectiveness of the delivery system is unknown. Future studies should compare the effects of BMP-2 treatment alone with BMP-2-loaded nHA-based scaffold to evaluate whether the delivery system improved the bone-forming ability of BMP-2.

**ACKNOWLEDGMENTS:** The authors would like to express appreciation for the support of the sponsors [Project Number = FRGS/1/2019/STG05/UKM/02/1].

## REFERENCES

- [1] Heubel B, Nohe A. *J. Dev. Biol.*, 2021. 9(3)
- [2] Zhou M, Geng YM, Li SY, Yang XB, Che YJ, Pathak JL, Wu GJ. *Nanomater.*, 2019.
- [3] Canillas M, Pena P, de Aza AH, Rodríguez MA. *Boletín de la Sociedad Española de Cerámica y Vidrio*, 2017. 56(3)
- [4] Zhou H, Lee J. *Acta Biomater.*, 2011. 7(7)
- [5] Ghiasi B, Sefidbakht Y, Rezaei M. In *Nanomaterials for Advanced Biological Applications*. 2019, Springer, Cham.



## Synthesis of Hydroxyapatite/Montmorillonite Nanocomposite as a Carrier for Methotrexate Drug

Rosnah Nawang<sup>1,\*</sup>, Mohd Zobir Hussein<sup>1</sup>, Khamirul Amin Matori<sup>1,2</sup> and Che Azurahaman Che Abdullah<sup>1,2</sup>

<sup>1</sup>*Institute of Nanoscience and Nanotechnology, Universiti Putra Malaysia, Serdang, Selangor, Malaysia*

<sup>2</sup>*Department of Physics, Faculty of Science, Universiti Putra Malaysia, 43400 UPM Serdang, Selangor, Malaysia*

\*Corresponding Author's Email: rnawang@upm.edu.my

**Abstract:** Hydroxyapatite/montmorillonite clay nanocomposite was prepared by the powder sintering technique to be used as a nanocarrier for methotrexate drug. Drug loading was performed using the adsorption method by soaking the pellet samples in the drug solution. The addition of montmorillonite clay into hydroxyapatite reduced the specific surface area of the resulting nanocomposite hence resulting in a lower percentage of drug loading into the nanocomposite. However, the addition of montmorillonite clay has prolonged the release time of the drug from the nanocomposite which suggested the potential use of the nanocomposite as a carrier for slow drug release application.

**Keywords:** Hydroxyapatite, montmorillonite, methotrexate, powder sintering.

### INTRODUCTION

Methotrexate (MTX) is a widely used drug for various cancer treatments, including bone cancer. MTX is administered into the body by oral or by injection. Although it can kill cancer cells, it also gives adverse side effects to the patients. The common side effects are nausea, vomiting, feeling tired and loss of appetite, whereas the major side effect is hepatotoxicity (1). To reduce/avoid the unwanted adverse side effect, a controlled drug release system can be used to give high efficiency and low toxicity of chemotherapy. Hydroxyapatite-based drug carrier for controlled drug release system has attracted many researchers because of its chemical similarity with the human bone as well as its ability to deliver the drug in a sustained manner. Therefore, in this work, hydroxyapatite (HA)/montmorillonite (MMT) clay nanocomposite was prepared to explore its potential use as a drug nanocarrier for a slow drug release system.

### MATERIALS AND METHODS

The hydroxyapatite (HA)/montmorillonite (MMT) nanocomposite was prepared by mixing HA powders with MMT clay in the ratio of HA: MMT 50:50 (wt/wt %) on a rolling mill at 50 rpm for 26h. The nanocomposite powder was then pressed into a cylindrical shape of pellet and then sintered at 800 °C for 2 hrs. The Brunauer-Emmett-Teller (BET) specific surface area analysis was performed by the adsorption-desorption of nitrogen gas at liquid nitrogen temperature (77K). Drug loading was done by soaking the pellet samples in MTX drug solution at 37 °C in a water bath shaker for 24 hrs. Drug release was carried out in a phosphate buffer saline (PBS) solution at 37 °C. The concentration of the drug solution was measured using a UV-Vis spectrophotometer.

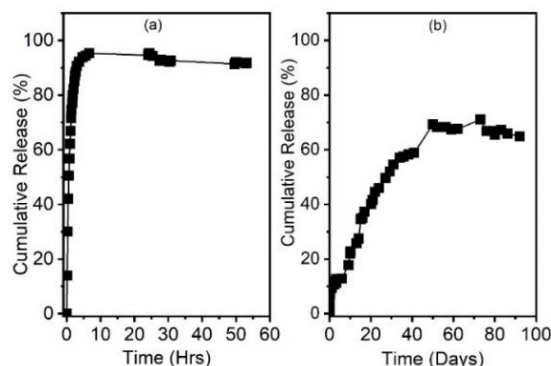
## RESULTS AND DISCUSSION

Table 1 shows the BET specific surface area (SSA), total pore volume (TPV), average pore width, and the percentage drug loading for HA and the nanocomposite carrier. The addition of MMT reduced the SSA, TPV and average pore size of the nanocomposite due to the improvement of packing density. The nanocomposite shows a lower percentage of drug loading compared to HA which could be contributed to the lower SSA, TPV and pore width of the nanocomposite (2).

Figure 1 shows the drug release profile for HA and the nanocomposite. HA showed two stages of MTX release. The fast release occurred within the first 90 min. About 70% of MTX was released in this stage. After that, the release rate is much slower and then reached its maximum release of approximately 95% after 6 hrs. The nanocomposite shows a longer release time compared to HA. The fast release occurred within the first two days with 10% of MTX release. It reached its maximum release of about 70% on day 50.

**Table 1.** BET specific surface area, total pore volume and average pore diameter of HA and nanocomposite carriers and the percentage drug loading of the carriers

Drug carrier	BET specific surface area m <sup>2</sup> /g	Total pore volume cm <sup>3</sup> /g	Average pore width (nm)	% Drug loading
HA	20	0.045	5.38	17.88
nanocomposite	13	0.037	5.27	6.93



**Fig. 1.** The in-vitro release profiles of a) HA and b) its nanocomposite

## CONCLUSIONS

The addition of MMT clay reduced the percentage of drug loading due to the reduction of SSA, TPV and pore size of the nanocomposite, but it prolonged the drug release time.

**ACKNOWLEDGMENT:** The authors would like to express appreciation to Universiti Putra Malaysia for providing Putra Geran [GP-IPM/2019/9678500, Vot No. 9678500].

## REFERENCES

- [1] **Webpage:** <https://www.ncbi.nlm.nih.gov/books/NBK556114/>
- [2] Bavnhoj CG, Knopp MM, Madsen CM, Löbmann K. *Int J Pharm X*. 2019;1(December 2018):1–5.

## Theranostic System using Novel Chitosan-based Nanoimmunosensing Antibody/Aptamer Assembly for Dual Application Sites of Bladder Cancer Cell Targeting and Drug Release

Fariza Aina Abd Manan<sup>1</sup> and Nor Azah Yusof<sup>1,2\*</sup>

<sup>1</sup>Institute of Nanosciene and Nanotechnology, Universiti Putra Malaysia, 43400 UPM Serdang, Selangor, Malaysia

<sup>2</sup>Department of Chemistry, Faculty of Science, Universiti Putra Malaysia, 43400 UPM Serdang, Selangor, Malaysia

\*Corresponding Author's Email: [azahy@upm.edu.my](mailto:azahy@upm.edu.my)

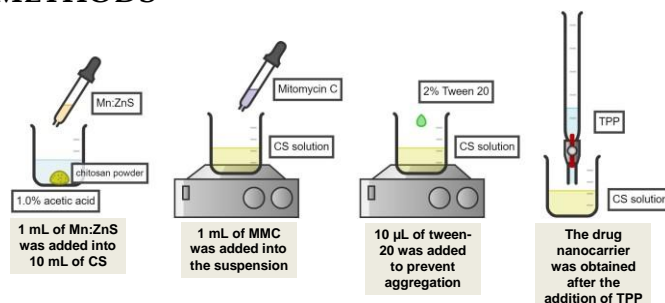
**Abstract:** In this current work, we reported the synthesis and characterization of Mn:ZnS quantum dots conjugated chitosan-based nanocarriers for encapsulation of Mitomycin C labelled as MMC@CS-Mn:ZnS nanocarriers. The drug loading capacity, drug encapsulation efficiency and release properties of the MMC@CS-Mn:ZnS nanocarriers system were evaluated at a fixed wavelength of 358 nm using a NanoDrop UV-Vis spectrophotometer. The cumulative release of MMC was calculated as 62.48% and 60.22% in medium with pH 6.8 and pH 7.2, respectively. The formulated nanocarrier system of Mitomycin C exhibit efficient delivery of the drugs at target cancerous site in non-muscle invasive bladder diseases.

**Keywords:** chitosan nanoparticles; quantum dots; drug delivery systems; nanocarriers, cancer cell therapy

### INTRODUCTION

The conventional method for the administration of several drugs by chemotherapeutic approaches exhibit excellent curative effects; however, they suffered from poor pharmacokinetics, poor selectivity, poor distribution, high toxicity, slow clearance of the administered drugs, and drug resistance over a period of therapy. Hence, drug delivery system has been implemented with high specificity, good biodistribution, prolonged systemic circulation, low toxicity, and invasive molecular imaging for targeted and controlled drug delivery system [1]. Besides, drug delivery system has improved the biocompatibility of drug with the cells and tissues, increase the intracellular uptake, retain the stability of drugs and improve the ability of drugs to be delivered to the targeted specific cells or tissues while sparing the normal cells [2]. In this study, we successfully synthesized chitosan based-nanocarrier conjugated with Mn:ZnS quantum dots (CS-Mn:ZnS) to improve the bioavailability of mitomycin c (an anticancer drug) for active targeted cancer cell therapy.

## MATERIALS AND METHODS



## RESULTS AND DISCUSSION

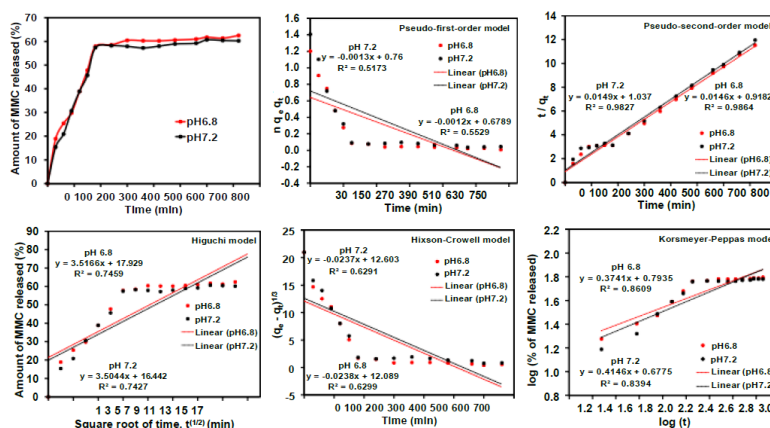


**Fig. 1.** Drug release data fitted with five different pharmacokinetics models at release medium with pH 6.8 and pH 7.2.

## CONCLUSIONS

In conclusion, excellent MMC@CS-Mn:ZnS drug delivery system for non-muscle invasive bladder cancer has been successfully developed with moderate drug loading capacity that improve chemotherapeutic efficiency. Hence, MMC@ CS-Mn:ZnS nanocarriers could be contemplated as an appropriate drug delivery system with suitable efficiency for non-muscle invasive bladder cancer, which necessitate further in vivo investigations in future work.

**ACKNOWLEDGMENT:** The authors acknowledged the research grant that was funded by Universiti Putra Malaysia (UPM) and the Ministry of Higher Education of Malaysia under the IPB research grant vote no. 9660200 (GP-IPB/2018/9660200).

## REFERENCES

- [1] D. Kukkar, P. Kukkar, V. Kumar, J. Hong, K. Kim, A. Deep, Biosensors and Bioelectronics Recent advances in nanoscale materials for antibody-based cancer theranostics, Biosens. Bioelectron. 173 (2021) 112787.
- [2] C. Alejandra, O. Pe, PLGA nanoparticle preparations by emulsification and nanoprecipitation techniques: effects of formulation parameters, (2020) 4218–4231.

## Structural and Antimicrobial Evaluation of Gamma Synthesized Ag/Kln Nanocomposites

Salmah Moosa<sup>1, 2</sup>, Anis Nadia Mohd Faisol Mahadeven<sup>1</sup> and Kamyar Shameli<sup>2</sup>

<sup>1</sup>Agrotechnology and Bioscience Division, Malaysian Nuclear Agency, Bangi 4300, Selangor, Malaysia

<sup>2</sup>Malaysia-Japan International Institute of Technology, Universiti Teknologi Malaysia, Jalan Sultan Yahya Petra, 54100 Kuala Lumpur, Malaysia

\*Corresponding Author's Email: salmahmoosa@nm.gov.my

**Abstract:** A one-step silver kaolinite nanoparticles has been developed successfully using gamma irradiation technique with kaolinite as a stabilizer at room temperature and under ambient pressure. The Ag/Kln NPs produced by  $\gamma$ -irradiation technique are pure without chemical residues, with good distribution and enhanced antibacterial properties. The effects of different experimental parameters, such as concentration of Ag<sup>+</sup> and irradiation dose on the formation of NCs were studied. The successful formation of Ag/Kln NPs has been confirmed by UV-visible spectroscopy, XRD, TEM and FESEM-EDX analysis. A study on the antimicrobe susceptibility was undertaken to determine the antibacterial properties of silver nanoparticles on two test microbes from Gram positive and Gram negative bacteria namely were used as test microorganisms. Ag/Kln NPs synthesized using gamma irradiation showed significantly large zone of inhibition relative to control which indicates high antimicrobial activity compared to Ag/Kln NPs synthesized chemically. The Ag/Kln NPs of 20kGy showed highest antibacterial activity against *Enterococcus faecalis* (Gram positive) as well as *Escherichia coli* (Gram negative). These suggest that Ag/Kln NPs can be employed as an effective bacteria inhibitor and can be applied in medical field.

**Keywords:** Silver nanoparticles; kaolinite; antimicrobial;  $\gamma$ -irradiation; antimicrobial activity.

### INTRODUCTION

In the past few years, nanoparticles (NPs) have been the subject of interest among researchers for its exceptional properties that differ from other conventional macroscopic materials [1]. One of the extensively studied NPs is silver nanoparticles (AgNP). In this work, silver nitrate (AgNO<sub>3</sub>) precursor salt are adsorbed on the surface of kaolin (Kln) which acts as a reactor and synthesized using  $\gamma$ -irradiation to produce silver kaolinite nanoparticles (Ag/Kln NPs). When aqueous solution of AgNO<sub>3</sub> and Kln was exposed to ionizing radiation, Ag<sup>+</sup> is reduced to Ag<sup>0</sup> by reactive radical produced from water radiolysis. Kln, as layer structured clay mineral, is a natural material which does not swell in water hence provide support for AgNPs [10]. A study on antimicrobial susceptibility was undertaken to determine the antibacterial properties of AgNPs in the presence of gram-positive and gram-negative bacteria.

### MATERIALS AND METHODS

The silver precursor AgNO<sub>3</sub> (99%) were obtained from QR $\ddot{e}$ c (New Zealand). Meanwhile, the kaolin powder, used as solid supporter for the AgNCs was purchased from R & M Chemicals (UK). Two bacterial strains, namely *Escherichia coli* (ATCC 25922) and *Enterococcus faecalis* (ATCC 29212) were subjected to this analysis.

## RESULTS AND DISCUSSION

Results of on the microbial growth inhibition of Ag/KIn NPs produced by  $\gamma$ -irradiation synthesis against *E. coli* and *E. faecalis*, demonstrated a distinct inhibitory effect although they are larger in scale compared to AgNCs produced chemically (**Table 1**). AgNCs produced by  $\gamma$ -irradiation synthesis demonstrated a distinct inhibitory effect on the microbial growth of *E. coli* and *E. faecalis*, although they are larger in scale compared to AgNCs produced chemically. Similar results were obtained by previous studies where irradiation at 20 kGy enhanced antibacterial activity of composite films.

**Table 1:** Size of Ag/KIn NCs synthesized by chemical and  $\gamma$ -irradiation methods.

Diameter of Inhibition Zones Ag/KIn NPs				Diameter of Inhibition Zones Ag/KIn NPs	
Chemical Method				$\gamma$ -Irradiation Method	
Ag (%)	<i>E. coli</i>	<i>E. faecalis</i>	Dose (kGy)	<i>E. coli</i>	<i>E. faecalis</i>
0.5 %	9.00	6.70	7	10.61	11.00
1.0 %	8.00	6.70	13	10.67	11.04
2.0 %	8.70	7.00	<b>20</b>	<b>12.50</b>	<b>11.68</b>
<b>5.0 %</b>	<b>9.30</b>	<b>7.00</b>	30	12.00	11.57
10.0 %	8.30	7.00	40	11.50	11.25
			65	11.27	11.17
			80	11.43	11.03
<b>Gm (10 <math>\mu</math>g/ml)</b>	<b>24.30</b>	<b>13.30</b>		<b>24.30</b>	<b>13.30</b>

## CONCLUSIONS

Gamma irradiation is a powerful tool, causing radiolysis and breaking of the strong Van der Waals bonding allowing the release of Ag<sup>+</sup> and increasing the antibacterial potential of the gamma synthesised NPs. Gamma synthesized NPs showed higher antimicrobial activity (63-107%) with a significant difference of  $p < 0.005$  compared to the result of chemical synthesis (33-77%). This manifests future potential of these NPs against pathogenic microorganisms and creates more window of opportunity for research in this subject. Further studies for dose optimisation and toxicity of these materials are needed to enable its implication and use of these NPs to formulate novel antibacterial materials for various applications.

**ACKNOWLEDGMENTS:** The authors indebted to Ministry of Higher Education for full funding under FRGS/1/2018/TKT10/MOSTI/02/2 and to Director of Malaysian Nuclear Agency for providing necessary facilities. The authors would like to express appreciation for the support of  $\gamma$ -irradiation by Sinargama facility group and the MTEG department for XRD, TEM and FESEM analysis facility.

## REFERENCES

- [1] S. S. Behera, S. Jha, M. Arakha, and T. K. Panigrahi, "Synthesis of Silver Nanoparticles from Microbial Source-A Green Synthesis Approach , and Evaluation of its Antimicrobial



## Hydrothermal Synthesized Stable and Reusable Tin Sulfide Filled Cellulose Photocatalysts and their Application in Dye Degradation

Jyoti Bala Kaundal<sup>1,2\*</sup> and Y. C. Goswami<sup>1,2</sup>

<sup>1</sup>Nano research lab ITM University Gwalior,

<sup>2</sup>SOS Physics, Jiwaji University Gwalior

\*Corresponding Author's Email: [ycgoswami@gmail.com](mailto:ycgoswami@gmail.com), [kaundal.jyoti@gmail.com](mailto:kaundal.jyoti@gmail.com)

**Abstract:** SnS nanostructures were grown using the hydrothermal method. Samples were characterized by structural, morphological, and optical studies. All the peaks in the X-ray diffractogram are identified and indexed as orthorhombic structure. Scanning electron microscopy studies confirm the formation of orthorhombic structures obtained. EDS confirms the composition of SnS nanoparticles. An optical study shows good luminescence in the visible region. A strong quantum effect was evident from the far blueshifted optical direct and indirect band gap. 90% to 98 % of Methylene red dye removal from wastewater.

**Keywords:** Nanostructures, hydrothermal method, Photocatalyst bag, SnS

### INTRODUCTION

Semiconductor nanostructures, owing to their particular application in electronic and sensor devices have gained great research potential interest. Since the photon energy should be equal to or greater than the bandgap energy of the photocatalyst, activation wavelength is an important parameter in the photocatalytic process [1]. In the visible and near-infrared regions of the spectrum, metal sulfide semiconductor nanoparticles produce light; therefore, it makes them visible light-driven photocatalysts [2-3]. At the nano range, these photocatalytic properties of semiconductors are morphological and structural dependent [3-4]. Tin sulfide (SnS) nanostructure is a p-type semiconductor with a direct bandgap between 1.39 eV and 2.33, and indirect bandgap of between 1 eV and 1.5 eV, which depend on the preparation method and its heat treatment temperature [5]. Due to the unique properties of SnS such as low toxicity, earth abundance, and high chemical stability, it has attracted a large number of research interests [1,6]. In this paper, we will observe the changes in photocatalytic activity of SnS nanoparticles when we manipulate the pH concentration.

### MATERIALS AND METHODS

Tin (II) chloride ( $\text{SnCl}_2 \cdot 2\text{H}_2\text{O}$ ) and sodium sulfide ( $\text{Na}_2\text{S}$ ) were taken as tin and sulfur sources respectively and Ethylene Glycol (EG) was used as a solvent. 0.1M of  $\text{SnCl}_2 \cdot 2\text{H}_2\text{O}$  dissolved in 90ml of EG and 0.1M of  $\text{Na}_2\text{S}$  in 80ml of EG continuously stirred for 3 hour, then kept in ultrasonicator for other 30 mins at 60°C. 0.1M  $\text{SnCl}_2 \cdot 2\text{H}_2\text{O}$  solution was added dropwise into the  $\text{Na}_2\text{S}$  solution and the solution is kept in an oven at 180°C. The precipitated particles were centrifuged and washed with ethanol and distilled water for several times. The reusable photocatalyst fillers were prepared by adding SnS particles in non-woven cellulose paper fillers. Photocatalytic degradation activity of SnS nanoparticles was performed with anionic methylene red dye in the visible region of the wavelength 400 nm to 700 nm.

## RESULTS AND DISCUSSION

In Fig. 1, the anionic dye, the adsorption is bigger at an occasional pH2 value and reduces, because the pH increased because a more charged sulfonate group is present within the methyl Red dye. About 90% dye degraded within 60 minutes.

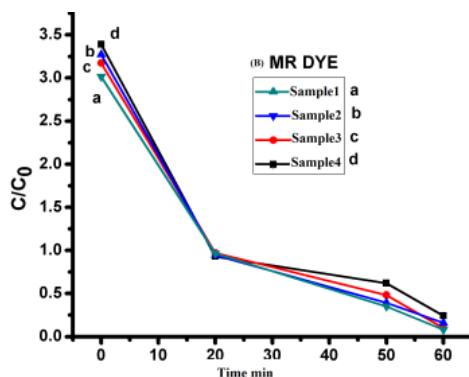


**Fig. 1.** The rate of concentration and percentage of degradation of MR dye within 60 min in the first cycle (A) Sample1 (B) Sample2 (C) Sample3 (D) Sample4

## CONCLUSIONS

This work presents the hydrothermal growth of SnS Nanoparticles and inclusions in now oven cellulose files to be used as photocatalysts. The crystallinity decreases as the pH values increases. SEM confirms the formation of SnS nanoparticles with the help of data. The SnS material shows excellent 92% degradation of dyes and stability up to three cycles as photocatalyst.

**ACKNOWLEDGMENT:** Authors are thankful to P C ray lab ITM University Gwalior for characterizations facilities like UV-Vis spectroscopy, PL FTIR.

## REFERENCES

- [1] Li X, Yu J. G, and Jaroniec M., *Chem. Soc. Rev.*, 2016, **45**, 2603.
- [2] Caldwell M. M., *BioScience*, 1979, **29**, 9, 520-552.
- [3] Kumar V, Rajaram P, and Goswami YC, *Optic*, 2016, **127**, 2490-2494.
- [4] Goswami YC, Kumar D, Sharma R and Singh R, *Cont. Eng.Science*, 2012, **5(1)**, 1-8.
- [5] Wang Y and Herron N, *J. PHys. Chem*, 1991, **95**, 2, 525-532.
- [6] Zhang X, Zhang P, Wang LJ, Gao HQ, Zhao JT, Liang CH, Hu JH, and Shao G. S., *Appl. Catal. B*, 2016, **192**, 17.

## Photodegradation Performance by Zinc Oxide Filled in Cellulose Nanofibril Membranes and Aerogel for Decolouration of Organic Dye

Azima Azmi<sup>1,2</sup>, Kam Sheng Lau<sup>1</sup>, Siew Xian Chin<sup>3</sup>, Sarani Zakaria<sup>1</sup> and Chin Hua Chia<sup>1</sup>

<sup>1</sup>*School of Applied Physics, Faculty of Science and Technology, Universiti Kebangsaan Malaysia, 43600 UKM Bangi, Selangor, Malaysia*

<sup>2</sup>*Biotechnology and Nanotechnology Research Centre, MARDI Headquarters, Persiaran MARDI-UPM, 43400 Serdang, Selangor, Malaysia*

<sup>3</sup>*ASASIpintar Program, Pusat GENIUS@Pintar Negara, Universiti Kebangsaan Malaysia, 43600 Bangi, Selangor, Malaysia*

*\*Corresponding Author's Email: chia@ukm.edu.my*

**Abstract:** This paper discussed the photodegradation performance of cellulose filled zinc oxide (ZnO) in membranes and aerogels for the decolouration methylene blue (MB). A Photocatalysis study with a 26-watt UV lamp was done to show the efficiency of both regenerated cellulose membranes and aerogels in the process of decolouration of an organic dye such as MB which recorded optimum decolouration of 91.6% and 50.3% for membranes and aerogels respectively. A study on the effect of initial pH has also been done to ensure the best condition for the catalysis and shows pH6 is the most suitable condition for both forms

**Keywords:** : Cellulose nanofibril (CNF), membranes, aerogels, ZnO and photocatalysis

### INTRODUCTION

Cellulose has the most abundant resources in the world despite its desirable properties such as being biodegradable, biocompatible, green and containing a huge amount of hydroxyl (OH) groups [1]. Because of its remarkable performance as a scaffolding loading catalyst, it has been used to support heterogeneous catalysts such as silver nanoparticles, palladium nanoparticles, iron oxide nanoparticles and zinc oxide nanoparticles [2]. In the past few years, zinc oxide (ZnO) is among the favourable heterogeneous catalysts because of its non-toxic, cheap, low-corrosion, recyclability and minimum execution properties [3]. When irradiated by UV light, changing of electron energy state from the valence band (VB) to the conduction band (CB) forms electron-hole pairs ( $h^+$ ) that lead to excitation of radical forms for the decolouration of methylene blue (MB) as described  $\text{OH} \cdot + \text{MB} \rightarrow \text{CO}_2 + \text{H}_2\text{O}$ . In this study, a comparison of performance via photocatalysis between two forms of regenerated cellulose embedded with ZnO has been done. MB was chosen as a model of pollutant because it is widely used in various industries as organic dyes such as textiles, paint, aquaculture and medicine.

### MATERIALS AND METHODS

0.4g of 1.6 wt% ZnO in membranes (CMZ) and aerogels (CAZ) were cut to dimensions of 1×1 cm and aerogel dimensions of 1×1×1 cm and was then immersed respectively in 100 mL of MB solution (5 mg/L) in a beaker with a magnetic stirrer equipped with a 26-watt UV lamp ( $\lambda \leq 390$

nm). The amount of decolourized MB was determined according to this equation;

$$\text{Removal percentage (\%)} = \frac{C_0 - C_e}{C_0} \times 100$$
 where  $C_0$  and  $C_e$  are the initial and equilibrium concentrations of MB, respectively

## RESULTS AND DISCUSSION

The efficiency of CMZ and CAZ were studied via the photodegradation process which also involved CM and CA as blank control together with ZnO powder to show the capability of ZnO as the catalyst as shown in Fig 1 (a). All samples have reached the equilibrium phase at 50 minutes as confirmed at 60 minutes. Compared to ZnO powder; CM, CA, CMZ and CAZ have better absorption in the dark period with CMZ recording the highest % decolouration by 70.9%. After exposure to UV light, ZnO powder excite to be the highest photodegradation performance among all samples because of direct exposure to UV light without any barrier such as cellulose component. At 100 minutes, ZnO powder started to go plateau and achieved its maximum decolouration at 94.7% decolouration. Meanwhile, CMZ has shown better performance with 91.6% compared to CAZ with just 50.3%. This may be caused by membranes having a higher surface area and better adsorption than aerogels that allow better irradiation of ZnO by UV light.

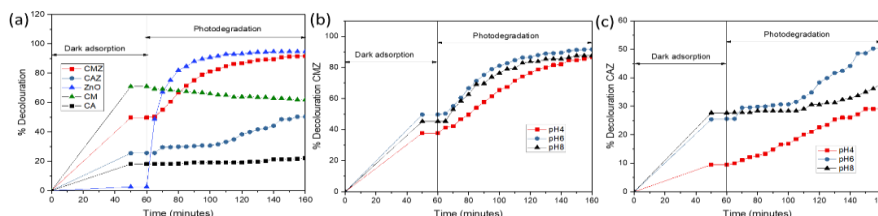


**Fig. 1.** Photocatalysis study for (a) comparison of % decolouration for ZnO powder, CMZ, CAZ with CM and CA as blank control, (b) effect of initial pH for CMZ and (c) effect of initial pH for CAZ

## CONCLUSIONS

CMZ shows a better performance compared to CAZ. This may be caused by membranes having higher surface area and better liquid penetration compared to aerogels for better irradiation of UV light on ZnO.

**ACKNOWLEDGMENT:** The author would like to acknowledge financial support from Universiti Kebangsaan Malaysia (FRGS/1/2019/STG01/UKM/02/11).

## REFERENCES

- [1] Moon, R. J., Martini, A., Nairn, J., Simonsen, J., & Youngblood, J. (2011). Cellulose nanomaterials review: Structure, properties and nanocomposites. In *Chemical Society Reviews* (Vol. 40, Issue 7).
- [2] Salas, C., Nypelö, T., Rodriguez-abreu, C., Carrillo, C., & Rojas, O. J. (2014). Current Opinion in Colloid & Interface Science Nanocellulose properties and applications in colloids and interfaces ☆ Fiber deconstruction. *Current Opinion in Colloid & Interface Science*, 19(5), 383–396.
- [3] Barakat, M. A. (2011). New trends in removing heavy metals from industrial wastewater. *Arabian Journal of Chemistry*, 4(4), 361–377.

## Synthesis and Characterization of TiO<sub>2</sub> Nanoparticles Using Alkaline Fusion Method for Potential Photocatalyst Application

Muhammad Azri Muhd Yusop<sup>2</sup>, Emmellie Laura Albert<sup>1</sup>, Dharshini Perumal<sup>3</sup>, Ashreen Norman<sup>1,2</sup>, and Che Azurahaman Che Abdullah<sup>1,2,3\*</sup>

<sup>1</sup>Nanomaterial Synthesis and Characterisation Laboratory, Institute of Nanoscience and Nanotechnology, Universiti Putra Malaysia, 43400 Serdang, Selangor, Malaysia.

<sup>2</sup>Biophysics Laboratory, Department Physics, Faculty of Science, Universiti Putra Malaysia, 43400 Serdang, Selangor, Malaysia.

<sup>3</sup>UPM-MAKNA Cancer Research Laboratory Institute of Bioscience, Universiti Putra Malaysia, 43400 Serdang, Selangor, Malaysia

\*Corresponding Autor's Email: azurahaman@upm.edu.my

**Abstract:** The current research involves the preparation of titanium-based nanoparticles having potential for photocatalytic of pollutants or dyes. The titanium dioxide (TiO<sub>2</sub>) nanoparticles were synthesised using alkaline fusion method using natural Ilmenite as a Ti precursor. Fourier transform infrared spectroscopy (FTIR) and powder X-ray fluorescence were used to characterise the synthesised nanoparticles. The results indicated that increasing the calcination temperature decreased the degradation rate of Ofloxacin due to increased particle size and surface area. The photocatalytic degradation of Ofloxacin established that TiO<sub>2</sub> was an effective catalyst for antibiotic removal from water samples.

**Keywords:** Synthesis, Nanoparticles, Titanium dioxide and Photocatalytic

### INTRODUCTION

Iron (III) Oxide (IO), Aluminum Oxide (Al<sub>2</sub>O<sub>3</sub>), Zinc Oxide (ZnO), and Titanium Dioxide (TiO<sub>2</sub>) are among metal oxide nanoparticles that have garnered significant attention due to their exceptional physicochemical properties, which make them highly desirable and sought after for a variety of consumer products and industrial technologies. Due to their unique physiochemical and photocatalytic properties, nanoparticles eventually play a significant role in antimicrobials, water purification, the removal of pollutants and also germs, as well as as a biosensor [1-4]. The purpose of this study is to determine whether the TiO<sub>2</sub> produced using alkaline fusion method from natural Ilmenite can be a degradation nanoparticle or not. We dissolved some titanium dioxide in methyl orange and monitored the colour change every hour for six hours.

### MATERIALS AND METHODS

All chemicals and solvents were purchased and used without further purification from Merck and Sigma-Aldrich (Germany). The process begins with selection of the ratio and in this case the chosen ratio is 2:1. 50g Ilmenite and 100g sodium hydroxide, NaOH required for an alkaline fusion process with various temperatures ranging from 550 -850 °C. The mixture of Ilmenite and NaOH then placed in the furnace and heated to 850°C for 3 hours. The product was then be washed and filtered with DI water. After washing, the leaching process started. Prepared samples then characterised using an ED-XRF machine to ascertain their true composition and the



distinction between anatase and rutile. Chemical elucidation of the synthesised  $\text{TiO}_2$  NP was accomplished using the FTIR spectrum. In addition, in this study the potential application was evaluated using organic dyes to resembles pollutant. Methyl orange was used at a concentration of 100ppm to investigate the effect of  $\text{TiO}_2$  on the dye solution.  $\text{TiO}_2$  at different percentage (1%, 3%, and 5%) in the solution were added to a 100ml solution of 100ppm methyl orange (MO) and used as a catalyst following ultraviolet lamp irradiation.

## RESULTS AND DISCUSSION

Samples prepared using alkaline fusion method revealed to be in rutile and anatase phases with 99%. The chemical fingerprints was investigated using FTIR. Photocatalytic had been tested by added some of the prepared samples using 50ppm of methyl orange dye. Gradually, the dye degradation of methyl orange occurs over time confirming the capability of the degradation using  $\text{TiO}_2$  nanoparticles.

## CONCLUSIONS

Several methods can be used to prepared  $\text{TiO}_2$  nanoparticles. A high yield of high quality  $\text{TiO}_2$  successfully achieved using Ilmenite as Ti precursor. The nacre was extracted from the shells using EDTA. XRF analysis of shows  $\text{TiO}_2$  in both rutile and anatase phases. A high quality  $\text{TiO}_2$  that been produced depends on the temperature and ratio used through the process. Most importantly it has a photocatalytic properties that can be activated under the UV light. The results indicated that increasing the heating temperature decreased the degradation rate of the dye solution.

**ACKNOWLEDGMENT:** The authors are grateful for the financial support from the Ministry of Higher Education of Malaysia under Fundamental Research Grants Scheme (FRGS) (Vot. No. 5524949) and Dana Tautan Grant (DT0021) from UPM.

## REFERENCES

- [1] Kordzadeh-Kermani, V., Schaffie, M., Rafsanjani, H. H., & Ranjbar, M. (2020). A modified process for leaching of ilmenite and production of  $\text{TiO}_2$  nanoparticles. *Hydrometallurgy*, 198, 105507.
- [2] Al-Qaradawi, S., & Salman, S. R. (2002). Photocatalytic degradation of methyl orange as a model compound. *Journal of Photochemistry and photobiology A: Chemistry*, 148(1-3), 161-168. Luo, X., Morrin, A., Killard, A. J., & Smyth, M. R. (2006). Application of nanoparticles in electrochemical sensors and biosensors. *Electroanalysis: An International Journal Devoted to Fundamental and Practical Aspects of Electroanalysis*, 18(4), 319-326
- [3] Hussain, M., Ceccarelli, R., Marchisio, D. L., Fino, D., Russo, N., & Geobaldo, F. (2010). Synthesis, characterization, and photocatalytic application of novel  $\text{TiO}_2$  nanoparticles. *Chemical Engineering Journal*, 157(1), 45-51. Ravishankar Rai, V. (2011). Nanoparticles and their potential application as antimicrobials



## Physical Properties Characterization of Ancient Nanostructured Biomaterials (Nacre Layer) Retrieved using Ethylenediaminetetraacetic Acid (EDTA)

Nur Farahah Mohd Khairuddin<sup>1</sup>, Nur Shuhada Zaharia<sup>2</sup>, Mohd Luqman Mokhtar<sup>2</sup>, Emmellie Laura Albert<sup>1</sup>, Nicholas Khong<sup>3</sup> and Che Azurahaman Che Abdullah<sup>1,2,3\*</sup>

<sup>1</sup>Nanomaterial Synthesis and Characterization Laboratory, Institute of Nanoscience and Nanotechnology, Universiti Putra Malaysia, 43400 Serdang, Selangor, Malaysia.

<sup>2</sup>Biophysics Laboratory, Department Physics, Faculty of Science, Universiti Putra Malaysia, 43400 Serdang, Selangor, Malaysia.

<sup>3</sup>UPM-MAKNA Cancer Research Laboratory Institute of Bioscience, Universiti Putra Malaysia, 43400 Serdang, Selangor, Malaysia

\*Corresponding Author's Email: azurahaman@upm.edu.my

**Abstract:** Nacre can be found in many seashells species made up of about 95% of volume of multilayer structure of crystalline aragonite. The physical characteristics of the retrieved nacre powder from the nacre layer by using ethylenediaminetetraacetic acid (EDTA) method were analyzed by means of yield percentage and X-ray fluorescence (XRF). Yield percentage found to be 44%. XRF analysis revealed the high content of calcium carbonate in comparison to the untreated nacre. Here, we successfully prepared nacre powder and evaluated the properties of the ancient nanostructured nacre retrieved using EDTA for future application in bone tissue engineering.

**Keywords:** Nacre, ethylenediaminetetraacetic acid, calcium carbonate, biomaterial

### INTRODUCTION

Nacre can be found in many seashells species. Since it is primarily consisted of brittle ceramic, so the structure has become the strongest structure found in the shells [1]. Nacre toughness is 3000 tougher compared to aragonite since it is mostly made up of aragonite. For over a thousand years, nacre powder also known as pearl powder has been used in cosmetics as well as health food substitute [2-3]. It is high in protein and minerals and has been used in biomedical for example treat skin and bone disorders [3].

### MATERIALS AND METHODS

Raw nacre shells of *Modiolus philippinarum* species were collected from the Merambong Shoal seagrass bed at the Pulai River Estuary in Johor, Malaysia. The shells were cleaned. Then it was dried in normal ambient. 100 shell samples were used to determine the average mass and size. The nacre shells were introduced into the crushing and grinding process to transform it into a fine powder.

## RESULTS AND DISCUSSION

### A. Yield Percentage

The initial weight for each method was about 60 grams. Following EDTA treatment, 26.7 grams was obtained. EDTA treatment led to the loss for more than half with percentage yields of 44.2%.

### B. X-Ray fluorescence (XRF) analysis

Table 1 showing the compositions of samples tested by using X-Ray Fluorescence (XRF) to know the dominant and trace element compounds for EDTA treated nacre sample.

**Table 1.** The XRF data for the major element and their percentages

Sample	Element (%)	
	Dominant	Trace
Control	Ca=98.389	Sc, Sr, K, Fe, Cu, Se
EDTA	Ca=99.055	Sr, Cu

## CONCLUSIONS

The nacre was extracted from the shells using EDTA. The treatment yielded 44.2 percent nacre. The nacre was then characterised by XRF. XRF analysis of nacre powder shows calcium as the dominant element. The EDTA method led to the nacre with least trace elements.

**ACKNOWLEDGMENT:** The authors are grateful for the financial support from Universiti Putra Malaysia through Putra Grant (Inisiatif Putra Muda IPM) Vot No 9406000.

## REFERENCES

- [1] Rousseau M, Meibom A, Gèze M, Bourrat X, Angellier M, Lopez E., *Journ. of Struct. Bio.*, 2009, **165(3)**, 190-195.
- [2] Ramos-Silva P, Benhamada S, Le Roy N, Marie B, Guichard N, Zanella-Cléon I, Plasseraud L, Corneillat M, Alcaraz G, Kaandorp J, Marin F, *ChemBioChem*, 2012, **13(7)**, 1067-1078.
- [3] Bertoldi K, Bigoni D, Drugan W J, *Comp. Sci. and Tech.*, 2008, **68(6)**, 1363-1375.

## Synthesis of Thymol Encapsulated in Chitosan Nanoparticle for Active Food Packaging Application

Ruzanna Ahmad Shapi'i<sup>1</sup>, Siti Hajar Othman<sup>1,2,\*</sup>, Mohd Nazli Naim<sup>2</sup> and Intan Syafinaz  
Mohamed Amin Tawakkal<sup>2</sup>

<sup>1</sup>Institute of Nanoscience and Nanotechnology, Universiti Putra Malaysia, 43400 UPM Serdang, Selangor, Malaysia

<sup>2</sup>Department of Process and Food Engineering, Faculty of Engineering, Universiti Putra Malaysia, 43400 UPM  
Serdang, Selangor, Malaysia

\*Corresponding Autor's Email: s.hajar@upm.edu.my

**Abstract:** In this study, thymol was encapsulated in chitosan nanoparticles (CNP-thymol) at varying ratios of chitosan to thymol (1:0, 1:0.25, 1:0.5, 1:0.75, 1:1). The average sizes of CNP-thymol were measured using dynamic light scattering (DLS) and transmission electron microscope (TEM). The antimicrobial activity of CNP-thymol on *Staphylococcus aureus* (*S. aureus*) and *Salmonella typhi* (*S. typhi*) was evaluated. DLS and TEM analysis revealed that the smallest size of CNP-thymol was produced when the ratio of chitosan to thymol was 1:0.5 (DLS: 157±0.75 nm; TEM: 10±0.25 nm). The antibacterial study of CNP-thymol demonstrated the reduction in bacterial counts, thus confirming the antimicrobial properties of CNP-thymol.

**Keywords:** chitosan nanoparticle, encapsulation, essential oil, ionic gelation, thymol

### INTRODUCTION

Nanoencapsulation of antibacterial agents such as thymol in chitosan nanoparticle (CNP-thymol) emerged as a new alternative to control the release of highly volatile thymol in the food package, thus maintaining the quality of food. To the best of our knowledge, only Medina et al. [1] and Cakir et al. [2] have studied the encapsulation of thymol in CNP. Nevertheless, both previous studies produced CNP-thymol with sizes larger than 100 nm which were not in the range of the nanoparticle size. Previous studies on the encapsulation of oregano oil and carvacrol revealed that the nanoparticle size increased with the increase in the ratio of chitosan to essential oil [3, 4]. Meanwhile, the optimization study of nanoencapsulation parameters by Cakir et al. [2] found that the ratio of chitosan to thymol was an insignificant parameter for nanoparticle size. Regardless of this contradiction, this study is directed to investigate the effect of the ratio of chitosan to thymol on the particle size of CNP produced via the ionic gelation method. Then, the antibacterial activity of the produced CNP-thymol was investigated.

### MATERIALS AND METHODS

Thymol was encapsulated into CNP via the ionic gelation process with sodium tripolyphosphate (0.09g) at varying ratios of chitosan (0.45g) and thymol (1:0, 1:0.25, 1:0.5, 1:0.75, 1:1). An amount of 0.3g of Tween 80 was added as an emulsifier for thymol. The particle size of CNP-thymol was measured using DLS and TEM. The antibacterial activity of the CNP-thymol was investigated via the liquid growth inhibition assay against *S. aureus* and *S. typhi*.

## RESULTS AND DISCUSSION

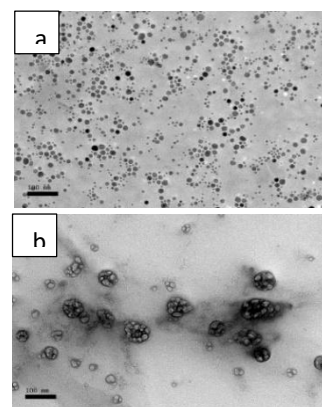
DLS analysis (Table 1) reveals that the smallest size of CNP-thymol was obtained when the ratio of chitosan to thymol was 1:0.5. Fig. 1 (a) shows the round and regular shape of particles for 1:0.5 CNP-thymol with an average size of  $10 \pm 0.25$  nm. Meanwhile, 1:1 CNP-thymol (Fig 1 (b)) exhibited irregular shapes of particles with an average size of  $48 \pm 3.91$  nm and aggregations. Excess thymol was also appeared around the CNP shell due to the same ratio of chitosan and thymol.

Table 1. Effect of ratio of chitosan:thymol on the average particle size

chitosan:thymol (w/w)	Average diameter (nm)
1:0.00 (CNP)	$106.34 \pm 1.69$
1:0.25	$172 \pm 2.42$
1:0.50	$157 \pm 0.75$
1:0.75	$177 \pm 2.67$
1:1.00	$177 \pm 1.36$

Table 2. Effect of ratio of chitosan:thymol on the antibacterial activity

Treatment	Bacterial count (cfu/ml)	
	<i>S. aureus</i>	<i>S. typhi</i>
Control	$1.93 \times 10^8$	$2.51 \times 10^8$
CNP	$5.20 \times 10^6$	$3.90 \times 10^4$
CNP-thymol (1:0.5)	$7.85 \times 10^5$	$2.45 \times 10^4$
CNP-thymol (1:1)	$1.55 \times 10^5$	$3.90 \times 10^3$



**Fig 1.** TEM image of (a) 1:0.5 CNP-thymol (b) 1:1 CNP-thymol.

The antibacterial study (Table 2) demonstrates the reduction of both gram-positive (*S. aureus*) and gram-negative (*S. typhi*) bacteria for CNP from 8 to 6 log CFU/ml and 8 to 4 log CFU/ml, respectively thus confirming the antibacterial properties of CNP. Both 1:0.5 CNP-thymol and 1:1 CNP-thymol also showed great improvement of antibacterial activity compared to the empty CNP. The improvement of antibacterial activity of CNP-thymol was due to the synergizing effect, whereby both CNP and thymol inhibit the bacterial growth via different mechanism [1].

## CONCLUSIONS

A significant effect of the ratio of chitosan to thymol on the CNP-thymol size was proven by DLS analysis and TEM images. CNP-thymol exhibited a good synergizing effect as antibacterial agent for both *S. aureus* and *S. typhi*. Further study on the other parameter of nanoencapsulation that affect the properties of CNP-thymol should be embarked on to ensure the promising application of the produced CNP-thymol.

**ACKNOWLEDGMENT:** The authors would like to acknowledge the financial support provided by Fundamental Research Grant Scheme of the Ministry of Science, Technology, and Environment, Malaysia [Project Number = 5540542].

## REFERENCES

- [1] Medina E, Caro N, Abugoch L, Gamboa A, Díaz-Dosque M, and Tapia C. J. Food Eng., 2018, **240**, pp. 191–198.
- [2] Cakır MA, Icyer NC, and Tornuk F. Int. J. Biol. Macromol., 2020, **151**, pp. 230–238.
- [3] Hosseini SF, Zandi M, Rezaei M, and Farahmandghavi F. 2013, **95**, pp. 50–56.
- [4] Keawchaon L and Yoksan R, Colloids Surfaces B Biointerfaces, 2011, **84**, pp. 163–171.

## Influence of Grinding Techniques During *Chromolaena Odorata* Leaves Preparation Towards the Formation of Biosynthesized SnO<sub>2</sub> Nanoparticles

Irmaizatussyehdany Buniyamin<sup>1\*</sup>, Rabiataladawiyah Md Akhir<sup>1,3</sup>, Noor Asnida Asli<sup>1,3</sup>  
Zuraida Khusaimi<sup>1,3</sup> and Mohamad Rusop Mahmood<sup>1,2\*\*</sup>

<sup>1</sup>NANO-SciTech Laboratory, Centre for Functional Materials and Nanotechnology (CFMN), Institute of Science, Universiti Teknologi MARA (UiTM), 40450 Shah Alam, Selangor, Malaysia

<sup>2</sup>NANO-ElecTronic Centre, Engineering College, Universiti Teknologi MARA (UiTM), 40450 Shah Alam, Selangor, Malaysia

<sup>3</sup>Faculty of Applied Sciences, Universiti Teknologi MARA (UiTM), 40450 Shah Alam, Selangor, Malaysia

Corresponding Author's Email: \*syehdany@uitm.edu.my; \*\*nanouitm@gmail.com

**Abstract:** In this study, tin oxide nanoparticles (SnO<sub>2</sub> NPs) were synthesized via a green protocol using bioactive compounds from *Chromolaena odorata* leaves which stand as a reducing and capping agent. The leaves underwent two types of grinding techniques to investigate which technique would provide bioactive compounds in effective concentration to assist the biosynthesis process: ball-mill and electronic blender. The prepared SnO<sub>2</sub> NPs were characterized by Fourier-Transform infrared (FTIR), X-ray diffraction analysis (XRD), field emission scanning electron microscopy (FESEM), energy dispersive X-ray spectroscopy (EDX) and UV-visible diffuse reflectance spectroscopy (DRS). FTIR spectra evidenced the pertinent functional groups of SnO<sub>2</sub> NPs. From XRD analysis, both samples developed in tetragonal structure whereby ball-mill and electronic blending techniques gave average crystallite size of 7.85 and 11.60 nm respectively. Uniform distribution of agglomerated spherical shape of SnO<sub>2</sub> NPs was observed from the FESEM images and EDX analysis confirmed the presence of Sn and O elements. The reflectance percentage of SnO<sub>2</sub> NPs was found to be 48 % with energy band value of 3.13 eV produced from ball-mill technique, while 37 % reflectance and 3.39 eV from latter technique. Band gap values suggested this synthesized SnO<sub>2</sub> NPs using both techniques are practical candidates for optical function.

**Keywords:** Tin oxide nanoparticles, *Chromolaena odorata*, bioactive compound, biosynthesis, band gap.

## INTRODUCTION

In this report, we demonstrate the preparation of SnO<sub>2</sub> NPs via a green approach using bioactive compound from leaves of *Chromolaena odorata*. The leaves underwent two types of grinding techniques; ball-mill and conventional blender, to indicate which technique is more effective towards the grinding associated with the releasability of the bioactive compounds. Previously, the green synthesis using plant extract towards SnO<sub>2</sub> NPs had been carried out using *Plectranthus amboinicus* [1], *Persia Americana* [2], *Pruni spinosae flos* [3], etc which stated these approaches possessed simplicity and mild reaction. The extract solution of *C. odorata* was mixed with precursor salt solution of tin chloride and later involved with calcination process to furnish SnO<sub>2</sub> NPs as the outcome. SnO<sub>2</sub> NPs showed tetragonal structure with agglomerated spherical-like

morphology while the absorption bands proved the pertinent functional groups. The obtained band gap is within the range of requirements for practical photocatalytic applications.

## MATERIALS AND METHODS

The leaves of *C. odorata* were dried and ground using a ball-mill machine or conventional blender. The fine powder was boiled into water and the prepared extract was mixed with solution of tin chloride pentahydrate. Later, the centrifugation process took place, and the gelatinous product was dried, followed by calcination [4].

## RESULTS AND DISCUSSION

Fig. 1 shows the index of the XRD pattern for the prepared SnO<sub>2</sub> NPs, whereby it is found to have good compatibility with earlier reports [5]. The construction of SnO<sub>2</sub> is recommended as a tetragonal structure. From the calculation using Scherrer's equation, the average particle size for samples A and B is 7.8 and 11.6 nm, respectively.

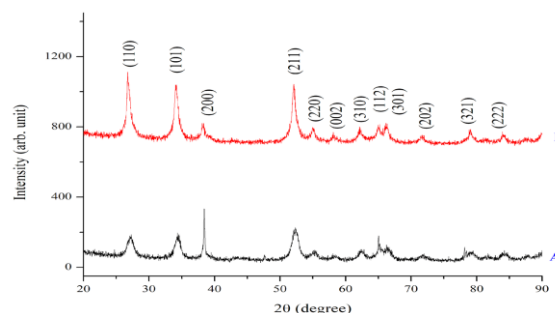


**Fig. 1.** XRD spectra of SnO<sub>2</sub> NPs using ball-mill (A) and conventional blender (B)

## CONCLUSIONS

SnO<sub>2</sub> NPs had been effectively produced using the extract solution of *C. odorata* leaves, in which the leaves ground either using ball-mill or conventional blender. Both techniques proved to be effective in furnishing the bioactive compounds required for the biosynthesis process. The spectroscopic analysis is evidenced to meet all requirements for the SnO<sub>2</sub> NPs construction. It is found that the obtained band gap is not of much divergent value and is still within the practical requirement for application such as photocatalytic.

## REFERENCES

- [1] Fu L, Zheng Y, Ren Q, Wang A, Deng B. *J Ovonic Res.*, 2015, **11**, 21.
- [2] Elango G, Mohana Roopan S. *Journal of Photochemistry & Photobiology, B: Biology*, 2016, **155**, 34.
- [3] Dobrucka R, Dlugaszewska J, Kaczmarek M. *Inorg Nano-Metal Chem*, 2019, 1.
- [4] Buniyamin I, Akhir RM, Asli NA, Khusaimi Z, Rusop M. *AIP Conference Proceedings*, 2021, **2368**, 020006.
- [5] Sudhaparimala S, Gnanamani A, Mandal AB. *AJNNR*, 2014, **2**, 75.



## The Effect of EM4 Addition to Stale Rice Substrate on the Production Potential of Methane in a Biogas Reactor

I Kadek Dwi Saputra, M. Ramdhan Kirom, Asep Suhendi\*

*Engineering Physics, Telkom University, Bandung, Indonesia*

*\*suhendi@telkomuniversity.ac.id*

**Abstract:** Anaerobic digester is a method of processing organic waste that has a high potential in producing methane gas by breaking down organic compounds in with the help of microorganisms without the need for oxygen. In this study, the effect of EM4 addition to stale rice substrate on the potential for methane gas production produced in a simple biogas reactor. The addition of EM4 bioactive to the substrate material is considered appropriate in accelerating the fermentation process of organic matter; bacteria are more measurable, works at mesophilic temperatures, and do not cause unpleasant odors when compared to the use of other bioactive. The biogas reactor in this study used the batch method and accommodated an influent volume of 12.67 liters working at room temperature. In this study, there were five variations of the addition of EM4 from 0% - 15%. The results show that without the addition of EM4 resulted in total gas production of 20.420 ml, and the estimated volume of methane gas is 108.0334 ml with 0.529% methane efficiency. However, the addition of EM4 to the stale rice substrate resulted in smaller methane gas production, so that the addition of EM4 bioactive decreased methane production efficiency.

**Keywords:** anaerobic-digester, organic-waste, EM4, substrate-variation, methane.

### INTRODUCTION

Low handling of organic waste causes various environmental problems. One of them is the release of free methane gas in the air, resulting in greenhouse gases 25 times greater than carbon dioxide [1]. One of the organic waste treatment methods is using the anaerobic digestion method. Anaerobic digestion is the process of breaking down organic matter contained in waste to be converted into methane gas without the need for oxygen [2]. In this research, the author will study the addition of bacteria (EM4) to obtain more optimal gas results with variations in the EM4 in stale rice waste with a batch reactor filling system. The measurement of methane gas content from the volume of gas produced in a simple biogas reactor was also carried out. Thus, it is expected to determine the variation of the addition of EM4 to the most optimal substrate in the production of methane gas in a simple biogas reactor.

### MATERIALS AND METHODS

In the tests carried out, stale rice was obtained from rice cooked by itself and allowed to stand for two days. The rice waste used is a mixture of stale rice and water with one kg of stale rice to two liters of water. Rice that is left closed so as not to be contaminated with outside bacteria. The use of rice waste as a substrate because it has a high carbohydrate and water content.

### RESULTS AND DISCUSSION

In this study, the measurements of total gas volume, methane gas volume, average gas

concentration, initial and final pH and room temperature were carried out. The results of observations of biogas production can be seen in Table 1. Table 1 shows that the variation that produces the highest gas volume and volume of methane gas content is the 0% variation (without the addition of EM4) with the gas recovery of 20,420 ml and 108,0334 ml.

**Table 1 Biogas Production Observation**

Information	0%	9% Variation	11% Variation	13% Variation	15% Variation
<b>Total Gas Volume (ml)</b>	20,420	4,580	10,560	5,410	8,630
<b>Concentration Average (ppm)</b>	5148.9	991.6	606.16	516.05	74.54
<b>Estimated Methane Volume (ml)</b>	108.0334	4.95167	7.54431	3.03097	0.52491
<b>Efficiency (%)</b>	0.529%	0.108%	0.071%	0.056%	0.006%

In this initial phase, the gas produced at 9%, 11%, 13%, 15% EM4 additions is very small, ranging from 40-50 ml, considering that this phase is an adaptation phase or an early growth phase. Therefore, from day 0 to day 1 is the adaptation phase. In contrast to the variation without the addition of EM4, on the first day, the gas produced from the 0% variation reached 1440 ml. Furthermore, from day 1 to day 2, there was an increase in gas yield but not much (for variations 9%, 11%, 13%, 15%).

## CONCLUSIONS

The effect of adding EM4 bioactive to the stale rice substrate on the potential for methane gas production in an anaerobic process using a simple reactor has been carried out. By adding EM4 solution to the stale rice substrate, an average concentration value produced is smaller than the variation without the addition of EM4, which impacts smaller methane gas production. The efficiency value of methane gas content obtained from the 0% variation is 0.529%, and the efficiency value from the 9% variation is 0.108%. So that from these two variations have a very high-efficiency reduction of 79.58%. It is hoped that further research and development will be carried out to improve the shortcomings of this research.

**ACKNOWLEDGMENT:** The author would like to acknowledge a research grant of PDUPT from the Ministry of Research and Technology Republic of Indonesia/National Research and Innovation Agency.

## REFERENCES

- [1] M. Chakraborty, C. Sharma, J. Pandey, N. Singh, and P. K. Gupta, "Methane emission estimation from landfills in Delhi: A comparative assessment of different methodologies," *Atmos. Environ.*, vol. 45, no. 39, pp. 7135–7142, 2011.
- [2] G. Náthia-Neves, M. Berni, G. Dragone, S. I. Mussatto, and T. Forster-Carneiro, "Anaerobic digestion process: technological aspects and recent developments", *Int J Environ Sci Technol*, vol. 15, pp. 2033–2046, 2018.

## The Effect of Variation of Stale Rice and EM4 Rice Substrate Filling time on Methane Gas Production Potential using Mesophilic Biogas Reactor

Lely Kusniawaty Gopar, M. Ramdhan Kirom and Asep Suhendi\*

*Engineering Physics, Telkom University, Bandung, Indonesia*

**Abstract:** Abstract Rice is a staple food for Asian countries so that rice waste can be easily encountered. If not managed properly, this waste has a negative impact on the environment. This research will process ricewaste to observe its potential as an alternative energy source. Rice waste has a high carbohydrate content which can be used as a raw material for producing biogas. The process was carried out by mixing rice waste with bioactive EM4 and water so that it becomes liquid waste that is ready to ferment anaerobically at mesophilic temperatures range in the biogas reactor. This study aims to determine the effect of differences in substrate filling time on the amount of gas produced. The time variations applied in this study were, 1, and 2 days. The results of the stability test on substrate filling per 2 days produced an average gas of 1,850 liters/day. The methane gas produced is estimated to be around 0.865 ml/day or 0.0467% of the total gas.

**Keywords:** hydraulic-retention-time, anaerobic-digestion, biogas, semicontinuous-filling, filling-time.

### INTRODUCTION

Indonesia ranks second in terms of food waste generation [1]. It is estimated that the amount of food waste produced by one person is around 300 kg per year. This food waste has a negative impact on the environment by contributing to greenhouse gas emissions due to uncontrolled release of methane and depletion of natural resources [2-3]. If methane gas is released into the air, it will create an impact almost 25 times greater as a greenhouse gas compared to carbon dioxide [4]. Anaerobic digestion is considered the most attractive method for treating and recycling organic solid waste and producing energy-rich gases such as hydrogen and methane thereby reducing the volume of waste [5]. The focus of this research is to observe and analyze the effect of the time and volume of filling the rice waste substrate with the addition of EM4 bacteria (Effective Microorganisms) on the production of methane gas which is expected to produce good alternative energy potential.

### MATERIALS AND METHODS

For the initial substrate, the total volume of substrate in this study was made as much as 12.67 liters. To carry out a variation of the study, 4.1 kg of rice was stale for two days in a closed container and then mixed with water using a blender for 30 seconds with a ratio of 1:2 to obtain a liquid stale rice substrate. Then the liquid substrate is transferred to the mixing tank to add 9% EM4 or 1.14 liters.

### RESULTS AND DISCUSSION

The following graph shows the change in the average maximum concentration per 12 hours:

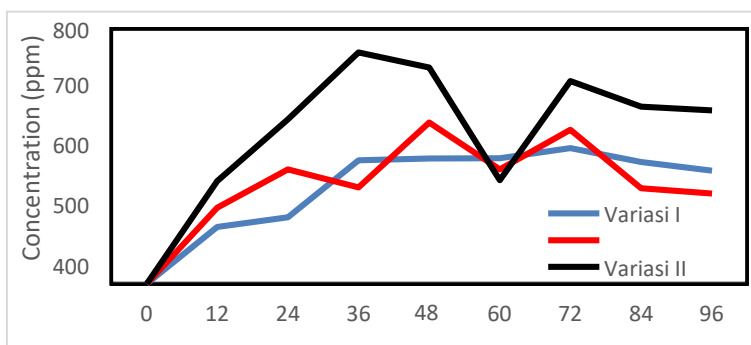


**Fig. 1.** Produced gas concentration

Of the three variations of the study, each showed fluctuating concentrations of methane. The concentration of methane tends to decrease after filling the new substrate into the reactor and then rises again as the anaerobic process occurs. This indicates a 'disturbance' to the methane concentration when each reactor is fed a new substrate. The highest average concentration was achieved by variation III with a peak reaching 726 ppm.

## CONCLUSIONS

Based on the test of the substrate filling time, the substrate filling time of 2 days produced the most superior gas compared to or 1 day filling. The volume of gas obtained reached 7.59 liters of gas in 4 days. After testing the stability of gas production for 10 days, the 2-day filling time was able to produce 18.5 liters of gas and 8.653 ml of methane gas. Production stability was obtained after the 4th day where the gas produced reached 1.774 liters/day with methane gas content of 0.8433ml/day or equivalent to 0.047% of the total gas.

**ACKNOWLEDGMENT:** The author would like to acknowledge a research grant of PDUPT from Ministry of Research and Technology Republic of Indonesia/National Research and Innovation Agency.

## REFERENCES

- [1] F. S. Index, "Food Loss and Waste," 2019. [Online]. Available: <http://foodsustainability.eiu.com>.
- [2] F. Girotto, L. Alibardi, and R. Cossu, "Food waste generation and industrial uses: A review," *Waste Manag.*, vol. 45, pp. 32–41, 2015.
- [3] E. Papargyropoulou, R. Lozano, J. K. Steinberger, N. Wright, and Z. Bin Ujang, "The food waste hierarchy as a framework for the management of food surplus and food waste," *J. Clean. Prod.*, vol. 76, pp. 106–115, 2014.
- [4] M. Chakraborty, C. Sharma, J. Pandey, N. Singh, and P. K. Gupta, "Methane emission estimation from landfills in Delhi: A comparative assessment of different methodologies," *Atmos. Environ.*, vol. 45, no. 39, pp. 7135–7142, 2011.
- [5] J. Mata-Alvarez, S. Macé, and P. Llabrés, "Anaerobic digestion of organic solid wastes. An overview of research achievements and perspectives," *Bioresour. Technol.*, vol. 74, no. 1, pp. 3–16, 2000.

## Preliminary Study on Methyl Jasmonate Nanoemulsion for Paddy Growth Modulation

Hazalina Zulkifli<sup>1</sup>, Noor Azlina Masdor<sup>1</sup>, Khalisanni Khalid<sup>1</sup>, Nur Sabrina Wahid<sup>1</sup>, Nor Fadilah Abd Halim<sup>2</sup>, Shahida Hashim<sup>3</sup>, Siti Nadzirah Padrillah<sup>1</sup>, Nadia Izati Fadzil<sup>1</sup>, Mohd Nor Mohd Rosmi<sup>1</sup>, Nor Suzaida Mohd Nor<sup>1</sup>, Ahmad Shazwan Ismail<sup>1</sup> and Muhamad Shafiq Abd Karim<sup>1</sup>

<sup>1</sup>Biotechnology and Nanotechnology Research Centre, MARDI Headquarters, 43400 Serdang Selangor, Malaysia

<sup>2</sup>Soil Sciences and Fertilizer Research Centre, MARDI Headquarters, 43400 Serdang Selangor, Malaysia

<sup>3</sup>Paddy and Rice Research Centre, MARDI Seberang Prai, 13200 Kepala Batas, Penang, Malaysia

\*Corresponding Author's Email: hazalina@mardi.gov.my

**Abstract:** Methyl jasmonate (MeJA), are phytohormone that crucial in plant signaling responses to biotic and abiotic stresses. The emulsion nanofertilizer containing 20% (v/v) of MeJA diluted in soybean oil was developed to improve tillers elongation, consequently increase the yield using the ternary phase diagram (TPD) approach. Each tube with formulation at 90% water with different percentage of oil and surfactant (HLB 8-15) were ultra-sonicated. A few formulations in HLB 14 shows a droplet size below than 100 nm with polydispersity index value in a range of 0.06 to 0.107 will be further studied on their stability and performance as paddy nanofertilizer.

**Keywords:** Methyl jasmonate, nanoemulsion, nanofertilizer, colloidal system, hidrofilic lipofilic balance

### INTRODUCTION

Proper management in fertilization is essential for increasing production of rice to meet the demand. Jasmonates are phytohormone involved in several vegetative growth and development processes, such as the increase of fruit size and mass and the development of the root system [1]. The study objective is to develop emulsion nanofertilizer containing a plant hormone (MeJA) using TPD and high energy emulsification approach to increase the rice production.

### MATERIALS AND METHODS

MeJA, sorbitan monooleate (Span 80) and polyoxyethylene sorbitan monooleate (Tween 80) were purchased from Sigma (USA). Soybean oil was purchased from hypermarket in Malaysia. Soybean oil is popular as an oil phase in colloidal system among other selected oils [2,3]. This study targeting an oil in water (o/w) nanoemulsion formulation, the screening of the hidrofilic lipofilic balance (HLB) value from 8 and above were performed. Tween 80 (HLB 15) and Span 80 (HLB 4.3) were blend together as surfactant mixture (Smix) with different percentage ratio according to Rodrigues et al. [4]. Aqueous titration method was used for the construction of the TPD which involves stepwise addition of water to each weight ratio of oil and surfactants, and then mixing the components with the help of vortex mixer at 25 °C [5]. The TPD was constructed using CHEMIX School version 10.0. Each tube with the last formulation at 90% water (aqueous phase) with different percentage of soybean oil and Smix were proceed for high

energy emulsification process using ultrasonicator at 125 kHz, 100% amplitude for 3 minutes. The droplet (particle) size and PDI were determined using Zetasizer (Brookhaven Instruments, USA).

## RESULTS AND DISCUSSION

For an example TPD for HLB 14 was shown below in figure 1a. The blue area in TPD has represented one phase of microemulsion formulation with creamy, clear or cloudy and gel like structure. The pink area has represented one phase of formulation with different range of surfactant (0 – 10.0%), oil (0 – 10.0%) and water (90%) after performing ultrasonication.

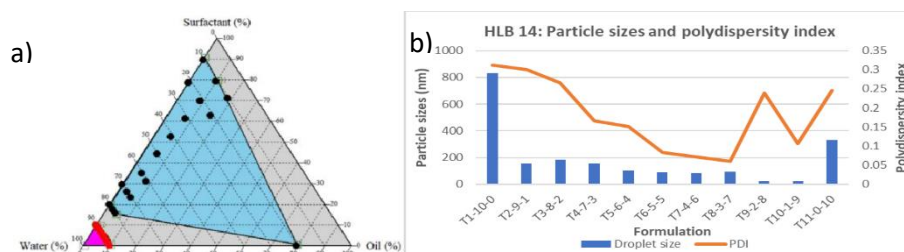


**Fig. 1. a) TPD of emulsion nanofertilizer b) Graph on droplet sizes and PDI of HLB 14**

Physicochemical characteristic of emulsion nanofertilizer such as particles sizes and PDI value were plotted in the graph at figure 1b. A few formulations in HLB 14 shows a droplet size below than 100 nm with PDI value in a range 0.06-0.107 will be a potential formulation to be further studied on their stability and performance as nano fertilizer to increase rice production.

## CONCLUSIONS

Emulsion nanofertilizer containing MeJA was developed and the potential formulations at HLB 14 will be explored further on their stability and its application as paddy nanofertilizer.

## ACKNOWLEDGMENTS

This project was financed by RMK-12 Development Project Fund (PRB-502), MARDI, Selangor

## REFERENCES

- [1] Martinez H. J., Demers, L. E., Grosser, K., Schedl, A., van Dam, N. M., & Bede, J. C. *Frontiers in Plant Science*, 2020, **10**.
- [2] Moghaddasi, F., Housaindokht, M. R., Darroudi, M., Bozorgmehr, M. R., & Sadeghi, A. *Journal of Molecular Liquids*, 2018, **264**.
- [3] Shevalkar, G., Pai, R., & Vavia, P. *AAPS PharmSciTech*, 2019, **20**, 5.
- [4] Rodrigues, R. F., Costa, I. C., Almeida, F. B., Cruz, R. A., Ferreira, A. M., Vilhena, J. C., Florentino, A.C., Carvalho, J.C.T. & Fernandes, C. P. *Revista Brasileira de Farmacognosia*, 2015, **25**.
- [5] Azeem, A., Rizwan, M., Ahmad, F. J., Iqbal, Z., Khar, R. K., Aqil, M., & Talegaonkar, S. *AAPS PharmSciTech*, 2009, **10**, 1.



## Effects of Carbon Quantum Dots on Growth of *Brassica Juncea* under Grow Lights

Yamuna A/P Chowmasundaram<sup>1</sup>, Tong Ling Tan<sup>1</sup>, Mohamad Fakri Zaky Bin Ja'afar<sup>2</sup>, Rosimah Nulit<sup>3</sup>, Mashitah Jusoh<sup>4</sup> and Suraya Abdul Rashid<sup>1</sup>

<sup>1</sup>*Institute of Advanced Technology, Universiti Putra Malaysia, 43400 UPM Serdang, Selangor, Malaysia.*

<sup>2</sup>*Department of Architecture, Faculty of Design and Architecture, Universiti Putra Malaysia, 43400 UPM Serdang, Selangor, Malaysia*

<sup>3</sup>*Department of Biology, Faculty Science, Universiti Putra Malaysia, 43400 UPM Serdang, Selangor, Malaysia.*

<sup>4</sup>*Department of Crop Science, Faculty of Agriculture, Universiti Putra Malaysia, 43400, Selangor, Malaysia*

*\*Corresponding Author's Email: gs58683@student.upm.edu.my, tongling@upm.edu.my, zakyjaafar@upm.edu.my, rosimah@upm.edu.my, mashitahj@upm.edu.my, suraya\_ar@upm.edu.my*

**Abstract:** In this work, Carbon quantum dots (CQD) was prepared and applied to green mustard (*Brassica Juncea*). The objective of the work was to observe the effects of various CQD concentrations on growth of plants in an indoor hydroponics system. The physiological response of the plant was analyzed using the one-way ANOVA test (Duncan). This study found that CQD concentrations of 100 mg/L and 150 mg/L boost plant growth and photosynthesis rate in the hydroponics system under grow light. Green mustard plants treated with 100 mg/L CQD showed a significant increase in plant height and net assimilation by 32%, and 23%, respectively. Correspondingly, plants treated with 150 mg/L CQD had a 29% increase in plant height and a 32% increase in net assimilation compared to control plants.

**Keywords:** Carbon quantum dot, plant growth, grow light, green mustard, statistical analysis

## INTRODUCTION

Carbon quantum dots (CQD) have attracted the attention of researchers in the agriculture field due to its unique properties such as non-toxicity, biocompatibility and environmentally friendly nature [1],[2]. CQD are zero dimension (0D) of carbon nanomaterial with a particle size of less than 10 nm [3],[4]. In comparison to the control plant, the CQD treatment enhances the photosynthesis rate of plants and subsequently increases the plant growth. It has been reported, the CQD improved rice and maize plants' assimilation rate, stomatal conductance, height and biomass [5]. This study uses a simple acid-free microwave-assisted procedure to prepared CQD from empty fruit bunch biochar as an eco-friendly approach and evaluates their effect on green mustard at various concentrations. Previous MTT cytotoxicity studies also showed that concentration range used is non-toxic, thus, it is deemed safe and appropriate for use in agricultural applications [5].

## MATERIALS AND METHODS

CQD was synthesized by microwave-assisted method as previously reported [6]. The CQD was then diluted to 50, 100, 150, 200 and 400 mg/L. Green mustard plants were treated with 1.5 mL of CQD at the various concentrations. The prepared CQD were applied in-vivo (spray) on the leaf surface for twice a month until the end of heading period. Distilled water was sprayed in the control treatment. In this experiment, a full spectrum grow light was used, the temperature of the system was

maintained at 30°C and humidity maintained at 46% with a photoperiod of 12 h day/12 h night. The photosynthetic photon flux density (PPFD) was maintained at  $130 \mu\text{mol m}^{-2} \text{s}^{-1}$  at the level of plant tips. The height and net assimilation of green mustard plants were measured at week 6.

## STATISTICAL ANALYSIS

The data were interpreted using statistical analysis and represented in the bar chart form. Significant differences among all the treatments were analysed using the one-way ANOVA test (Duncan) at a significance level of 0.05, and all analyses were conducted in triplicate.

## RESULTS AND DISCUSSION

As shown in Fig. 1(a), the plant height of 100, 150 and 200 mg/L CQD treated plants were significantly increased by 32%, 29% and 12%, respectively, compared to the control. Based on Fig. 1(b), 100, 150 and 400 mg/L CQD treated plants showed a higher net assimilation compared to other treatments. Each CQD concentration had varied net assimilation, whereby, 150 mg/L treatment increased the net assimilation by 32%, followed by 400 mg/L and 100 mg/L at 30% and 23%, respectively, when compared with control. The data assembled in the figures shows that all CQD treated plants significantly increased the plant height and net assimilation. The findings of 100 mg/L and 150 mg/L are nearly same, with significantly increased plant height and net assimilation, but there is no significant difference between them. Increased  $\text{CO}_2$  assimilation resulted in higher electron transport rates as CQD promotes electron transfer and assimilation [5-7]. The higher the plant's net assimilation, the higher the photosynthesis rate, which leads to increased plant growth [8-10].

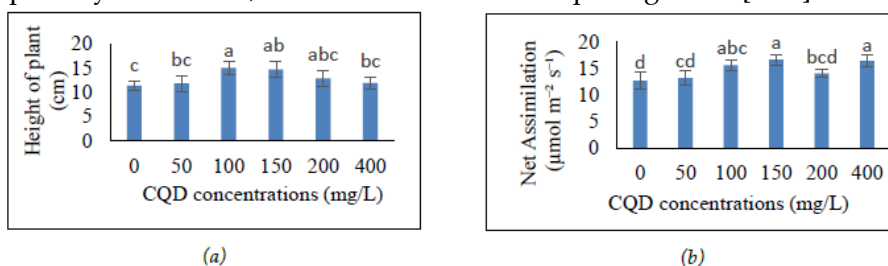


**Fig. 1.** (a) Height of plants. (b) Net assimilation of treated plants.

**ACKNOWLEDGMENT:** The authors gratefully acknowledge the financial support from Universiti Putra Malaysia for the Fundamental Research Grant Scheme (FRGS/1/2019/TK05/UPM/02/8: 5540329).

## REFERENCES

- [1] Zhu C, Chen Z, Gao S, Goh LB, Bin Samsudin I, Lwe KW, Wu Y, Wu C and Su X, *Prog. Nat. Sci. Mater. Int.*, 2019, 29, 628–640.
- [2] Zhang Q, Zhang X, Bao L, Wu Y, Jiang L, Zheng Y, Wang Y and Chen Y, *J. Anal. Methods Chem.*
- [3] Das R, Bandyopadhyay R and Pramanik P, *Mater. Today Chem.*, 2018, 8, 96–109. [4] Molaei M J, *RSC Adv.*, 2019, 9, 6460–6481.
- [5] Tan TL, Zulkifli NA, Zaman ASK, Jusoh M, Yaapar MN and Rashid SA, *Plant Physiol. Biochem.*, 2021, 162, 737–751.
- [6] Jamaludin N, Tan TL, Zaman ASK, Sadrolhosseini AR and Rashid SA, *Materials (Basel)*, 2020, 13, 1–22.
- [7] Iermak I, Vink J, Bader AN, Wientjes E and Van Amerongen H, *Biochim. Biophys. Acta - Bioenerg.*, 2016, 1857, 1473–1478.
- [8] Calfapietra C, Gielen B, Galema ANJ, Lukac M, Angelis PD, Moscatelli MC, Ceulemans R and Scarascia-Mugnozza G, *TreePhysiol.*, 2003, 23, 805–814.
- [9] Simkin AJ, López-Calcano PE and Raines CA, *J. Exp. Bot.*, 2019, 70, 1119–1140.
- [10] Weigel HJ and Manderscheid R, *Eur. J. Agron.*, 2012, 43, 97–107.

## Cellulose-Based Hydrogel for Seed Germination

Swarna Devi Palanivelu <sup>1,2</sup>, Kushairi Mohd Salleh <sup>2</sup>, Keith Lindsey <sup>3</sup>, Fareed Sairi <sup>1</sup>, Muhamad Hafiz Che-Othman <sup>1\*</sup> and Sarani Zakaria <sup>2\*</sup>

<sup>1</sup>Department of Biological Sciences and Biotechnology, Faculty of Science and Technology, Universiti Kebangsaan Malaysia, 43600 UKM Bangi, Selangor, Malaysia

<sup>2</sup>Bioresources and Biorefinery Laboratory, Faculty of Science and Technology, Universiti Kebangsaan Malaysia, 43600 UKM Bangi, Selangor, Malaysia

<sup>3</sup>Department of Biosciences, Durham University, United Kingdom

\*Corresponding Author's Email: szakaria@ukm.edu.my, hafiz87@ukm.edu.my

**Abstract:** Application of hydrogel in hydroponics techniques is one of the advances in urban farming. The main objective of this research is to assess the rate of seed germination in cellulose-based hydrogel for *Ipomoea aquatica*, *Brassica juncea*, *Lactuca sativa* and *Solanum lycopersicum* in comparison with perlite and soil. Each species had 150 seeds sown directly in each media and results were recorded after 15 days. The result confirmed that the hydrogel was the best germination medium for *Lactuca sativa* plant species with seed germination percentage of 70%. Hydrogel demonstrates huge prospects in emerging as an alternative medium for seed germination.

**Keywords:** urban farming, hydrogel, seed germination

### INTRODUCTION

Urban farming has complemented food security by providing urban areas with fresh produce witnessed by 100-200 million urban farmers [1]. Lacking of arable land, water shortage to crops and manpower are serious issues in conventional farming. Hydrogel has been applied in the soil as a soil conditioner and controlled-release fertilizer, found efficient as a water-holding reservoir and nutrient mobilizer when used in the soil [2]. Hydrogel used in combination with other substrates such as vermiculite, pine bark and perlite has also proven to have a positive effect. Cellulose-based hydrogel offers an environmental-friendly solutions. Due to the hydrogel capacity of holding water and delivery system, it will have the ability to supply water to the seeds for germination to take place [3]. The fundamental requirements for seed germination are water availability, conducive temperature, oxygen supply, and light intensity depending on plant species. The main aim of this study is to assess the performance of seed germination in cellulose-based hydrogel compared soil and perlite. The relationships between germination percentage and the characteristic of the germinating media are discussed.

### MATERIALS AND METHODS

#### A. Preparation of Cellulose Hydrogel

Hydrogel was prepared from an alkaline solvent solution kept in the freezer overnight. About 3 g of cotton was dissolved in the aqueous solvent at -13°C. The resulting mixture was crosslinked with a crosslinker and stirred continuously to get a homogenous solution and followed by storing in the fridge.

### B. Seed germination Percentage

Plant species *Ipomoea aquatica*, *Brassica juncea*, *Lactuca sativa*, and *Solanum lycopersicum* were sown onto the soil, perlite and hydrogel. The seed germination experiment was conducted in the growth room at 22°C under the 4000 K LED light source and results were obtained after 15 days.

### C. Characterization of Germinating Media

The morphology aspects of the germinating media were observed under variable pressure scanning electron microscope (VPSEM).

## RESULTS AND DISCUSSION

### A. Seed germination Percentage

The germination rate of *Lactuca sativa* in the hydrogel was 70% while for *Ipomoea aquatica*, *Brassica juncea*, and *Solanum lycopersicum* was 86%, 85%, and 90%, respectively in perlite.

### B. Microscopic view of Perlite and Hydrogel

The hydrogel produced in this study is porous. The well adapted amorphous perlite is captured through VPSEM. Thousands of  $\beta(1-4)$  linked D-glucose units in the cellulose chain of the hydrogel carry plenty of hydroxyl groups. The hydrophilic functional groups help water absorption and retain water [4]. During the formation of hydrogel, the crystalline structure of cellulose is transformed to amorphous regions. The crosslinking process that occurred leads to a decreased crystallinity index. The transformation of structure from crystalline to amorphous state has led to a higher porosity of the hydrogel[3]. The porous structure allows oxygen to be available to the seeds. These features may have encouraged higher seed germination rate of *Lactuca sativa* plant species in hydrogel.

## CONCLUSIONS

Perlite is the best germination medium for *I. aquatica* and *S. lycopersicum*. Hydrogel shows comparable performance as perlite and soil to germinate *B. juncea* and *L. sativa*. Cellulose-based hydrogel has huge prospects as a suitable germinating medium, and there are more room for improvements in terms of hydrogel preparation and customization to be used as plant growth medium.

**ACKNOWLEDGMENTS:** The authors would like to thank Universiti Kebangsaan Malaysia (UKM) for the financial support via the research project grant LRGS/1/2019/UKM-UKM/5/1.

## REFERENCES

- [1] F. Orsini, R. Kahane, R. Nono-Womdim, G. Gianquinto, Urban agriculture in the developing world: A review, *Agron. Sustain. Dev.*, 2013, 33, 695.
- [2] D. Sarmah, N. Karak, Biodegradable superabsorbent hydrogel for water holding in soil and controlled-release fertilizer, *J. Appl. Polym. Sci.*, 2020, **137**, 1.
- [3] H. Tang, L. Zhang, L. Hu, L. Zhang, Application of Chitin Hydrogels for Seed Germination, Seedling Growth of Rapeseed, *J. Plant Growth Regul.*, 2014, **33**, 195.
- [4] M.A. Rahman Bhuiyan, M.A. Hossain, M. Zakaria, M.N. Islam, M. Zulhash Uddin, Chitosan Coated Cotton Fiber: Physical and Antimicrobial Properties for Apparel Use, *J. Polym. Environ.*, 2016, **25**, 334.

## Synthesis of Dazomet-Micelle Fungicide Nanodelivery System for Combating Ganoderma Disease in Oil Palm

Isshadiba F. Mustafa<sup>1</sup>, Mohd Zobir Hussein<sup>1\*</sup>, Abu Seman Idris<sup>2</sup>, Nur Hailini Z. Hilmi<sup>2</sup> and Sharida Fakurazi<sup>3</sup>

<sup>1</sup>Institute of Nanoscience and Nanotechnology (ION2), Universiti Putra Malaysia, 43400 UPM, Serdang, Selangor, Malaysia

<sup>2</sup>Malaysian Palm Oil Board (MPOB), Bandar Baru Bangi, 43000, Kajang, Selangor, Malaysia

<sup>3</sup>Faculty of Medicine and Health Sciences, Universiti Putra Malaysia, 43400 UPM Serdang, Selangor, Malaysia

\*Corresponding author: mzobir@upm.edu.my

**Abstract:** Dazomet-micelle nanodelivery systems (DAMINs) were prepared using ionic surfactants; sodium dodecylbenzene sulfonate and sodium dodecyl sulfate, and a non-ionic surfactant, Tween 80. Their physicochemical properties such as crystallinity and particle size distribution were studied. The particle size of DAMINs was found to be dependent on surfactant type and their concentration. This study found that DAMINs prepared using sodium dodecylbenzene sulphonate (SDBS), labeled as DMBS gave the highest inhibitory activities towards *Ganoderma boninense* compared to the one prepared using sodium dodecyl sulfate and Tween 80. This is towards the new generation of nanofungicides of better efficacy.

**Keywords:** Dazomet, nanodelivery, surfactant, micelle, *Ganoderma boninense*

### INTRODUCTION

Currently, there are very limited studies on the basal stem rot (BSR) disease which causes significant loss in the oil palm industry. The micellization process for pesticide nanoformulation is one of the ways to overcome the hydrophobic and poor water-soluble agrochemicals [1]. Recently, we have reported that the hexaconazole-micelles is a potential agronanochemical, but to the best of our knowledge, no work seems to have been done for agronano fungicide based on dazomet-micelle nanodelivery system.

### MATERIALS AND METHODS

The chemical, dazomet was obtained from Shanghai, China and all the surfactants were provided by Sigma-Aldrich (USA). Dazomet-micelle nanodelivery system was prepared by mixing 0.4 M dazomet with 1.226 g of SDBS, SDS or T80, separately. The suspension was immersed in an oil bath shaker at 70 °C before they were dried in an oven. The collected samples were labeled as dazomet-based sodium dodecyl benzene sulfonate (DMBS), dazomet-based sodium dodecyl sulfate (DMDS) and dazomet-based Tween 80 (DMT).

### RESULTS AND DISCUSSION

Figure 1 shows the X-ray diffractograms of DMBS, DMDS and DMT. The presence of the fungicide, dazomet was detected in the micelle systems, as shown in Fig. 1 (D-F), where typical diffraction peaks of dazomet at 16.1, 16.8, 18.3, 19.44, 21.16, 22.94, 28.08, 30.04, 31.3 and 32.5° (♦) were observed. Based on Table 1, it can be seen that the increase of surfactant concentration



lowers the particle size of the dazomet-micelles which is due to the interaction forces between molecules in the samples [2]. Treatment on *Ganoderma boninense* using the poison agar assay showed the smaller size of the DAMINs gave better efficacy.

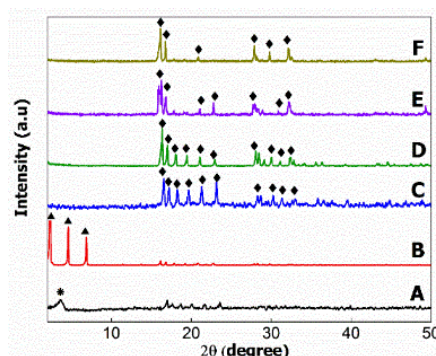


**Fig 1.** The XRD patterns of the physical mixture of DMBS (A), DMDS (B), DMT (C) and their dazomet-micelle nanodelivery systems (DAMINs); DMBS (D), DMDS (E) and DMT (F)

**Table 1.** Particle size distribution (mean value) of dazomet-micelle nanodelivery systems synthesized using various surfactant concentrations

Surfactant	Surfactant Concentration (% w/v)	Formulation label	PSD* Intensity (nm)	
			Initial	After 6 months of storage
Sodium dodecyl benzene sulfonate	1	DMBS-1	110	243
	2	DMBS-2	91	217
	4	DMBS-4	37	276
Sodium dodecyl sulfate	0.5	DMDS-0.5	206	290
	1	DMDS-1	153	204
	2	DMDS-2	98	200
Tween 80	6	DMT-6	130	228
	7	DMT-7	125	252
	8	DMT-8	109	194

## CONCLUSIONS

Dazomet-micelle nanodelivery systems (DAMINs) were prepared using various types of surfactants and varying their concentrations, and subsequently used to treat *Ganoderma boninense* using the poison agar assay. The findings demonstrated that the type of surfactants and their concentration is important in controlling the size of the agronanochemicals, where smaller sizes gave better efficacy.

## REFERENCES

- [1] M. Kah and T. Hofmann, "Nanopesticide research: Current trends and future priorities," *Environ. Int.*, vol. 63, pp. 224–235, 2014
- [2] P. Kumari, S. Kaur, S. Sharma, and H. K. Kashyap, "Impact of amphiphilic molecules on the structure and stability of homogeneous sphingomyelin bilayer: Insights from atomistic simulations," *J. Chem. Phys.*, vol. 148, no. 16, p. 165102, 2018, doi: 10.1063/1.5021310.



## Surface Modification of Nanocellulose: A Brief Overview

Nurul Ain Nadirah Jamaluddin<sup>1</sup>, Latifah Jasmani<sup>2</sup>, Rafeadah Rusli<sup>2</sup> and Sarani Zakaria<sup>1</sup>

<sup>1</sup>*Bioresources and Biorefinery Laboratory, Faculty of Science and Technology, Universiti Kebangsaan Malaysia, 43600 UKM Bangi, Selangor, Malaysia.*

<sup>2</sup>*Forest Products Division, Forest Research Institute (FRIM), 52109 Kepong Selangor, Malaysia.*

<sup>ok\*</sup>*Corresponding Autor's Email: P104438@siswa.ukm.edu.my*

**Abstract:** The increased popularity in sustainable technology recently has resulted in the rapid use of renewable material in many application fields. Nanocellulose is considered as one of the alternative materials to minimize our dependency on fossil resources and has the highest potential to be green nanomaterial across various research disciplines. This tremendous level of attention from scientist to focus on nanocellulose is due to its amazing physicochemical properties such as high mechanical strength, high surface area and ease of modification. Nanocellulose is hydrophilic in nature thus can only be used in related water-based application field. Surface modification is necessary to confer functionalities such as hydrophobicity onto nanocellulose in order to provide extra feature as well as to broaden its use in various application industries. The ease of functionalization on nanocellulose is due to the presence of abundant hydroxyl group on its surface. This review summarizes the surface modification process that have been conducted to date which focusing on the physical and chemical modification.

**Keywords:** nanocellulose, surface, modification, functionality.

### INTRODUCTION

Cellulose has been known for its availability, low cost, non-toxic as well as its remarkable mechanical and physical properties such as high strength, high flexibility and stiffness, and lightweight. However, the hydrophilic nature of nanocellulose hinders its application in any process or product that could not use water and cannot be readily corporates in most non-polar matrices [1]. Due to the presence of hydroxyl group on the surface of the nanocellulose, it provides an effective platform for surface modification to confer the hydrophilic behavior [2]. This mini review provides an overview of modification of nanocellulose using two types of pathways, physical and chemical modification in which both focused to alter its hydropilicity properties. Basically, there are three types of nanocellulose: Nanocrystalline cellulose (NCC), Nanofibrillated cellulose (NFC) and Bacterial cellulose (BC). NCC is commonly prepared by bleached wood pulp via an acid hydrolysis using inorganic acids. As opposed to NCC, NFC is produced via mechanical methods using high pressure homogenizer, microfluidizer, cyrocrushing and milling.

### SURFACE MODIFICATION

Recently, there has been growing interest on nanocellulose due to its incomparable properties whenever material strength, high aspect ratio or flexibility is required. However, the hydrophilic nature of nanocellulose hinders its application in any process or product that could not use water and cannot be readily corporated in most non-polar matrices [1]. Several modifications have been studied

and tested on nanocellulose to extend their compatibility in a diverse of matrices through physical adsorption or by chemical approach.

## PHYSICAL ADSORPTION

Based on this method, the surface of cellulose nanoparticles is modified using surfactants or electrostatic interaction between an anionic substrate and cationic polyelectrolyte. These interactions with the nanocellulose are performed through electrostatic attractions, hydrophilic affinity, hydrogen bonds or van der Waals forces. One of the examples of research that had been conducted using surfactant is the use N-hexadecyltrimethylammonium bromide (also called cetyltrimethylammonium bromide CTAB) [3-4]. As a result, the adsorbed layer of CTAB was proved to increase in its hydrophobicity without causing mechanical degradation.

## POLYMER GRAFTING MODIFICATION

Polymer grafting is another method that gain the interest of most researchers as it does not only improve their hydrophobicity, it also will provide better compatibility in the target polymer (Zhou et al., 2018). For instance, the synthesis of NCC and poly-L-lactic acid (PLLA) via in-situ ring open polymerization (ROP). This type of modification consists of two types of routes: 'grafting from' and 'grafting to'.

## COVALENT MODIFICATION

Covalent modification involves esterification (acetylation, butyration and palmitoylation), amidation and silylation. Owing to its simple and straightforwardness, esterification has been widely studied. Among all esterification process, acetylation has been considered as one of the best methods to modify the hydrophilicity of cellulose fibers as it helps in reducing the absorption of moisture in fibers.

## CONCLUSIONS

Nanocellulose is perceived as one of the most fascinating, biodegradable, renewable and sustainable polymer due to its inherent properties. This reviews, provide an overview to alter the surface of nanocellulose using two types of pathways, physical and chemical modification in which both focused to modify its hydrophilicity properties. Concisely, surface modification offers new wealth and revenue for the world as it helps to widen the application of nanocellulose not only in polar solvents but also in non-polar matrices.

## REFERENCES

- [1] Mariano, M., El Kissi, N., & Dufresne, A. (2014). Cellulose nanocrystals and related nanocomposites: Review of some properties and challenges. *Journal of Polymer Science, Part B: Polymer Physics*, 52(12), 791–806.
- [2] Domenek, S., Belgacem, N., & Bras, J. (2014). *Green Process for Chemical Functionalization of Nanocellulose with Carboxylic Acids*.
- [3] Miao, C., & Hamad, W. Y. (2016). In-situ polymerized cellulose nanocrystals (CNC) — poly (l -lactide) (PLLA) nanomaterials and applications in nanocomposite processing. *Carbohydrate Polymers*, 153, 549–558.
- [4] Morandi, G., & Thielemans, W. (2012). Synthesis of cellulose nanocrystals bearing photocleavable grafts by ATRP. *Polymer Chemistry*, 3(6), 1402–1407.

## Preliminary Study of Cellulose Nanofibre Produced through the Tri-solvent Technique

Mohamad Zaki Abdullah<sup>1</sup>, M Shuaib B M Saheed<sup>1</sup>, Mohd Fazli Mohammat<sup>2</sup> and Shahrul Nizam Md Salleh<sup>1,3\*</sup>

<sup>1</sup>Mechanical Engineering, Universiti Teknologi PETRONAS, Persiaran UTP, Seri Iskandar, Perak, Malaysia

<sup>2</sup>Institute of Science (IOS), Universiti Teknologi MARA, Level 3, Block C, UiTM 40450 Shah Alam, Selangor, Malaysia

<sup>3</sup>Centre of Innovation in Nanotechnology, SIRIM KULIM, Lot 34, Jalan Hi-Tech 2/3, Kulim Hi Tech Park, 09000 Kulim, Kedah

\*Corresponding Author's Email: shahrul\_19001715@utp.edu.my

**Abstract** This paper presents a preliminary study of the multi-solvent effect on the formation of cellulose nanofibre through the electrospinning method. Due to cellulose nanofibre's potential application in various fields, a different solvent was suggested to produce consistent quality of cellulose nanofibre. The solvent utilised in the study were acetone and water, while ethanol was added to the formulation. An attempt to add ethanol to acetone/water mix-solvent was performed to determine whether the tri-solvent technique could produce the nanofibre. The produced nanofibre was characterised using SEM to study the nanofibre morphology. The tri-solvent approach efficiently produced cellulose nanofibre with relatively low electrostatic field strength (EFS) and non-beaded nanofibre.

**Keywords:** electrospinning, nanofibre, multi-solvent, electrostatic field strength (EFS)

## INTRODUCTION

Nanofibre was defined as fibre which diameter range from 1 to 1000 nm the length to diameter ratio is more than 100 [1]. The researchers suggested several methods to produce the nanofibre, such as chemical vapour deposition (CVD), electrospinning, melt air spinning, conjugate spinning, and meltblown [1]. Electrospinning has emerged as one of the essential processes in producing nanofibre due to a wide range of materials such as synthetic and natural polymers, metals, ceramics, and composite systems.

## MATERIALS AND METHODS

CA (acetyl content 39.8%, Mw = 30,000), ethanol and acetone were purchased from Aldrich Co. and used as received. The difference tri-solvent mixtures were labeled as S1, S2, S3 and S4. The CA concentration was fixed at 5% w/v. The EFS was set at 10 kV with a 5 cm working distance and flow rate of 5 ml/h

## RESULTS AND DISCUSSION

The viscosity of the tri-solvent solutions was reported as 115, 101, 105 and 109 cps for S1, S2, S3 and S4, respectively. Figure 1 shows the SEM micrograph of S1, S2, S3 and S4 solutions.

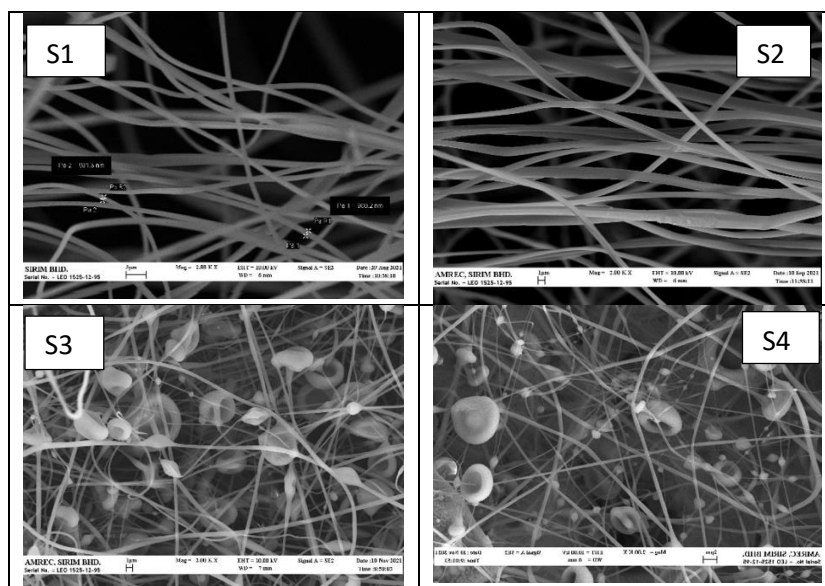


**Fig.1** Electrospun CA Nanofibre

The average diameter measured from the SEM micrographs was 831,914,514 and 396 nm for S1, S2, S3 and S4, respectively.

## CONCLUSIONS

In summary, a tri-solvent solution of a CA polymer consisting of an acetone, water and ethanol solution successfully produced the cellulose nanofibre. The S2 tri-solvent mix with 5% w/v CA produces the nanofibre comparable to the result reported elsewhere. No extensive studies on the tri-solvent system were reported in the journal. However, detailed studies including surface tension, EFS value, optimum feed rate, needle distance and roller drum rotation need to be considered.

## REFERENCES

- [1] Akihiko Tanioka and Mitsuhiro Takahashi. Nanofibers. In Japan The Society of Fiber Science and Techno, editor, High-Performance and Specialty Fibers: Concepts, Technology and Modern Applications of Man-Made Fibers for the Future, Springer Japan, Tokyo, 2016, pp. 273–283.

## Refinement Technique for Nanocellulose Extraction from Corn Cobs

Ismail K. Ibrahim Al-Khateeb <sup>1,\*</sup>, Yusra M. Al-Obaidi<sup>2</sup> and Sabri M. Hussain<sup>2</sup>

<sup>1</sup>Dijlah University College, Baghdad, Iraq.

<sup>2</sup>Department of Chemistry, College of Science, University of Anbar, Ramadi, Iraq.

Corresponding Author's Email address: dpt.head@duc.edu.iq

**Abstract:** Here we will discuss our novel extraction method that allows scalable fabrication of nano-cellulose materials with notes bile precision, combined with promising practical techniques. Nanocellulose (NC) was obtained from native corn cobs as agriculture waste. A modified method using ultrasonic technology followed by sulfuric acid hydrolysis with range of 30% to 60% was reliance by this investigation. The chemical analysis of the resultant NC as indicated by FTIR revealed a significance removal of hemicellulose and lignin from raw materials.

**Keywords:** Nanocellulose, Sonication, Acid-hydrolysis, Corn cobs, Isolation

### INTRODUCTION

The main goal of this work is to discuss the novel extraction procedure of cellulose and nano-cellulose from raw material of corn cobs. Cellulose is the most considerable polymer and it is the major composition of most plant biomass [1]. Regardless, cellulose has numerous worthy virtual purposes such as entity renewable, recyclable, eco- intimate, inexpensive, and prevailing many mechanical power [2]. The number of leftover plants has been selected as the origin for the manufacture of cellulose nanoparticles like corn cobs, rice straw etc [3]. Nano cellulose (NC) is one of the durable and rigid organic molecules very altitude surface areas, hydrophilic, and totally adjustable to surface activation. Meanwhile, nano-cellulose (NC) and its derivatives were used to prepare significance and the potential materials such as membranes [4] and industrial implementations [5].

### MATERIALS AND METHODS

The corn cob samples were washed with distilled water, dried at 100°C for 48 h and bleached at 80°C for 4 h using 0.1 % sodium hydro chlorite. The bleached fibers were filtered and washed several times with distilled water and dried. Ten grams of bleached fibers coming from bleaching step have been hydrolyzed in 100 ml of a sulfuric acid at various concentration (30,40,50,60%) using vigorous stirring. For termination of the reaction, 100 ml of deionized water mixed with the solution, cooled at 10°C. The pH was adjusted to 7 by using 1% of NaOH. The suspension was filtered, collected and sonicated by ultra sonicator (UP400S). with amplitude 80 for different periods of time (30,60,120 min). The subsequent NC was dried, converted to powder and stored for later use.



## RESULTS AND DISCUSSION

The peaks at  $1431\text{ cm}^{-1}$ ,  $1373\text{ cm}^{-1}$  and  $1317\text{ cm}^{-1}$  are correlated with twisting vibrations of  $-\text{CH}_2$ ,  $\text{C}-\text{H}$  and  $\text{C}-\text{O}$  groups of the aromatic rings respectively. These peaks manifested in Fig. 1. The peaks located at  $1031\text{ cm}^{-1}$  to  $1162.9\text{ cm}^{-1}$  attributed to the distortion of the  $\text{C}-\text{H}$  rocking vibration and the  $\text{C}-\text{O}-\text{C}$  pyranose ring skeleton [6,7]. Finally, the absorbance peak observed at  $896$  was assigned to the symmetric  $\text{C}-\text{O}-\text{C}$  stretching at (1-4)-glycosidic linkage [8] which became lower in intensity for NC spectra matched to that of unsonicated sample.

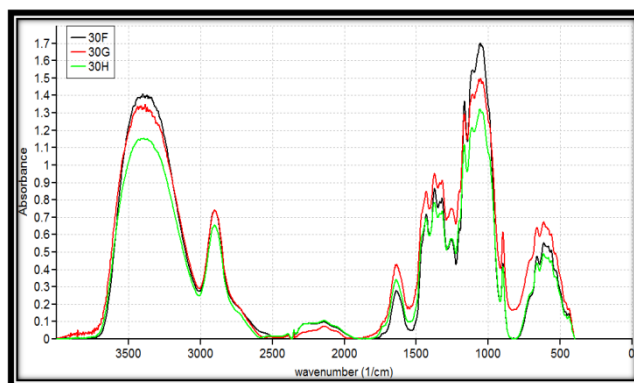


**Fig. 1.** FTIR Spectrum patterns comparisons of nanocellulose prepared from Corn Cobs at different sonification time (30, 60, 120) min at 30% acid

## CONCLUSIONS

The use of sonication technique coupled with hydrolysis method has been successfully used in synthesizing cellulose nano particles. The preferable outcomes under sonication situation used are coming from remediation of 30% acid sonicated for 120 min. Although cellulose nanoparticles of fairly well-defined dimensions were result in using this procedure, the precise cause for the differences in the sizes of nanoparticles synthesized using corn cobs addressed under the two different conditions studied here (sonication time and acid concentration) has to be further inspected.

## REFERENCES

- [1] Eduardo. E. Cellulose Nanocrystals Properties and Applications in Renewable Nanocomposites. Ph.D. thesis. Clemson University, Clemson, USA. 2011.
- [2] Chang C, Wang I, Hung K, Perng YJ. *Taiwan Sci.*, 2010, **25**, 251.
- [3] Mandal A, Chakrabarty D, *Carbohydr. Poly*, 2011, **86**, 1291.
- [4] Al-Rawi A, Al-Khateeb I, Zaidan T, *Enviro. Nanotechn. Monit. Manag*, 2021, **16**, 100529
- [5] Ergun R, Huebner-Keese B, *Encyclopedia of Food and Health Academic Press*, 2016.
- [6] Kumar A, Negi Y, Choudhary V, Bhardwaj N, *J.Mater.Phys.Chem*, 2014, **2**, 1.
- [7] Nazir M, Bambang W, Yussof A, *J. Bio. Reso.*, 2013, **8**, 2161
- [8] Wang Y, Wei X, Li J, *J. Mater. Sci. Chem. Engine.*, 2013, **1**, 49.



## Investigation on Thermal Stability Behaviour and Mechanical Properties of Polylactic Acid-Based Polymer Composite Filled with Different Nanofillers

Natasha Ramli<sup>1</sup>, Norkhairunnisa Mazlan<sup>2,3\*</sup>, Yoshito Ando<sup>4</sup>, Khalina Abdan<sup>5</sup>, Zulkiflle Leman<sup>6</sup>

<sup>1</sup>Laboratory of Biocomposite, Institute of Tropical Forestry and Forest Products (INTROP), Universiti Putra Malaysia, 43400 Serdang, Selangor, Malaysia

<sup>2</sup>Department of Aerospace Engineering, Faculty of Engineering, Universiti Putra Malaysia, 43400 Serdang, Selangor, Malaysia

<sup>3</sup>Institute of Advanced Technology, Universiti Putra Malaysia, 43400 UPM Serdang, Selangor, Malaysia

<sup>4</sup>Department of Biological Functions and Engineering, Graduate School of Life Science and Systems Engineering, Kyushu Institute of Technology, 2-4 Hibikino, Wakamatsu-ku, Kitakyushu, Fukuoka 8080196, Japan.

<sup>5</sup>Department of Biological and Agricultural Engineering, Faculty of Engineering, Universiti Putra Malaysia, 43400 Serdang, Selangor, Malaysia

<sup>6</sup>Department of Mechanical and Manufacturing Engineering, Faculty of Engineering, Universiti Putra Malaysia, 43400 Serdang, Selangor, Malaysia

\*Corresponding Author's Email: norkhairunnisa@upm.edu.m

**Abstract:** With growing worries about finite fossil fuel supplies and the impact of human activities on the environment around the world, biobased and biodegradable plastics and composites have emerged as viable options. Among the most widely used bioplastics is Polylactic Acid (PLA), synthesis by direct polycondensation of lactic acid as well as by ring-opening polymerization of lactide (LA), a cyclic dimer of lactic acid. Polylactic Acid (PLA), a renewable resource-based, was melt-processed with three different nanofillers to produce sustainable biocomposite. The addition of the fillers improved the mechanical properties of biocomposite at 40 wt% filler loading. An increase in flexural modulus was also observed. On the other hand, the strength, elongation-at-break and impact strength increased. The thermal stability of the PLA-based biocomposite was slightly reduced compared with the neat PLA. The degradation of PLA and the formation of unstable imperfect crystals were revealed by differential scanning calorimeter (DSC) analysis. Higher filler contents resulted in reduced crystallinity, indicating more pronounced effect on polymer chain mobility restriction.

**Keywords:** Polylactic acid, Biocomposite, Nanofiller, Impact strength, Crystallinity, Thermal stability

### INTRODUCTION

Thermal stability behaviour and mechanical properties of polylactic acid-based polymer composite filled with different nanofillers will be discussed. The performance of reinforced nanocomposites is superior than that of unreinforced nanocomposites [1]. A little amount of nanofiller increases thermal and mechanical conduction by allowing greater dispersion within the polymer matrix [2].

## MATERIALS AND METHODS

Three types of nanofillers were dispersed through the PLA polymer matrix during layer-upon-layer deposition of material extrusion-based additive manufacturing to fabricate a layered nanocomposite structure for the means of industrial applications. The mixture of PLA-nanofillers then moulded by hotpress method to become a composite. Then, samples will be tested regarding to thermal and mechanical properties behaviour.

## RESULTS AND DISCUSSION

Based on figure 1, it showed flexural strength behaviour on samples of PLA-nanofiller through one of mechanical testing. Three different types of nanofillers with 5 different loading will be tested. The amount of nanofillers start from 0.2%, 0.5%, 1%, 2% and 5%. Nanoclay shows 5% of loading is the best because it stated the highest flexural strength which is 16.5Mpa. Graphene and Geopolymer shows 0.5% and 1% respectively are the best performance for both which are 20.7Mpa and 20.78Mpa.

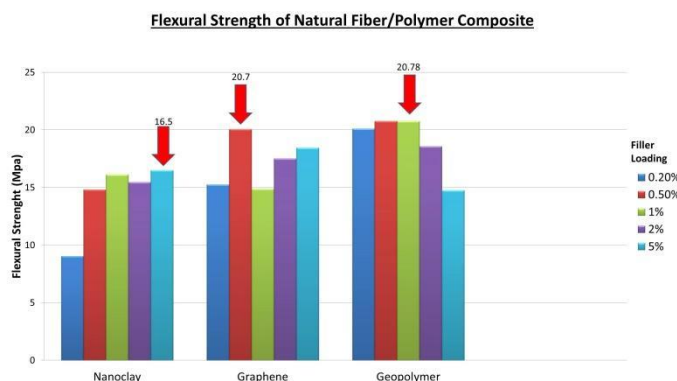


**Fig. 1.** Flexural strength of PLA-nanofiller mixture

## CONCLUSIONS

For the conclusion, a small amount of nanofiller can be affected the mechanical strength of PLA mixture. As PLA is one of favourite polymer use to create a better environmentally friendly composite, it still needs a supportive material in it to overcome its weakness. So that, this study used an addition layer of fibre to enhance its strength. This biocomposite can be used in aviation and automotive industry in the future because there are too many potentials to discover by researcher.

## REFERENCES

- [1] Rouway, M., Nachtane, M., Tarfaoui, M., Chakhchaoui, N., Omari, L. E. H., Fraija, F., & Cherkaoui, O. (2021). Mechanical Properties of a Biocomposite Based on Carbon Nanotube and Graphene Nanoplatelet Reinforced Polymers: Analytical and Numerical Study. *Journal of Composites Science*, 5(9), 234.
- [2] Sutar, H., Mishra, B., Senapati, P., Murmu, R., & Sahu, D. (2021). Mechanical, Thermal, and Morphological Properties of Graphene Nanoplatelet-Reinforced Polypropylene Nanocomposites: Effects of Nanofiller Thickness. *Journal of Composites Science*, 5(1), 24.

## Excess Population of the Dipole Moment Controls the Total Moment in Bulk Tetrahydrofuran

Mohd Farid Ismail<sup>1,2\*</sup>

<sup>1</sup>Department of Chemistry, Faculty of Science, Universiti Putra Malaysia, 43400 UPM Serdang, Selangor, Malaysia

<sup>2</sup>Integrated Chemical Biophysics Research, Faculty of Science, Universiti Putra Malaysia, 43400 UPM Serdang, Selangor, Malaysia

\*Corresponding Author's Email: mohd\_farid@upm.edu.my

**Abstract:** This work investigates the behavior of the individual dipole moment and its relation to the total moment in a bulk tetrahydrofuran (THF) solvent. Molecular dynamics simulation with carefully parametrized partial charges and Van der Waals parameters was used to reproduce the bulk static dielectric constant and the density of THF. The effect of the individual dipole moment of the THF molecules was analyzed and compared to the total moment of the bulk THF. From the simulation, the excess population of the THF molecules was determined to be the main factor that controls the behavior of the total moment.

**Keywords:** Total moment, molecular dynamics simulation, bulk solvent, THF.

### INTRODUCTION

The static dielectric constant of a bulk solvent determines the relative polarity of the solvent, a property that plays an important role in various field of chemistry. In statistical mechanics, the static dielectric constant is directly proportional to the total moment of the bulk solvent,  $\mathbf{M}$ , where  $\mathbf{M}$  is (a vector) defined as the addition of all individual dipole moment,  $\boldsymbol{\mu}$ , (vector) of the molecules of the bulk solvent [1]. As the molecules of the bulk solvent is free to move, the value of  $\mathbf{M}$  is affected by the angle and the direction of each individual  $\boldsymbol{\mu}$ . If the angle is perpendicular to  $\mathbf{M}$ , the contribution of  $\boldsymbol{\mu}$  to  $\mathbf{M}$  is small, whereas if the angle is parallel to  $\mathbf{M}$ , the contribution to  $\mathbf{M}$  is large. If the direction of  $\boldsymbol{\mu}$  is in the same direction as  $\mathbf{M}$ , then  $\boldsymbol{\mu}$  will contribute to increase the value of  $\mathbf{M}$ , and vice versa. Despite the obvious cause-and-effect between  $\boldsymbol{\mu}$  and  $\mathbf{M}$ , the relation between  $\boldsymbol{\mu}$  to  $\mathbf{M}$  is not known. Most of the studies related to the total moment fluctuation is related to the Stockmayer fluid [2]. This work looks at the behavior of the dipole moment  $\boldsymbol{\mu}$  and the way that it affects the total moment  $\mathbf{M}$  in the commonly used tetrahydrofuran (THF) solvent.

### MATERIALS AND METHODS

Molecular dynamics simulation was performed using the AMBER16 molecular dynamics software packages [3]. Electrostatic and Van der Waals parameters were modified such that the simulation produces bulk density and static dielectric constant from experiment. The data were collected at 1ps and 298K. The dipole moment was obtained with AMBERTOOLS [3] and analyzed using custom made C++ programs.

## RESULTS AND DISCUSSION

From the simulation, at any instantaneous moment, there are  $\mu$  that point in the same direction as  $\mathbf{M}$ , and  $\mu$  that point in the opposite direction of  $\mathbf{M}$ . While most of the time, the number of  $\mu$  that point in the same direction as  $\mathbf{M}$  is in excess, there are a few instances where the number of  $\mu$  that point in the opposite direction of  $\mathbf{M}$  is in excess. Using the dot product of each individual  $\mu$  and the total moment  $\mathbf{M}$ , the angle between the two variables were calculated. The average angle of all  $\mu$  that are in the same direction as  $\mathbf{M}$  was plotted. This analysis showed that there are no relationship between the two variables. The excess  $\mu$  that points in the same direction as  $\mathbf{M}$  was analyzed. The plot of the excess  $\mu$  versus  $\mathbf{M}$  is shown in Fig. 1. As can be seen from the plot, the number of excess  $\mu$  shows trends that is similar to  $\mathbf{M}$ . The direction of the plot of  $\mathbf{M}$  can be predicted by only looking at the plot of the excess  $\mu$ . The result suggests that the excess  $\mu$  is the determinant of the value of  $\mathbf{M}$ .

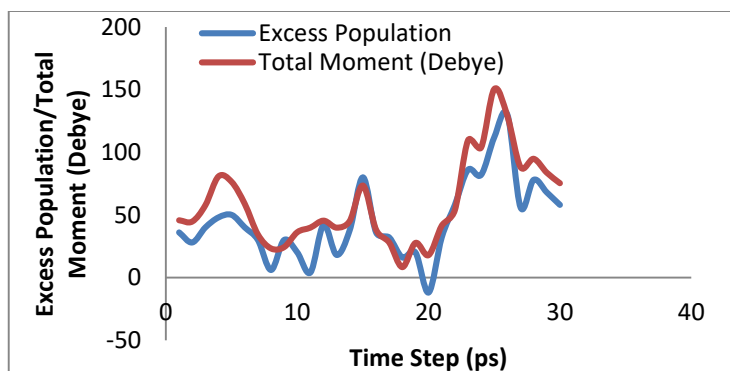


Fig. 1. The plot of Excess Population of  $\mu$  (blue) versus  $\mathbf{M}$  (red).

## CONCLUSIONS

From the results, the excess population of the individual dipole moment predicts the total moment in the bulk solvent really well. On the other hand, the angle of the individual dipole moment appears to have no control of the total moment in the bulk solvent. It can be concluded that at the molecular level, the static dielectric constant value for a bulk solvent depends on the total excess individual dipole moment of the constituent molecules that point to the same direction as the total moment in the bulk solvent.

**ACKNOWLEDGMENT:** The author would like to thank Universiti Putra Malaysia for the support of this work via the Inisiatif Putra Muda (IPM) grant scheme (Reference code: UPM/700-2/1/GP-IPM/2015/9455900, Project Code: GP-IPM/2015/9455900).

## REFERENCES

- [1] Neumann, M. *Mol. Phys.*, 1983, **50**, 841-858.
- [2] See for example: Martin T. *J. Chem. Phys.*, 2010, **133**, 174105.
- [3] D. A. Case, et. al. (2016), AMBER 2016, University of California, San Francisco

## **Modeling Techniques of MTJ's in Spin Based Devices and Its Results Comparison**

Maryala Praveen<sup>1</sup> and Atul Kumar Nishad<sup>2</sup>

<sup>1</sup>Department of Electronics & Communication Engineering, National Institute of Technology Warangal,  
Telangana, India

<sup>2</sup>Department of Electronics & Communication Engineering, National Institute of Technology Warangal,  
Telangana, India

**Abstract** – This paper describes an initiative study about the modelling techniques of MTJ block with consideration of different no. of terminals to MTJ and its results comparison. MTJ modelling can be extended to include different Spintronic phenomena like basic ‘Spin transfer torque’ (STT) – 2 terminal to further ‘Voltage Controlled Magnetic anisotropy’ (VCMA) – 2 terminal, ‘Spin orbit Torque’ (SOT) – 3 terminal w.r.t SHE and Rashba effect, Ferro electric tunnel junction (FTJ) – 3 terminals. These above modelling techniques of MTJ are observed in this paper and finally will compare their functionality results with respect to basic STT 2-terminal modelling of MTJ.

**Keywords** – MTJ, STT, VCMA, SOT, FTJ, SHE.

### **INTRODUCTION**

‘SPINTRONICS’ is blend of electronics with Spin, refers to the study of role played by electron “SPIN” in Solid state physics. The basic building block of any Spin based devices is “Magnetic Tunnelling Junction (MTJ)”. Magnetic tunnel junction (MTJ) is a device whose electrical resistance is variable and depends on the magnetic state [3]. Magnetic Tunnel Junction (MTJ) device is structured as thin Insulated layer is separated by both Ferromagnetic layers in which one layer is constituted with Fixed Spin orientation and when the Spin polarized current passes through both FM fixed layer and Insulating /Oxide layer the Spin orientation in the Free FM stand either in Parallel to Fixed layer or Anti-Parallel to Fixed layer; such switching happens in MTJ device. Here are some listing the different type modelling techniques of MTJ's are:

(1). Spin Transfer Torque (STT) – Basic model, (2). Voltage controlled Magnetic Anisotropy (VCMA), (3). STT\_Spin Orbit Torque (STT\_SOT), (4). Ferro Electric Tunnel Junction (FTJ).

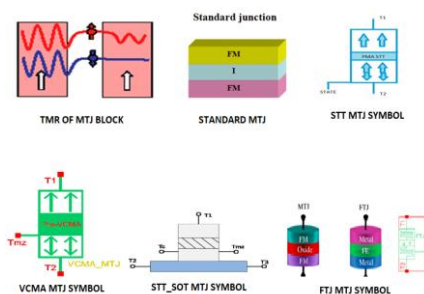


**Fig.1** Symbols of TMR, MTJ, STT, VCMA, STT\_SOT, FTJ

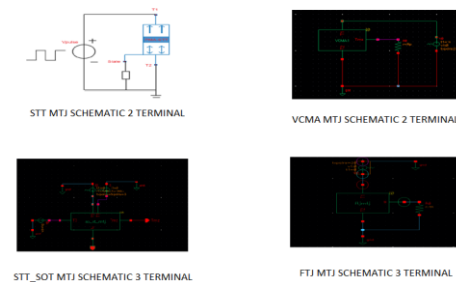


**Fig.2** Schematics of STT, VCMA, STT\_SOT, FTJ



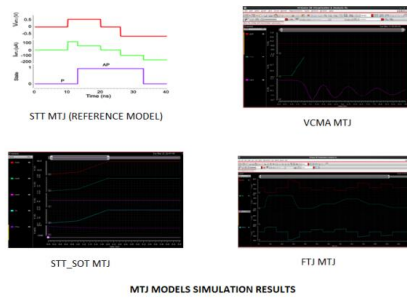


Fig.3 Simualtion results of  
STT,VCMA,STT\_SOT,FTJ

S.no	Parameters/ Modules	STT	VCMA	STT_SOT	FTJ
1.	Structures	PL-NM-FL	PL-NM-FL	PL-NM-FL-HM	EL(PL)-NM-EL(FL)
2.	No.of Terminals	02	02	03	03
3.	Model Technique	STT	STT+ External Bias voltage	STT+SOT (RASBHA+ SHE)	TMR & TER
4.	Model Output	I <sub>on</sub> vs STATE	I <sub>on</sub> vs V <sub>appl</sub>	I vs I <sub>on</sub>	I vs V <sub>appl</sub>
5.	Model Input	T1 & T2	V <sub>appl</sub> - T1 & T2	I <sub>on</sub> - T1 & T2 & V <sub>dc</sub> -T3	V <sub>appl</sub> - T1& T2
6.	Switching	Internal STT current	External Bias Voltage	STT- TMR & SOT- (SHE +RASBHA)	TER- FN Tunneling & TMR- Direct Tunneling
7.	Delay	~2.1ns	~2ns	~1.6ns	~1ns

Table.1 MTJ models Results comparision

## RESULTS AND DISCUSSION

All the MTJ models are simulate through Cadence Virtuoso Tool considering different input modelling technique to each model and observe the results in terms of Functionality Speed and Delay measured for each model. Here, STT MTJ is considered as Basic modeling technique and then its Limitations is overcome in VCMA MTJ model by sepearating both 'Writing' & 'Reading'paths to avoid error-rate. And Further STT\_SOT is combination of both STT & Spin-Orbit Torque functioning by 'Spin-hall Effect' & 'Rasbha Effect' – the overall betterment in terms of Functionality and Delay time. The above 3 models are purely observed as magnetic variation without consideration of electric mode. Final model of FTJ MTJ is an inclusive of electric charge as input to MTJ and output observed as elegant manner than earlier models. Hence minimum delay observed when compared to STT, VCMA, STT\_SOT models.

STT > VCMA > STT\_SOT > FTJ --- Perfomance Delay

## CONCLUSIONS

We compared several parameters from **basic model STT technique** to every other models of **VCMA, STT\_SOT & FTJ**. The results best confirms that the 3 terminal device of **FTJ MTJ** i.e., faster switching comparing to earlier models. High TMR is resulting in FTJ MTJ model along with additionally TER effects came into existence. The drawbacks of STT MRAM of sharing common path for both 'READ' & 'WRITE' is overcome in VCMA MTJ technique and further with 3 terminal SOT\_STT MRAM shows better results with minimum delay and faster switching by both SHE + RASBHA effects. Finally, among all FTJ MTJ show better scope results with minimum delay of around ~1ns and resembles with faster switching by functionality of both TER – FN Tunnelling, TMR – Direct Tunnelling and Thermionic Tunnelling in device.

## REFERENCES

- [1]. Sonal Shreya and Brajesh kumar Kaushik, "Modeling of voltage-controlled Spin- orbit Torque MRAM for multi level switching application" *IEEE transactions on electron devices*,vol.67,no1,Jan2020.
- [2]. Mustafa mert Torunbalci ,Pranmey Upadhyaya,Sunil A.Bhaveand Kerem Y.Camsari,"Modular compact modeling of MTJ devices",*arXiv:1805.00066v2*,Aug 2018.
- [3]. Vincent Garcia & Manuel Bibes -"Ferroelectric tunnel junctions for information storage and processing".



## Simultaneous Extraction of Diffusion Length and Surface Recombination Velocity from an EBIC Line Scan using Artificial Neural Networks

Souhila Soualmia

*Departement of Physics, Faculty of Science, Batna University, 05000 Batna, Algeria*

**Abstract:** In this work, we present a new approach that uses artificial neural networks (ANN) to simultaneously extract two related semiconductor parameters that are: the diffusion length  $L$  and the normalised surface recombination velocity  $S$  from the same Electron Beam Induced Current (EBIC) as a function of beam position in a normal collector configuration. A set of parameters values is obtained with an error less than 1.7% for the diffusion length and less than 4% for the normalised surface recombination velocity in 95% of the cases, and an error less than 2.7% for the diffusion length and less than 8% for the normalized surface recombination velocity in 100% of the cases. The obtained results show the efficiency of our method.

**Keywords:** EBIC, parameter extraction, neural networks, diffusion length, surface recombination velocity.

### INTRODUCTION

For the characterization of semiconductor materials; Electron Beam Induced Current (EBIC) of the Scanning Electron Microscopy (SEM) is one of the widely used methods. The parameter extraction problem is a multi-minimum optimization problem and it can be solved using several optimization techniques [1]. We developed in this work a new parameter extraction technique, that extracts simultaneously two related semiconductor parameters: the diffusion length  $L$  and the surface recombination velocity  $S$ , using a feedforward artificial neural network. Basically, the ANN is trained to learn the inherent relationship between the input parameters ( $L$ ,  $S$ ) and the output parameter (EBIC signal versus electron beam position). Once the ANN has been trained, it is possible to observe the reverse process and extract the two parameters from any EBIC curve using an exhaustive search method. Our approach has the following advantages: 1) since it uses directly the data (experimental) for training it is independent of the theoretical model. 2) Once the ANN is trained it is able to generalize and extract the required parameters from any experimental data. 3) Since the whole search space is scanned, our approach ensures finding the optimum values for the parameters ( $L$ ,  $S$ ).

### THE PARAMETER EXTRACTION ALGORITHM

A normal collector configuration [2] is used here, the model of Donolato [3] is used to calculate EBIC current (Monte Carlo simulations and experimental data can be used as well). For the training data a set of the two parameters ( $L$ ,  $S$ ) are sampled and stacked into vectors  $\mathbf{L}^{train}$  and  $\mathbf{S}^{train}$ . All the possible combinations of the vectors  $\mathbf{L}^{train}$ ,  $\mathbf{S}^{train}$  form the input training set  $\mathbf{X}^{train}$ . The EBIC signal for different values of the beam position is evaluated (Donolato's model [3]). The results are stored in another matrix  $\mathbf{Y}^{train}$  (output training set). Same for the test samples  $\mathbf{L}^{test}$  and  $\mathbf{S}^{test}$ , all

their possible combinations form the input test set  $\mathbf{X}^{test}$  the theoretical EBIC signal for different values of beam position is calculated and stored in a matrix  $\mathbf{Y}^{test}$  (output test set). The ANN is trained to learn the functional relationship  $f$  between the input data set  $\mathbf{X}^{train}$  and the output data set  $\mathbf{Y}^{train}$ . Once the ANN has been trained, its ability to generalize is tested by applying a new set of input values not seen before. More samples are obtained by oversampling of the EBIC signal, the oversampled data set are used as a database for the exhaustive search.

## RESULTS AND DISCUSSION

The total number of samples used for training is 2077, the maximal error in 95% of the training set is 0.4% only, and for all the training set it is 1.2% only. Our ANN is tested with 2010 samples, the maximal error in 95% of the test set is 1.2% only, and for all the test set it is 1.5% only. The total number of input data samples used for oversampling the EBIC is 10769. The maximal error in 95% of the set is 0.45% and it is 1.26% in 100% of the set. Then, an exhaustive search procedure is used to determine the value of the oversampled EBIC that is the closest (in terms of Euclidian distance) to the EBIC for which we want to determine the input parameters. Then, a large set of randomly selected EBIC curves for which the input parameters ( $L$ ,  $S$ ) are known, is generated and used to test the parameter extraction algorithm. The percentage error between the true input parameter (nominal value) and the parameter determined using the proposed parameter extraction algorithm is calculated for each randomly selected EBIC curve. The error is less than 8% in all cases and less than 4% in 95% of the cases.

## CONCLUSION

We developed in this work a novel method based on neural networks and exhaustive search technique for the simultaneous extraction of the diffusion length and the surface recombination velocity from any theoretically/experimentally obtained EBIC signal. The derived results show that a unique set of parameter values can be obtained with error less than 8% from the true value. This shows that the proposed approach is efficient.

## REFERENCES

- [1] A. K. Hartmann, H. Rieger, "Optimization Algorithms in Physics", Wiley-VCH Verlag Berlin GmbH, Berlin (Federal Republic of Germany), 1<sup>st</sup> edition 2002.
- [2] L. Reimer, "Scanning Electron Microscopy physics of image formation and microanalysis", Springer 2<sup>nd</sup> edition 1998.
- [3] C. Donolato, "On the Analysis of Diffusion Length Measurements by SEM", *Solid State Electronics*, Vol. 25, No. 11, pp. 1077-1081, 1982.

## Simulation of AI & ML based Nano Mechanical Embedded Systems for Diagnostic Application Development in the field of Bio-medical Engineering

Madhu P. Asangi<sup>1</sup>, Pavithra G.<sup>2</sup> and T.C. Manjunath<sup>3</sup>

<sup>1</sup>, Dept. of ECE, USN - 1DS20LVS03, VLSI Design & Embedded Systems, Dayananda Sagar College of Engg.,  
Bangalore, Karnataka

<sup>2</sup>ECE Dept., Dayananda Sagar College of Engineering, Bangalore

<sup>3</sup> ECE Dept., Dayananda Sagar College of Engineering, Bangalore

Cell : 9449820361 9591071967 9663846781 Email : tcmanju@iitbombay.org, dr.pavithrag.8984@gmail.com

**Abstract:** The research work that is presented in this extended abstract aims to perform a simulation of AI & ML based nano mechanical systems for diagnostic application development in the field of bio-medical engineering, i.e., we simulate a nano-robot that could be used for the detection of cancerous diseases in human beings. We use some nano-technology based simulation tools such as the nano-hive software for the design & simulation of robots, further to use the simulated robot to detect the cancerous cells and give an intimation to the doctor and to the patient that the patient has been affected with cancer and if possible bring out the cancerous cell out of the human body. Simulation is carried out using nano-hive software tool & the results are presented. In this research work, we have developed some mathematical models for the dynamical movements of the nanorobots, we also simulated a nanorobot using simulation tools like nanohive or cadence or synapses tools. Once simulated & given a job to detect the cancer cells & destroy them, the effect of achieving the task is seen. Different simulation parameters were considered in the design process in the software. If there should be an occurrence of dynamic focusing on, nanoparticles containing the chemotherapeutic specialists were planned in such a manner as they straight-forwardly communicate with the deserted/infect cells and do the action preset.

**Keywords:** Nano-Robot, AI, ML, Simulation, Cancer, Bio-medical, Embedded.

## INTRODUCTION

In the fight against cancer disease, the early detection is a key factor for successful treatment & to save precious human life. The research work presented in this extended abstract relates to such an application-oriented work w.r.t. the simulation, design & development of nanorobots for cancer cure therapy & diagnostic applications in human beings using AI & ML tools with the help of software tool studies. The main objective of the research work is to carry out the following, which is combined in the form of 4 well-defined objectives as (1) To simulate a miniaturized nano-robot to detect the cancerous cell using simulation tools like nano-hive & cadence tools using the following concepts such as Locomotion, Propeller, Cilia/flagellate, Electromagnetic pump, Jet Pump, Membrane propulsion, Crawl along surface, Navigation, Ultrasonic parts, Radioactive dye parts, Power actuating device, Sources within the body, Generation of power from the bloodstream. (2) Studying the behaviour of the cancerous cells & to halt their behavioural growth by detecting that the cell is being affected with the cancer disease. (3) To kill or dis-infect the cancerous cell by injecting anti-cancerous nanoparticle and to make it inactive. (4) Devise some strategies to bring them out of the human body by collecting them.

## MATERIALS AND METHODS

The materials used are C in the design of the nano-robot along with some specifications. Basic constructional features of a Nanobot that is taken into consideration during the design process are - Nanorobot has a C- nanotube body, A bio-molecular n-motor that propels it & peptide limbs to orient itself, Composed of biological elements such as DNA & proteins, genomes, Hence, it can be easily removed from the body, Sensors, molecular sorting rotors, fins & propellers,  $\leq 6$  DOF, Sensory capabilities to detect the target regions, obstacles, C is the principal element comprising the bulk of a medical nanorobot. The software used is the nano-hive simulation tool. NanoHive-1 is a modular nanosys-simulator used for modeling the physical world at a nanometer scale. Purpose of the simulator is to act as a tool for the study, design, simulation, experimentation & development of nano & biological entities.

## RESULTS AND DISCUSSION

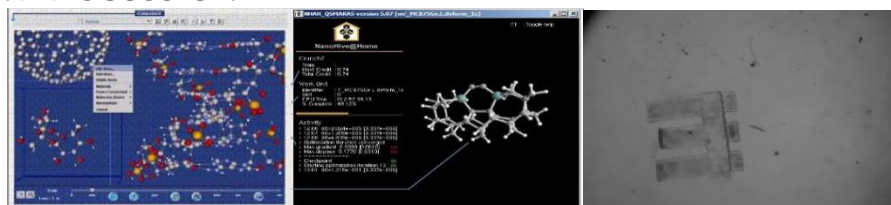


**Fig. 1:** Simulated Motion of the designed & developed Nanobot using Nano Hive-1 Ver 1.2.0 Beta-1 : Nano Systems Simulator Tool Material : C Nano-tubes ; Nano Hive-1 is a modular simulator used for modeling the physical world at a nanometer scale (adv : model the DNA / ribosomes) ; MNR navigation moving along the x-direction

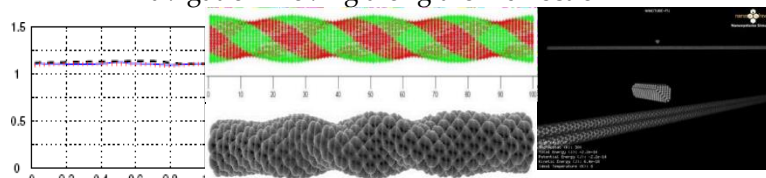


**Fig. 2:** Representation of predicted buckling mode-shapes Actual buckling mode-shape predicted using simulations; Result of a simulation designed to test various distributed computing mechanisms; While just a test, it's still an interesting simulation to watch; A diamonded carbon "knife" is pushed down on the nanotubes with a 5 nN force; Will the knife cut through the nanotubes? The system comprises ~20,000 atoms & runs for 5.5 ps of sim time

## CONCLUSIONS

A small review of the research work related to the design & development of nanorobots was presented here. This research work is developed w.r.t. rural community with less experienced doctors even in the field of cancer detection & its diagnosis in the field of bio-medical engineering, i.e., it has got wide applications in the field of bio-medical engineering that too in the detection of cancerous cells as the current techniques such as the chemotherapy & the other medical activities causes lot of nausea, hair loss, vomiting, stress, etc.

## REFERENCES

- [1] Dr. T.C.Manjunath, "Fundamentals of Robotics", Nandu Publishers, India, 2005.

## Ambipolar effect in Field Effect Transistors Based on Transition-Metal Dichalcogenides

Mehmet Ertugrul<sup>1</sup>

<sup>1</sup>*Department of Electrical Electronics Engineering, Engineering Faculty, Ataturk University, 25240 Erzurum, Turkey*

**Abstract:** Ambipolarity has become important for many applications in recent years. In addition to device fabrication from materials with ambipolar behavior, many factors such as the controllability of ambipolarity and the degree of ambipolarity have attracted the attention of researchers. Many factors causing ambipolarity have been reported in the literature. Especially, 2D dicalgonites such as WS<sub>2</sub> and MoS<sub>2</sub> are the leading materials for FET devices with ambipolar behavior. Besides the properties of these 2D materials, the geometry of the device also has an effect on ambipolarity. In this study, the effect of geometric properties of the FET device, such as channel thickness, on ambipolarity was investigated. For the FET device, it was seen that the instability starts from a few layers of channel thickness and then decreases again as the thickness increases. It was observed that as the thickness increased, the degree of ambipolarity approached zero. The degree of ambipolarity approaching zero indicated that the WS<sub>2</sub> channel exhibited natural n-type behavior and the ambipolar effect disappeared.

**Keywords:** TMDC, ambipolarity, FET

### 1. Introduction

The polarity of transistors can be categorized as unipolar (hole-dominant p-type or electron-dominant n-type) or bipolar (ambipolar) (hole and electron together) according to the switching characteristics and the dominant charge carriers in semiconductors. Ambipolar transistors are types of transistors that allow synchronous transport of electrons and holes in a semiconductor [1]. Unipolar devices (p-type and n-type) generally exhibit invariant electrical properties and therefore their application has certain limitations. Si itself is an ambipolar. Boron doped Si acts as P type, phosphorus doped Si acts as N type, so doped Si becomes unipolar p or n type. In practical applications, it is difficult to redope Si with the chemical element to change the type of major charge carriers. The electric field cannot completely control the semiconductor behavior and therefore it is difficult to control the polarity of the main charge carriers for bulk Si. Ambipolar devices can achieve comparable simultaneous transfer of electrons and holes, thus displaying p-type and n-type features within a single device. In ambipolar semiconductors, p or n-type semiconductor behavior can be obtained by electric field driving. This is why ambipolar semiconductors require electrical configurations like FETs. Unlike doping, electric field propulsion offers an efficient approach to quickly, dynamically and reversibly adjusting the type of main charge carriers [2-4].

Organic materials, ambipolar materials such as carbon nanotubes, 2D and perovskite materials, and various device architectures such as bilayer and blended structures have been fabricated to achieve ambipolar carrier transmission and other applications including solar cells, logic devices, neuromorphic devices, light-emitting transistors, gas sensors, and ambipolar flash memory [5]. Nanostructures such as 2D semiconductors make materials display ambipolar properties, effectively avoiding the screening effect. Among 2D materials, TMDCs stand out in device technology due to their ability to adjust their conductivity, large



surface/volume values, electronic properties depending on thickness, very high mechanical flexibility, and functionalization capabilities [6]. Currently TMDCs have attracted more attention due to their natural abundance and unique/diverse properties. The generalized chemical formula for TMDCs is  $MX_2$ , where M represents the transition metal (typically Ti, Zr, Hf, Mo, W, Nb, Re, V and Ni) and X is a chalcogen (S, Te and Se) (Figure 1). Currently, there are more than 40 different combinations of TMDC have been reported and have shown distinctive features [6].

## 2. Ambipolarity

The ambipolarity can be controlled with gate voltage which is described in the literature. When  $V_g - V_t > V_d$  and both are positive, the current is carried by electron (1). When  $V_g - V_t$  is positive and  $V_d$  is negative (6), the effective gate potential is positive across the entire channel. The transistor works as a unipolar n-type transistor in which source and drain are reversed. When  $V_g - V_t$  is negative and  $V_d$  is positive (3), the effective gate potential across the channel is negative. Ambipolarity can occur when  $V_d > V_g - V_t$  (2) and  $V_d < V_g - V_t < 0$  (5).  $V_g$ : gate bias,  $V_d$ : drain bias,  $V_t$ : threshold voltage.

Electron and hole mobilities vary depending on the thickness, and for TMDC materials. Materials with one or more layer thicknesses generally have p-type characteristics, over this thickness they are ambipolar in a certain range, and in thicknesses above that, they have n-type characteristics, which is the natural behavior of the material [9]. As can be seen from previous studies [10,11] the electron and hole mobilities can be obtained from the  $I_d$ - $V_{DS}$  graphics of the transistor, whose schematic drawing is given in Figure 3. By plotting the electron and hole mobilities against the channel thickness, it can be found at what intervals the materials exhibit ambipolar behavior (Figure 1).

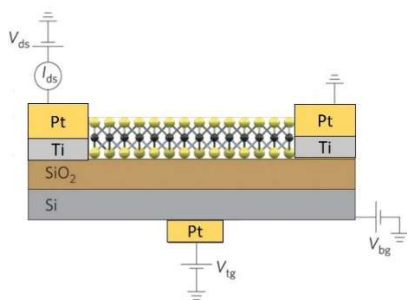


**Fig. 3.** A Schematic TMDC transistor

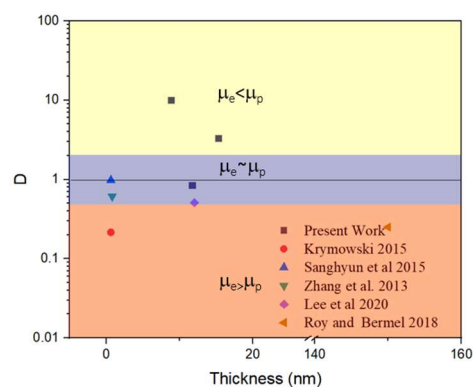


**Fig. 4.** Variation of ambipolarity behavior depending on channel thickness. (Here,  $D = \mu_h / \mu_e$ )

## 3. Conclusions

Ambipolarity behavior provides a FET device with significant advantages over conventional FET devices due to the gate voltage and polarity adjustment and rapid switching. However, the ambipolarity behavior may differ according to the material, process parameters, channel thickness, film growth technique and conditions. It is very important to understand the



mechanisms of these effects in order to produce suitable ambipolar FET devices. In this study, the effect of thickness on ambipolarity behavior was tried to be investigated. As a result, it has been observed that TMDC materials exhibit ambipolar behavior in a certain thickness range. In the thicknesses of a few atomic layers, it has been determined that the material shows a dominant p-type behavior, shifts towards n-type behavior as the thickness increases, and after a certain thickness, the dominant n-type behavior is effective. For WS<sub>2</sub> films, electron and hole mobility varies depending on many factors such as growth method, thickness, growth and annealing temperature, gate voltage, etc. It was observed that the WS<sub>2</sub> FET device exhibited ambipolar behavior in a certain thickness range as the thickness increased from monolayer to multilayer. A thicker channel has higher mobility compared to thinner ambipolar TMDC-based devices. The effect of channel thickness in TMDC-based devices can be associated with Coulomb scattering and quantum confinement. Coulomb interactions weaken the scattering of carriers, providing higher mobility for thicker FETs compared to their thinner counterparts. Further studies should be done for the effect of channel thickness on ambipolarity. Investigation of the effects of gate voltage, S/W ratio and other factors on ambipolarity together with channel thickness and reflecting the effects of these parameters on the degree of ambipolarity will make a significant contribution to the literature.

## References

1. Acar M, Mobtakeri S, Efeoğlu H, Ertuğrul M, Gür E., *Ceramics International*, 2020, 46(17), 26854
2. Yadav S, Jena SR, Bhavya MB, Altaee A, Saxena M, Akshaya KS, *Emergent Materials*, 2021, 901, 4
3. Hu W, Sheng Z, Hou X, Chen H, Zhang Z, Zhang DW, Zhou P, *Small Methods*, 2021, 5, 2000837.
4. Bisri SZ, Piliago C, Gao J, Loi MA, *Advanced Materials*, 2013, 26, 1176.
5. Zhou Y, Han ST, *Ambipolar Materials and Devices*, Royal Society of Chemistry, 2020.
6. Ahmed S, Yi J, *Nano-Micro Lett.*, 2017, 9, 50
7. Acar M, Ertuğrul M, *Erzincan University Journal of Science and Technology*, 2021, 14(2), 825.
8. Risteska A, Chan KY, Anthopoulos TD, Gordijn A, Stiebig H, Nakamura M, Knipp D, *Organic Electronics*, 2012, 13, 2816
9. Rani A, DiCamillo K, Hossain Khan MA, Paranjape M, Zaghloul ME, *Sensors*, 2019, 19(11), 2551
10. Koçak Y, Gür E, *ACS Appl. Mater. Interfaces*, 2020, 12, 15785
11. Schwierz F, *Nature Nanotechnology*, 2010, 5, 487

## Green Synthesized Nanomaterials as a Novel Support for the Immobilization of Some Industrial Enzymes and Their Applications

Hayrunnisa Nadaroglu\*

Department of Food Technology, Erzurum Vocational Collage, Ataturk University, 25240 Erzurum, Turkey  
Department of Nano-Science and Nano-Engineering, Institute of Science and Technology, Ataturk University,  
25240 Erzurum, Turkey

\*Corresponding Autor's Email: hnisa25@atauni.edu.tr

**Abstract:** Industrial enzymes immobilized on nano support materials are successfully used in the food industry, fuel, textile, paper and pulp, detergent, environment, medical and analytical fields. Nanoparticles obtained by green synthesis by using plant extracts in non-toxic, high yield, mild conditions were used for immobilization. Many different biodegradable nanoparticles or nanocomposite support materials have been used successfully in the immobilization of industrial enzymes. While pectin lyase, mannanase, lipase, protease, laccase, cellulase and chitinase enzymes were immobilized to the nanosupported materials, the activity and immobilization efficiency were preserved. As a result of the modification of the enzymes with Magnetic Fe<sub>3</sub>O<sub>4</sub> nanoparticles, the enzyme was easily recovered from the reaction medium. In addition, as a result of the immobilization of industrial enzymes, the steric bulk problem was minimized during the binding of the substrates to the active center.

From the findings obtained from our studies, it has been determined that the reusability of enzymes provides an average of over 80% activity preservation in 10 cycle reaction trials in almost all enzymes.

**Keywords:** Immobilization, Pectin lyase, Laccase, Mannanase, Phytase, Lipase, Chitinase

### INTRODUCTION

Within the scope of this paper, it is aimed to purification, characterization and immobilize pektin liyaz (polimetilgalakturonat liyaz; EC 4.2.2.10, PMGL), mannan endo-1,4- $\alpha$ -D-mannosidaz, fitaz (miyo-inositol heksakisfosfatfos phohidrolaz, EC 3.1.3.8), lipaz (EC 3.1.1.3), kitinaz (EC 3.2.1.14) ve lakkaz (EC 1.10.3.2), endo-b-D-mannanaz (EC 3.2.1.78) enzymes purified from different sources and using different methods to suitable nano support materials. In addition, it is aimed to increase and protect the stability of the immobilized industrial enzymes against environmental conditions such as high pH, temperature, metal ions, and to investigate suitable industrial applications (1).

### MATERIALS AND METHODS

#### Purification and Characterization of Some Industrial Enzymes

In our studies, enzymes were purified by using different chromatographic methods. For this purpose, enzymes were purified by using mostly ammonium sulfate precipitation, three-phase separation method (TPP method), ion exchange methods (2).

#### Determination of the Activity of Enzymes

In the characterization stages of all purified industrial enzymes, their activities were determined spectrophotometrically using the specific substrate of each enzyme. Enzyme

Unit for each enzyme; The optimal amount of enzyme that converts 1 mmol substrate to product under optimal conditions was calculated as EU/mL for each enzyme (3).

## RESULTS AND DISCUSSION

### Industrial Enzymes

The pectin polymer found in fruit structures is the natural support material of the plant cell structure. Pectin is formed as a result of the binding of 300-1000 galacturonic acid units with b(1-4) glycosidic bonds (3). Mannan is a homopolymer of D-mannose and constitutes 30% of the dry weight of the plant. Pectin Lyase, Mannanase and Amylase enzymes are widely used in the fruit juice industry to obtain clear and high yielding juice. At this stage, by using Pectin Lyase, Mannanase and Amylase enzymes to biodegradable, antibacterial modified nanomaterials, pectin, mannan and starch structures are hydrolyzed and fruit juice is obtained with a clearer and higher efficiency compared to free enzymes, and the use of enzymes can be achieved repeatedly (4).

**Proteases (EC: 2.3.1.1)** are members of the hydrolase enzyme group. It plays a role in the catalysis of the hydrolysis of peptide bonds. In particular, the loss of activity of the immobilized protease enzyme is prevented and more effective use is ensured. It is widely used in the food industry to make meat crispy and to obtain cheese by coagulating milk (5). Lipase enzyme (E.C.3.1.1.3; triglycerol acylhydrolases) is also a hydrolase group enzyme and it catalyzes hydrolysis reactions, especially esterification, alcoholysis, acidolysis and aminolysis reactions. In our group, after purification from microbial sources, it was covalently immobilized to the modified florisol surface with magnetic Fe<sub>3</sub>O<sub>4</sub> NPs obtained by green synthesis and used as a detergent additive material in formulations (1).

**Phytase enzyme** (myo-inositol 1,2,3,4,5,6 hexakis-dihydrogen phosphate) and chitinase (E.C. 3.2.1.14) enzyme are also hydrolase group enzymes. Phytase enzyme is one of the commercial enzymes that is important for human health, especially for the protection of the environment. In our study, phytase enzyme purified from non-toxic fungi was immobilized to the modified chitosan surface with magnetic Fe<sub>3</sub>O<sub>4</sub> NPs obtained by green synthesis, and phytic acid found in some cereal products was degraded into inorganic monophosphate, myo-inositol phosphates and free myo-inositol. performances were compared (6). **Chitinase enzyme**, on the other hand, is used as a preservative against plant pathogens, as well as being used in the hydrolysis of chitin, which causes environmental pollution. In our study, the chitinase enzyme was purified and its antifungal activity against *F. culmorum* was determined (7).

Finally, oxidoreductase **laccase** (Benzendiol: Oxygen Oxidoreductase, EC 1.10.3.2) is a member of the large group of enzymes called polyphenol oxidases, which contains copper atoms in its catalytic center and has three copper ions in its active center. In our studies, laccase enzyme purified from different materials was immobilized on the surface of modified support materials with metal NPs obtained by green synthesis, and its use in processes such as fruit juice clarification and azo dye removal from wastewater was investigated (8).

## CONCLUSION


By immobilizing the industrial enzymes it is summarized above to different non-toxic and biodegradable support materials modified with magnetic Fe<sub>3</sub>O<sub>4</sub> NPs obtained by green synthesis, more resistant and higher efficiency reactions against external factors will be realized and their reusability will be ensured. Thus, the use of immobilized systems is of great importance in terms of both their use in different industries and the elimination of environmental pollution (9).

## REFERENCES


1. Soleimani, S. S., Nadaroglu, H. & Kesmen, Z. Lactobacillus brevis lipase: Purification, immobilization onto magnetic florosil NPs, characterization and application as a detergent additive. Tenside, Surfactants, Detergents 54, (2017).
2. Tasgin, E., Babagil, A., Nadaroglu, H. & Allegretti, P. E. Immobilization of Purified Pectin Lyase from Acinetobacter calcoaceticus onto Magnetic Carboxymethyl Cellulose Nanoparticles and Its Usability in Food Industry. Journal of Chemistry 2020, 1–12 (2020).
3. Tasgin, E., Nadaroglu, H., Babagil, A. & Demir, N. Immobilization of Purified Pectin Lyase from Pseudomonas putida onto Magnetic Lily Flowers (Lilium candidum L.) Nanoparticles and Applicability in Industrial Processes. Molecules 25, 2671 (2020).
4. Nadaroglu, H., Adiguzel, G., Adiguzel, A. & Sonmez, Z. A thermostable-endo- $\beta$ -(1,4)-mannanase from Pediococcus acidilactici (M17): purification, characterization and its application in fruit juice clarification. European Food Research and Technology 243, 193–201 (2017).
5. Nadaroglu, H.; Polat, M. S. Chapter 6 - Microbial extremozymes: Novel sources and industrial applications. in Microbial Extremozymes Novel Sources and Industrial Applications 67–88 (2022). doi:0.1016/B978-0-12-822945-3.00019-1.
6. Onem, H. & Nadaroglu, H. Preparation and Properties of Purified Phytase from Oakbug Milkcap (Lactarius Quietus) Immobilised on Coated Chitosan with Iron Nano Particles and Investigation of Its Usability in Food Industry. Journal of Food and Nutrition Research 2, 938–945 (2014).
7. Senol, M., Nadaroglu, H., Dikbas, N. & Kotan, R. Purification of Chitinase enzymes from Bacillus subtilis bacteria TV-125, investigation of kinetic properties and antifungal activity against Fusarium culmorum. Annals of Clinical Microbiology and Antimicrobials 13, 35 (2014).
8. Kalkan, E. & Nadaroglu, H. Adsorptive removal of acid fuchsin dye using by-product silica fume and laccase-modified silica fume. Iranian Journal of Chemistry and Chemical Engineering 40, 551–564 (2021).
9. Nadaroglu, H. Exploring Plant Cells for the Production of Compounds of Interest - Chapter-Immobilization and Application of Industrial Enzymes on Plant-Based New Generation Polymers. (Springer International Publishing, 2021). doi:10.1007/978-3-030-58271-5.



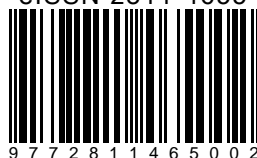
# iSAMN2021



**Organized by:**  
INSTITUTE OF NANOSCIENCE AND  
NANOTECHNOLOGY (ION2)  
UNIVERSITI PUTRA MALAYSIA (UPM)  
[www.ion2.upm.edu.my](http://www.ion2.upm.edu.my)



eISSN 2811-4655



9 7 7 2 8 1 1 4 6 5 0 0 2

AGRICULTURE • INNOVATION • LIFE

**BERILMU BERBAKTI**  
WITH KNOWLEDGE WE SERVE

[www.upm.edu.my](http://www.upm.edu.my)